SELECTIVE LASER MELTING OF Al-Cu12 IN-SITU ALLOYING

DEVELOPMENT FOR ANCHOR-LESS PROCESSING

By:

Rafael Martinez

A thesis submitted in partial fulfilment of the requirements for the degree of Doctor of Philosophy

Academic Supervisors:

Dr. Kamran Mumtaz

Professor Iain Todd

The University of Sheffield

Faculty of Engineering

School (or Department) of Mechanical Engineering

Submission Date 19th of September, 2019

Abstract

The feedstock used within the additive manufacturing process Selective Laser Melting (SLM) is generally deposited and laser processed in a pre-alloyed state. The full melting and rapid solidification of feedstock leads to the creation of components with mechanical properties comparable and sometime exceeding those of traditionally cast. For high performance applications within aerospace and automotive, pure elemental powdered blends for use within SLM are generally not used due to poor powder distribution and difficulty in controlling composition across the component. In-situ elemental blending of feedstock represents a route for testing the feasibility of different elemental mixtures, creating alloys in-situ in a cost-efficient way, however the resultant properties of component made using such a feedstock are not fully understood.

This research aims to develop an in-situ aluminium hardenable alloy using a novel Semi-Solid Processing (SSP) method known as, Anchorless Selective Laser Melting (ASLM). This method requires two or more separate materials within the feedstock to be in-situ alloyed under the action of the laser to form into various combinations of eutectic/hypo/hyper eutectic alloys in a stress reduced state. The ASLM method results in the elimination of supports required during manufacture due to maintaining the processed material in a semi-solid state.

In this investigation, Selective Laser Melting (SLM) was applied to an identified suitable candidate materials for ASLM processing requiring elemental blending and developed optimum processing parameters for the in-situ fabrication of an Al-Cu12 alloy from pure elemental blends of aluminium and copper powders. Design of Experiments (DOE) were applied for parameter optimisation in order to minimise internal defects and studying the influence of SLM parameters such as layer thickness, laser power, scan strategy, scan speed and hatch spacing concluding that 67º meander scanning strategy and a combination of high power source and reduced scanning velocities leads to a higher densification.

Findings shows that the use of elevated pre-heat temperatures created a coarser cellular-dendritic microstructure consisting of supersaturated Al-rich matrix with a uniform globular microstructure with finer Al_2Cu phase compared to as-fabricated samples at room temperature. It was found that Al-Cu12 in-situ processed samples achieved maximum tensile strength values comparable to cast AlCu12 alloy. Processing at elevated pre-heat temperatures created components with higher ultimate tensile strength and ductility and minimised warping distortion compared to standard room temperature built samples due to it assisting a more complete melting of Al and Cu particles. An in-situ age hardening resulted of the prolonged high temperature processing and slower cool down, producing an equilibrium $\alpha + \theta$ microstructure.

Acknowledgements

Journal Paper Publications

Vora, Pratik, Rafael Martinez, Neil Hopkinson, Iain Todd, and Kamran Mumtaz. 2017. "Customised Alloy Blends for in-Situ Al339 Alloy Formation Using Anchorless Selective Laser Melting." MDPI Technologies (2): 24. https://doi.org/10.3390/technologies5020024.

R. Martinez, Todd I & Mumtaz KA, 2019. "In-situ alloying of elemental Al-Cu12 feedstock using Selective Laser Melting". Virtual and physical Prototyping. 1(1), p.32.

Conference Papers

Ruihuan Ge, R. Martinez, A. Sciacovelli, M. Atallah, 2019 "3D printing manufacturability of a topology-optimized multi-tube latent heat storage system'" 16th UK Heat Transfer Conference UKHTC2019

Contents

List of Figures

List of Tables

Abbreviations

3D	Three Dimensional
3DP	3 Dimensional Printing
ADMAM	Anchorless Direct Metal Additive Manufacturing
AM	Additive Manufacturing
AMRG	Additive Manufacturing Research Group
ASLM	Anchorless Selective Laser Melting
ASTM	American Society for Testing and Materials
CAD	Computer aided Design
CT	X-ray Computer Tomography
DED	Design For Additive Manufacturing
DFMA	Direct Energy Deposition
DMLS	Direct Metal Laser Sintering
DOE	Design Of Experiments
DSC	Differential Scanning Calorimetry
FDM	Fused Deposition Modelling
FEA	Finite Element Analysis
FEM	Finite Element Modelling
FM	Full Melting
HF	Hydrofluoric Acid
HV	Vickers Hardness
LASER	Light Amplification by Stimulated Emission of Radiation
LPS	Liquid Phase melting
LS	Laser Sintering
LOM	Light Optical Microscopy
MRI	Magnetic Resonance Imaging
MTX	Melting Temperature of 'X' material
N2	Nitrogen
PA	Polyamide
PW	Process Window
SEM	Scanning Electron Microscopy
SL	Stereo lithography
SLS	Selective Laser Sintering
SLM	Selective Laser Melting
SSS	Solid State Sintering
SSP	Semi-Solid Processing

TA	Thermal Analysis
TGM	Temperature Gradient Mechanism
UC	Ultrasonic consolidation
UTS	Ultimate Tensile Strength
XRD	X-Ray Diffraction

Symbols

P	Pressure (Pa)
Tb	Bed temperature (K)
λ	Wavelength
ED	Energy density (W)
Ss	Scan Spacing (mm)
V	Scan Speed (mm/s)
PL	Laser Powder (W)
Tm	Melting Temperature
ρb	Bulk Density(kg/m^3)
Kb	Thermal Conductivity (W/mK)
Cp	Specific heat capacity (J/kgK)
Lf	Latent heat of fusion (J/kg)
Tv	Evaporation Temperature (K)
η	Dynamic Viscosity (Pa.s)
θ	Angle
γ	Surface energy (J/m^2)
A	Absorbance
γSV	Surface energy at solid-vapour interface (J/ m^2)
γLS	Surface energy at liquid-solid interface (J/ m^2)
γLV	Surface energy at liquid-vapour interface (J/ m^2)
Ma	Marangoni number
α	Solid phase of component A in eutectic phase diagram
β	Solid phase of component B in eutectic phase diagram
L	Liquid Phase in eutectic phase diagram
δ	Thermal diffusivity (mm^2/s)
μm	Micro (10^{-6} m)

Chapter 1: Introduction

1.1　Overview of Additive Manufacturing Technologies

Additive Manufacturing (AM) is officially defined by the ASTM F2792−12a standard terminology as "a process of joining materials to make objects from 3D model data, usually layer upon layer, as opposed to subtractive manufacturing methodologies" (ASTM Standard, 2013). AM is capable of processing a wide variety of materials such as polymers, metals and ceramics.

The raw material used in production could be in the form of wire, liquid or powder. Figure 1-1 shows an overview of AM processes. AM can be classified further based on medium used to consolidate the material such as laser and electron beam technologies. The metal AM technologies can be sub classified by the method of material deposition onto the build tray/platform and into powder bed deposition and powder feed deposition.

Nowadays, AM is mostly used to create complex geometries not possible to achieve by traditional methods such as machining or casting, as well to reduce the lead-time in functional prototyping.

Additive Manufacturing

Metal

Powder Bed Fusion
-Selective Laser Melting(SLM)
-Electron Beam Melting (EBM)
-Direct Metal Laser Sintering (DMLS)

Direct Energy Deposition
-Laser Engineering Net Shape(LENS)
-Electron Beam Additive Manufacturing (EBAM)
-Direct Metal Deposition(DMD)

Material Jetting
-NanoParticle Jetting(NJ)

Binder Jetting
-Binder Jetting(BJ)

Polymer

Powder Bed Fusion
-Selective Laser Sintering(SLS)
-Multi Jet Fusion (MJF)

Vat Photopolymerization
-Stereolithography(SLA)
-Digital Light Processing(DLP)
-Continuous Digital Light Processing(DLP)

Material Extrusion
-Fused Deposition Modelling(FDM)

Material Jetting
-Material Jetting(MJ)

Ceramic

Powder Bed Fusion
-Selective Laser Sintering(SLS)
-Selective Laser Melting(SLM)
-Fused Deposition of Ceramic(FDC)

Composite

Material Extrusion
-Fused Deposition Modelling(FDM)

Sheet Lamination
-Laminated Object Manufacturing(LOM)

Figure 1-1 Additive Manufacturing Technologies. Adapted Diagram (author's Image)

1.1.1   Selective Laser Melting

Selective laser melting (SLM) is one of the powder bed fusion technologies most widely investigated within the metal AM technologies due their large range of material options that can process, becoming one of the most versatile options for many researchers. For this process, near fully dense components can be manufactured by metallic powders layer by layer using laser beam (Mercelis and Kruth, 2006). SLM processing offers possibility to manufacture

net-shape parts without the need of any post-processing operations used in AM components such as heat treatment or final machining.

The main advantage of SLM are reflected in their resultant fine microstructure which is beneficial for the improvement of mechanical properties for a wide range of metallic alloys. Furthermore, mechanical properties of SLM components can be customised by varying different process parameters during the build process leading to a different microstructures that influence the mechanical behaviour (Prashanth et al. 2017).

1.1.2   In-situ Selective Laser Melting Alloys

Selective Laser Melting (SLM) is a manufacturing technology process that can produce complex geometries directly from CAD. The process uses a laser beam to locally fuse metallic powder layer by layer at the powder bed. Thus, introduces an opportunity to mixture different materials from elemental powders using in-situ alloying.

In-situ alloying processing in SLM consists to locally melt two or more distinct powdered materials under the action of laser forming different material combinations. The potential of the in-situ alloying processing approach is by now not well understood because of the absence of experimental knowledge

and details of the influence of process parameters on final microstructure, homogeneity, and mechanical properties of blended alloys (Yadroitsev 2017).

Recent studies focus attention on the benefits of elemental blending in-situ alloys processed by SLM to introduce materials with unique microstructure and mechanical properties were shown recently. Vora successfully demonstrated the creation of in-situ Al-339 by mechanically mixing two elemental custom alloys AlMg and SiCuNi (Vora et al. 2017). Sistiaga reported dense crack-free parts by mixing A7075 pre-alloy with 4% Si elemental powder (Sistiaga et al. 2016). Kang produced a eutectic in-situ aluminium alloy from Al and Si with an average particle size of 6- 42 µm demonstrating mechanical properties similar to AlSi12 pre-alloy processed by SLM (Kang et al. 2017). It was noted that the creation of an alloy in-situ through SLM could represents a low-cost and flexible methodology.

1.2   Novelty Statement

Recently, a considerable amount of literature has been published to understand SLM of metals. Processing metals under lasers has been studied in detail for effects related to the changing of process parameters, materials, and method of production. So far, very little attention has been paid to the role of in-situ alloying in SLM and the potential benefits for researches to quickly

manufacture powders at a laboratory scale for new alloy/application development. The potential development of customised powder mixtures with different properties has strong potential and represent a promising route in the future of AM (Aboulkhair et al. 2016).

The experimental work presented in this dissertation provides the first investigation into developing SLM parameters for pure elemental blends of binary system Aluminium-Copper to create an Al-Cu12 in-situ alloy, establishing analysis and results for microstructure, residual stress and mechanical properties (tensile behaviour, micro hardness) under room temperature and high temperature conditions.3.3

Secondly this research will provide insight into a novel method of removing or alleviating stress build up and the requirement for the additional material attached to the parts know as anchors that within SLM can achieved by preventing parts from completely solidifying during processing or maintaining in a stress reduced state. An in-situ Semi-Solid Processing (SSP) know as Anchorless Selective Laser Melting (ASLM) has been developed to prevent processed metal from completely solidifying during SLM build.

Processing metals without anchors will benefit SLM processing by improving manufacturing throughput, providing new opportunities for complex

geometries, cost, and efficiency. Until now, only one academic work has been performed in collaboration with the author of this thesis to examine this novel process, however it lacks in-depth understanding of material properties and industry applications.

1.3   Aims and Objectives

This research will focus on creating knowledge and in-depth analyses of a new in-situ aluminium Al-Cu12 elementally mixed from pure powder to meet requirements for ASLM processing method that eliminates supports. The research will be conducted in two phases; material development and material processing with ASLM. Material development will investigate on developing new feedstock material for standard SLM that will have good process ability and further applications. Material processing with ASLM will involve laser melting of identified alloy produced by mixing elemental components to assess the potential of design for additive manufacturing without supports and unlock design of freedom.

1.3.1 Objectives

The objectives for this project are to:

- Develop and optimise SLM process parameters for in-situ Al-Cu12 alloy from elemental mixture in order to achieve low internal defects and good mechanical properties comparable to cast alloys such as yield strength(σ) and ultimate tensile strength (UTS) .

- Investigate the influence of in-process preheating on microstructure development, chemical composition and mechanical properties for in-situ Al-Cu12 processing via SLM and ASLM.

- Design and development of in-situ pre-heating platform capable to obtain high temperature that would be able to eliminate the use of supports from metal powder bed.

- Produce overhang parts with novel material and process enhancing the free of design.

- Develop understanding into laser material interaction to build support less geometries with conventional SLM and ASLM for Al-Cu12.

1.4   Thesis Structure

A detailed flow diagram of the methodology steps used to accomplish the aims and objectives for this research is described in Figure 1.2. Most of the stages were undertaken in parallel during the entire project.
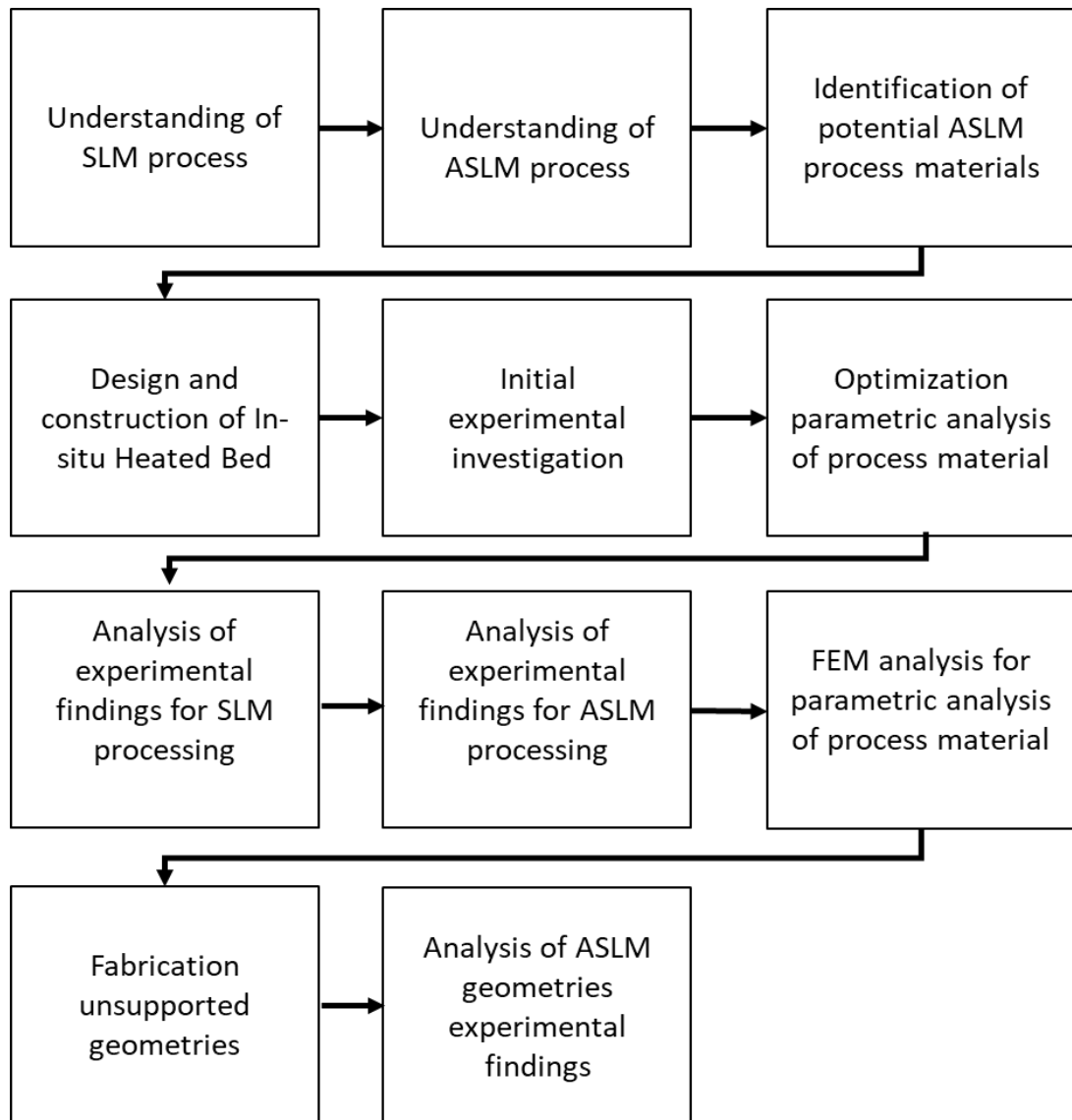
Figure 1-2 Project methodology flow diagram

Chapter 2 will introduce an extensive literature research in order to understand the following:

- Selective Laser Melting: process, parameters, materials, melt pool dynamics.
- Current research in SLM
- Metal phase transformation
- Processing in-situ alloys via SLM.
- Geometric limitations in Fusion Powder Bed AM

And explain in detail ASLM methodology used in this research. Provides detail of specials characteristics, establishing the super cooling effect for polymers and metals, as well of processing parameters, methodology requirements and initial research in metals.

Chapter 3 details the experimental methodology for the research. System information for equipment used to perform this research will be discussed, and will provide details on different apparatus used to prepare material used in research and test build geometries for process window, density, microstructures etc. It will explain in detail the design and development of the heated platform for laser melting as well machine modifications and installation.

Chapter 4 presents the utility of Design of Experiments (DoE) for optimising processing parameters to achieve a high dense in-situ Al-Cu12 and the use of Finite Element Analysis (FEA) modelling used to predict melt pool formation and experimental validation for trials conducted for this work. Providing a better understanding to minimise porosity by selecting right processing parameters.

Chapter 5 presents experimental results for the development of in-situ Al-Cu12 alloy from elemental mixing and the variation of processing parameters on microstructure and high temperature processing effects.

Chapter 6 focuses in the mechanical properties (UTS, hardness, elongation) of samples as built and processed at high temperature using optimum parameters this chapter shows a comparison of mechanical properties of samples built in in different built directions and presents results of residual stress measurements.

Chapter 7 presents the validation of ASLM fabrication methodology using the developed in-situ alloy for this research by processing unsupported geometries. The chapter will provide experimental research on overhang structures and limitations as well of the creation of more complex design and its advantages over standard SLM processing.

Chapter 8 will list the overall conclusions from this research and future work suggestions to improve current research and expand its application.

Chapter 2: Literature Review

2.1 Selective Laser Melting

2.1.2 Process

SLM is a laser powder bed fusion (LPBF) process utilising laser technology to produce metal 3D parts. Metal powder is spread over a substrate (a thick metal plate/platform) at a defined layer thickness (20µm-70µm) using a powder deposition mechanism. The layer thickness is adjusted through lowering the substrate after completion of each laser scan. The laser scans the layer and the powder material is melted, fusing it to the previously melted layer. Figure 2-1 shows a schematic of conventional SLM. In SLM the powder particles fully melt and theoretically a full density can be achieved. Several factors contribute to the production of fully dense parts.

The process variables involve energy density (ED), layer thickness (T_L), bed temperature (T_b) and scanning strategy. To obtain full melting, high laser power and temperatures are required; these cause large thermal gradients that can create thermal stress. To reduce thermal stresses, SLM systems are installed with powder bed heating systems to reducing the thermal gradient. The process chamber is isolated, and processing is performed in inert atmosphere (purged with argon, nitrogen gas etc.).
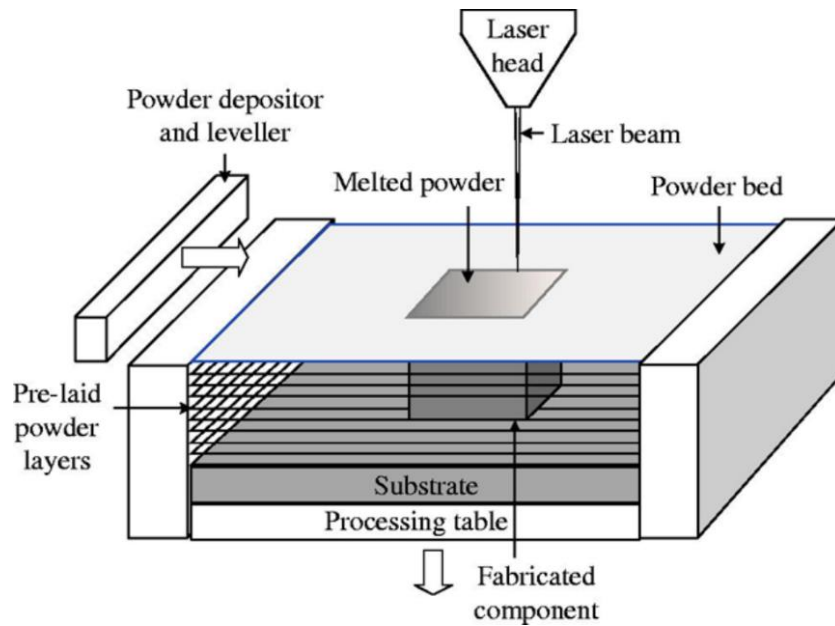
Figure 2-1 Selective Laser Melting Schematic diagram (Mumtaz and

Hopkinson, 2008)

2.2 Processing parameters and factors involved during SLM process

SLM part properties such as surface roughness, porosity and mechanical properties are all affected by processing parameters. Several factors are responsible for selection of processing parameters. These factors are shown in Figure 2-2. A brief description of the relevant parameters considered as relevant to the research will be introduced from section 2.2.1 to 2.2.6.

```
┌─────────────────────────────────────────────────────────────────┐
│          FACTORS AFFECTING SELECTIVE LASER MELTING PARAMETERS     │
└─────────────────────────────────────────────────────────────────┘

┌──────────────────┐   ┌──────────────────┐   ┌──────────────────┐
│   ENVIRONMENT    │   │      LASER       │   │     POWDER       │
│                  │   │                  │   │                  │
│  • INERT GAS     │   │  • MODE          │   │  • COMPOSITION   │
│  • PRESSURE      │   │  • WAVE          │   │  • GRANULAR SIZE │
│  • OXYGEN        │   │    LENGTH        │   │  • MORPHOLOGY    │
│    LEVEL         │   │  • INTENSITY     │   │                  │
│                  │   │    PROFILE       │   │                  │
└──────────────────┘   └──────────────────┘   └──────────────────┘

┌─────────────────────────────────────────────────────────────────┐
│                    PROCESSING PARAMETERS                          │
│                                                                   │
│       ENERGY DENSITY                   POWDER BED                 │
│                                                                   │
│   • SCAN SPACING                  • LAYER THICKNESS               │
│   • SCAN SPEED                    • BED TEMPERATURE               │
│   • LASER POWER                   • POWDER                        │
└─────────────────────────────────────────────────────────────────┘
```
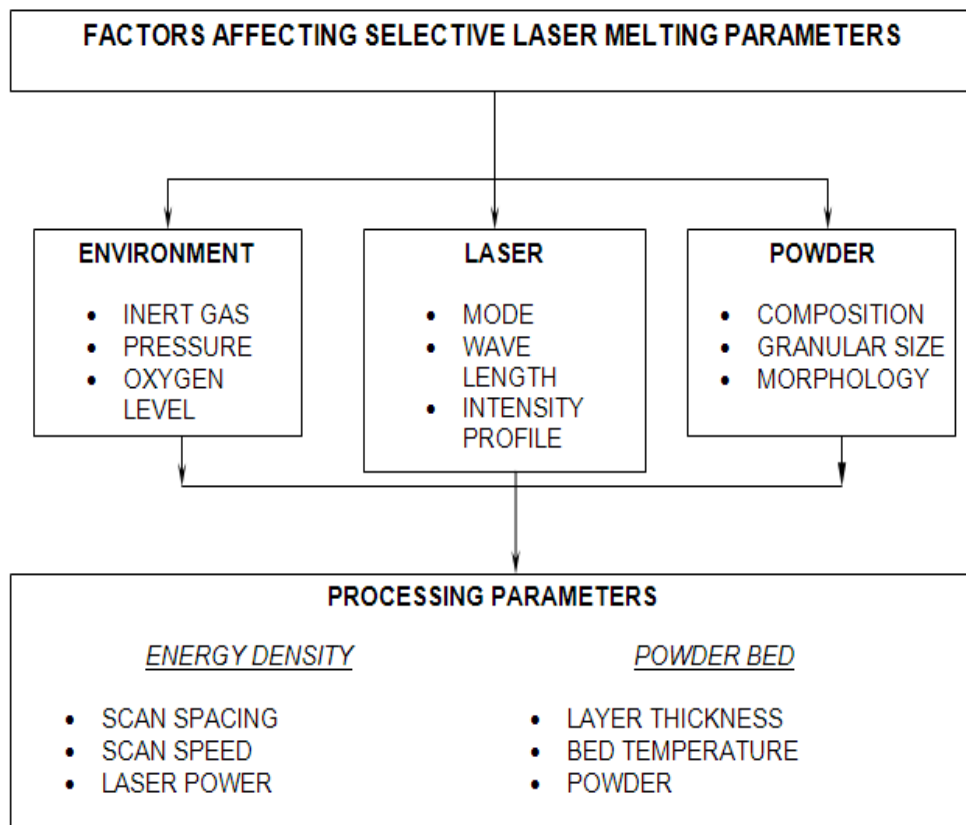
Figure 2-2 Factors affecting SLM parameters Adapted from (Arwala et al.

1995)

2.2.1 Environment

The environment involved the conditions inside the processing chamber of the
SLM machine. This is a key factor influencing the performance of the system and
the properties of the parts. The presence of reactive agents such as oxygen can
affect part mechanical properties as shown in Figure 2-3. Thus, the presence of

oxygen in the chamber should be controlled. SLM is conducted in the presence of inert gases such as nitrogen (N_2) and Argon (Ar).

Gases: Several gases are known to be inert and suitable for various applications. However, at elevated temperatures metals may react with certain gases and thus reduce the wetting properties by formation of metal oxides. For example, hydrogen and nitrogen cause embrittlement for Ti-alloys. Argon can be used with most of the materials. Although helium has good inert properties but is not ideal due to high cost and poor oxygen displacement properties.
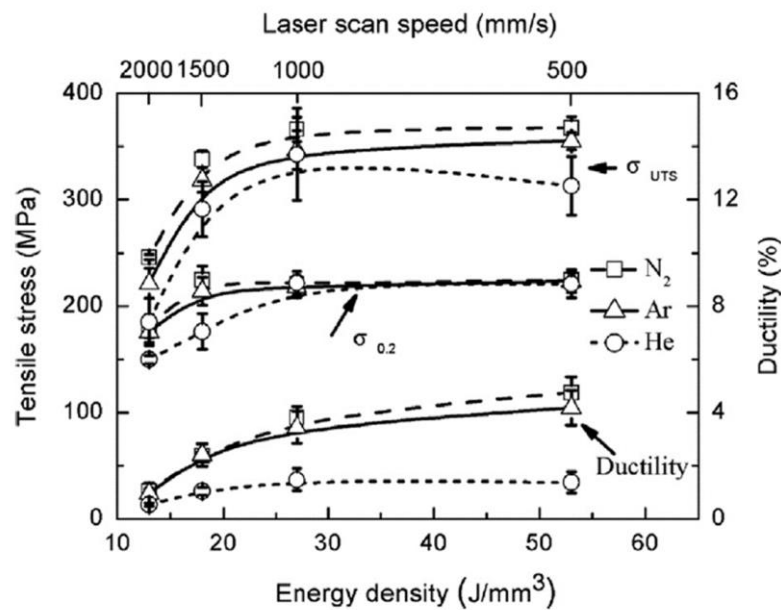
Figure 2-3 Influence in tensile stress and ductility by using different gases in the inert chamber for SLM processing (Olankanmi, 2013)

Pressure: It has been reported that pressure in the chamber has minimum influence on the material properties and parts built. However, increasing the pressure of inert gas within the chamber helps consistently maintain the oxygen level.

Oxygen Level: The presence of oxygen leads to the development of metal oxides at elevated temperatures. This leads to poor component properties and changes the wettability of a melt pool. Therefore, controlling the oxygen level in the chamber is an important factor to monitor. Several factors lead to the presence of oxygen in the chamber such as leaks, poor purity of inert gas or reduction of oxide coating over the powder.

Temperature: The bed temperature aids the process by reducing the heat input required by the laser to fully melt the material and reduces the thermal stress by reducing thermal gradient between layers. Metals at high temperature have high intrinsic absorptance (Poprawe 2011).

2.2.2   Laser

As shown in previous Figure 2-1 a laser irradiates the surface of a powder bed following the information received by the software. During the process the absorbed energy is transformed into heat and dissipates across the entire

powder bed due to the heat transfer properties of the powder bed and material processed.

The key parameters for lasers are explained in this section. Laser parameters are important in controlling the energy density required to melt the metal powder. Different laser systems are installed on machines provided by technology suppliers. The properties of SLM machines are mentioned in Table 2-1.

Table 2-1 Laser systems used in SLM equipment (Author's image)

Process	Product	Developer	Laser	Type of Laser Wavelength
SLM	Realizer 100/250	MTT/ MCP, Germany	20-200W CW	Fibre 1.03 µm
	Lumex 25C	Mastsuura, Japan	500W PW	CO_2 10 µm
	TrumaFoam LF250	Trumpf, Germany	250W CW	Disk Laser
	PM 100/250	Phenix System, France	200/ 50W CW	Fibre 1.03 µm

There are two modes of laser operation generally used within SLM machines, continuous wave and pulsed. Continuous laser mode output is constant due to the continuous excitation of the reactive medium and a pulsed laser emits bursts of energy containing a fixed amount of energy for a specified duration. Continuous wave lasers have two control parameters, laser power and scan speed whereas pulsed modes have at least four, pulse energy, repetition rate, pulse duration and scan speed (Steen et al. 2010). A schematic representation of the two modes are shown in Figure 2-4.
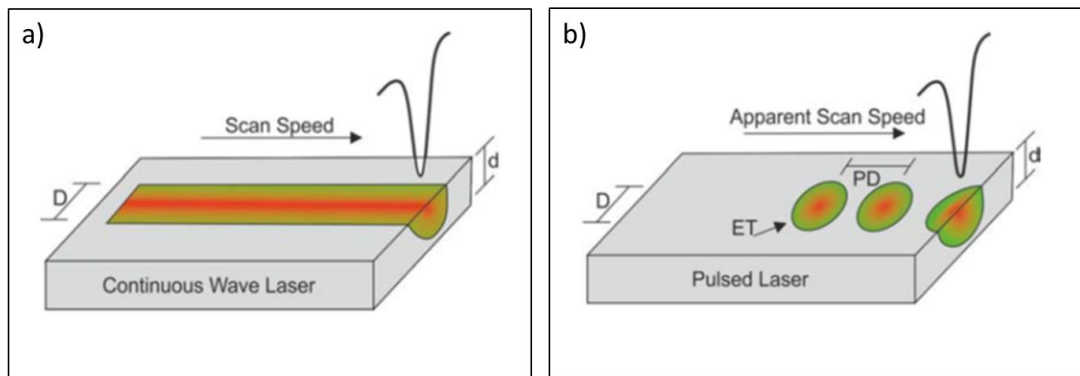
Figure 2-4 Different Lasers used for SLM (a) Continuous Wave Laser and (b) Pulsed Laser. (Adapted from Steen, 2010)

The wavelength (λ, µm) is the wavelength at which the laser energy propagates, it dictates the level of absorption of the laser by the material. The lasers are chosen in conjunction with the material property to absorb the energy emitted.

The intensity profile is the amount of energy added to material. This is an important factor for the SLM process. The factors on which intensity of laser profile depends are laser power, beam quality, frequency, and spot size.

2.2.3 Powder

Knowledge of material properties and effects on the process window is required for successful SLM processing. Some of the material properties that should be considered before processing includes: Particle size distribution (PSD), bulk density (ρ_b), melting temperature (T_m), boiling temperature (T_b), etc. (Rehme and Emmelmann 2006). However the powder should be testing inside the processing chamber using the recoater to test the flowability, the powder should spread uniformly without leaving any lumps.

The morphology is the physical shape of powder particles. Powder particles spherical in shape are ideal for SLM process and are generally produced using gas atomisation. Spherical shaped particles display good flowing properties and higher compaction ability with increased packing density (Das 1998; Karapatis et al. 2002). Figure 2-5 shows a typical spherical shape morphology used for SLM processing with an average particle size range of 15-63 µm.
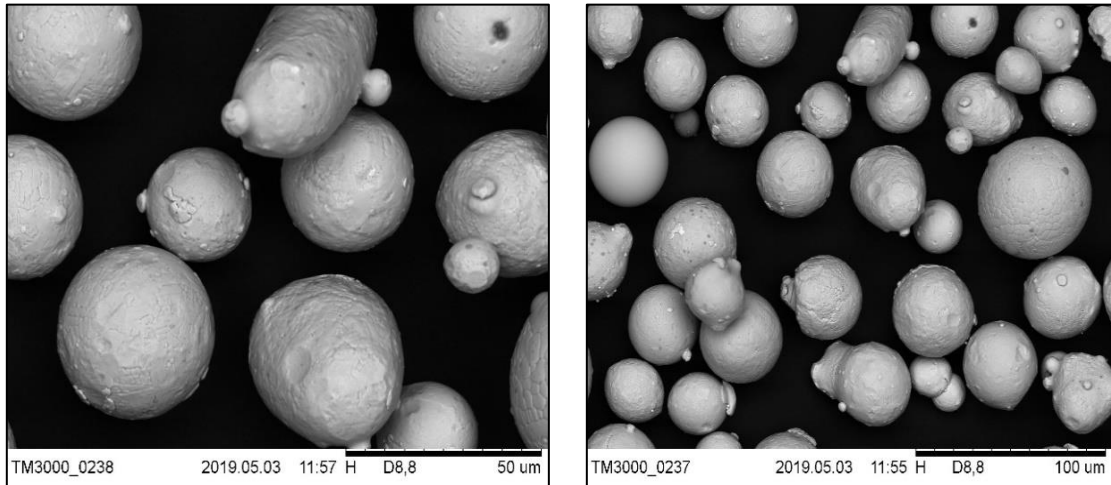
Figure 2-5 SEM image of Stainless Steel 316 L spherical-shaped powder morphology at different magnifications (author's Image)

Particle size distribution (PSD) is the distribution of particle size at given diameters. Selecting and optimum range of PSD is essential to identify prior processing. Having a wide range of PSD can be beneficial in improving bulk density (Mumtaz 2008) or may lead to increase porosity due to improper melting (Morgan et al. 2004). However using a narrow PSD range can improve the packing of particles but can also lead to additional cost of manufacturing and can also lead to powder agglomeration (Boivie 2001).

Bulk density determines the mass per unit volume. The volume includes particle volume, inter-particle void volume and internal pore volume (Lyon et al. 1947). The indication of compaction required for dense parts is obtained in comparison to density of powder bed (ρ_p, kg/m^3) (Van Elsen et al. 2007).

Thermal conductivity varies with temperature. This property shows the materials ability to conduct heat and affect the heat balance (Mumtaz 2008).

Specific heat capacity is the heat energy required to increase the temperature of a unit quantity of a material by unit temperature. C_p affects the heat balance.

Latent heat of fusion is the amount of energy required to change the state of a solid material to a liquid. The amount of energy required to change the state of a liquid to gas is known as the latent heat of vaporisation (L_v, J/kg).

Melting temperature is the temperature at which the material will transform into liquid state.

Evaporation Temperature is the temperature at which a material will transform into a vapour.

Dynamic viscosity is the resistance to flow encountered when one layer or plane of fluid attempts to move over another identical layer or plane of fluid at a given speed. Dynamic viscosity is also called absolute viscosity (Bansal 2005).

Surface free energy it measures the disruption of chemical bonds when a surface is transformed (Van Elsen et al. 2007).

Absorbance is defined as the ratio between absorbed energy and reflect transmitted energy.

2.2.4   Melt pool Dynamics

During SLM a laser melts material creating a melt pool under controlled atmosphere. The fluid behaviour of a melt pool is important in understanding resultant surface profile and final density of the material. The following sections will explain the factors affecting melt pool capillary instabilities and thermocapillary effects within a melt pool.

2.2.4.1 Wetting

The wetting of the melt material affects interlayer connections, porosity and strength of parts produced by SLM (Mumtaz 2008, Singheiser et al. 2001, Steen et al. 2010). Wetting behaviour determines the spreading of melted material over underlying surfaces. Excessive wetting leads to uncontrolled melt pool and poor wetting leading to breakage of the melt pool into cylindrical

or spherical segments due to variation in surface tension. The wetting behaviour explained by Eustathopoulos represents surface free energy at interfaces of liquid, vapour and solids respectively (Eustathopoulos et al. 1999). Consider a flat, solid, smooth, and non-reactive surface in contact with a liquid in presences of a vapour phase (see Figure 2-6). The liquid will intersect the solid surface at a contact angle θ and is governed by Young's equation.

$$Cos\theta = \frac{\gamma_{SV} - \gamma_{LS}}{\gamma_{LV}} \qquad \qquad \textit{Equation 2-1}$$
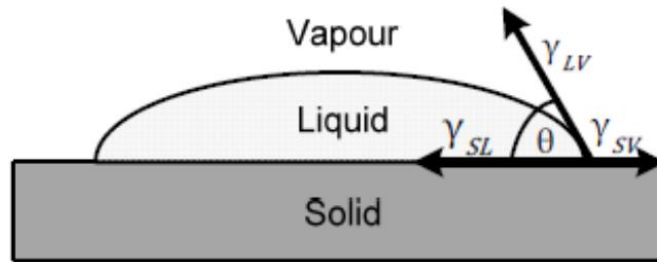
Figure 2-6 Three Phase equilibrium diagram and equation for wetting of a liquid on underlying solid (adapted from Eustathopoulos et al. 1999)

$\gamma_{LV}, \gamma_{SV}, \gamma_{LS}$ represent surface energy at the liquid-vapour, solid-vapour, and liquid solid interfaces respectively it can be observed from the Figure 2-6, better wetting is obtained with reduced θ. θ will be smaller than 90° if $\gamma_{LV} <$ γ_{SV}- γ_{LS}. With melting of same material over as the solid, θ would be close to zero (Eustathopoulos et al. 1999). This phenomenon is usually true with SLM and is known as homologous wetting. This is in good agreement with the

results for experiments conducted by Eustathopoulos (Eustathopoulos N. et al. 1999). Liquid metals generally exhibit poor wetting on a solid with an oxide film. This is true due to lower surface energy of metal oxides than the corresponding liquid-vapour surface free energy leading to higher angle of contact therefore, leading to balling effect (Das 1998). Figure 2-7 shows effects of poor wetting of a laser scanned track of steel powder.
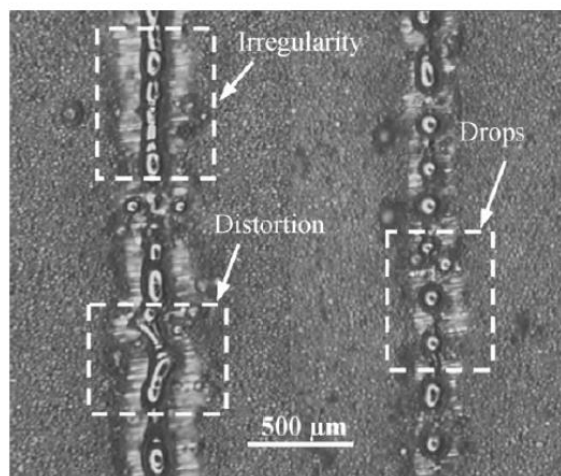
Figure 2-7 Poor wetting behavior causing breaking of laser scanned steel tracks (Yadroitsev et al. 2010)

The surface tension is a function of temperature. Kruth reported that as temperature increases γ_{LV} reduces, improving the wetting behaviour. Therefore, sufficient time must be given for the melt pool to achieve good wetting (Kruth et al. 2004).

A general practice used in soldering to improve the wetting of solder is to introduce in-situ deoxidiser or fluxing agent in solder. The same can be applied in SLM. This will improve spreading of liquid over solid and reduce the wetting (Agarwala et al. 1995). Studies undertaken have reported increased in recoil pressure by high laser peak powers exert a pressure on the melt pool reducing the contact angle made between liquid and substrate (Fischer et al. 2003, Morgan et al. 2004, Mumtaz 2008).

2.2.4.2 Capillary instabilities

The capillary effect causes the liquid to flow against the flow of gravity because of intermolecular forces. These intermolecular forces exist between the different states of masses are known as surface tension. The breakup of liquid into small entities in an attempt to reduce surface free energy/surface tension is related to capillary instability.

This phenomenon has a great impact on the SLM process as there are elongated melt pools in the direction of the laser path due to the heat input by the laser. In SLM this is known as balling and related to Plateau-Rayleigh instabilities (Mumtaz 2008). These small entities break into cylindrical or spherical shapes. Kruth reported that melt pool breaks when the surface tension of the pool increases. In order to avoid balling, the melt pool should be as small as

possible. Surface tension is a function of temperature (Kruth et al. 2004). Temperature variation in the melt pool causes a variation in surface tension and leads to breaking into smaller entities. Due to the temperature gradient at the edges of the melt pool, balling formation at the edges is often seen. The small entities may hinder the SLM process by increased part porosity, hamper the layer deposition and create improper interlayer connections (Fuh et al. 1995, Hauser 2003, Kruth et al. 2004). The spheres often scatter around the crystallised track/layer on the edges due to improper wetting of substrate (O'neill et al. 1998) causing vertical side roughness.

2.2.4.3 Thermocapillary flows

Density and surface tension of fluid both cause the convective fluid flow due to temperature variations. Laser energy melts the solid powder into a liquid state and when the laser has passed, the liquid rapidly solidifies. This process generates capillary instabilities in the fluid causing convective flows. These flows are known as Magrangoni flow and can affect the melt pool shape affecting part properties.

The variation of temperature along the melt pool in SLM induces a similar effect on the surface tension resulting low to high surface tension convective

flow called Marangoni flow. The strength of the flow can be determined by a dimensionless Marangoni number (M_a).

$$M_a = \frac{d\gamma_{LV}}{dT}\frac{dT}{ds}\frac{L}{2n\delta} \qquad\qquad \textbf{\textit{Equation 2-2}}$$

With $\frac{d\gamma_{LV}}{dT}$ the surface tension gradient, $\frac{dT}{ds}$ the thermal gradient, L the length of the melt pool, η is the viscosity and δ the thermal diffusivity.

Figure 2-8 (a) (b) illustrates a negative and positive Marangoni convection flows in a melt pool. Surface tension γ is a function of temperature, with increase in temperature the surface tension decreases. The thermal gradient (at point A, B & C) in the melt pool causes the surface tension variation as shown in Figure 2-8 [**a**: negative and **b**: positive surface tension gradient] an outward flow away from the centre (Beer S. Z. 1972) and vice versa.
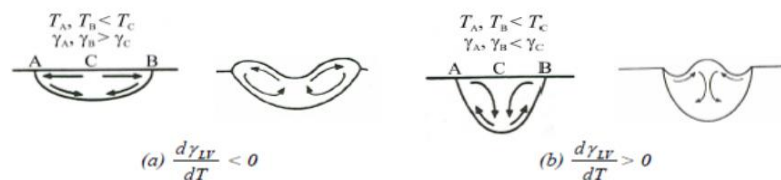
[**a**: negative and **b**: positive surface tension gradient]

Figure 2-8 Schematic of Marangoni convection flow due to thermal gradient (Mills et al. 1998)

2.2.5 Problems associated with SLM processing

Recent efforts in SLM research have helped improve its capabilities however; there still exists several issues leading to the production of poor quality parts. Studies have improved the understanding of the process by identifying the source of defects for various materials. Most commonly observed issues are warping, agglomeration, ball formation of melted material, rough surface finish, porosity etc.

The processing chamber for SLM is isolated and the process is done in presence of non-reactive gas. Often while processing, pores can form within parts, these can be formed due to gases being trapped due to the fast solidification of molten material (Fast J. D. 1965). These are caused due chemical reaction or decrease in the solubility of the dissolved elements in the molten pool during cooling and solidification.

Bubble formation is often observed when gases like nitrogen, oxygen or hydrogen is dissolved in the melt pool at high temperatures (Debroy et al. 1995, Fujii et al. 2004). Internal gas in SLM can also form due to the reaction of material elements reacting with chamber inert gas or the vapours of metals caused due to excessive energy. Kruth observed internal pores due to release of trapped gases in the micrograph of SLM iron parts (Kruth et al. 2004).

Partial melting of powder is one the issues observed in SLM. The laser beam is focused on the material spread over the substrate or previously consolidated material and scans the layer profile. It has been observed that insufficient energy to powder particles cause material to be partially melted. Morgan reported a wide particle size distribution within a batch of materials led to partial melting of larger particles while small particles are vaporised (Morgan et al. 2004). Experimental work done by Simchi reported thicker layers caused the density of part to be reduced due to improper melting. The laser energy was insufficient to penetrate the layer for full melting (Simchi et al. 2003).

2.2.5.1 Residual Stress

Residual stress can be simply as internal stresses, which exist within a part without any applied force or constraint. They are strongly associated with processing, and it has been said that every production process will introduce some amount of residual (Mercelis and Kruth, 2006). As their presence is inevitable, residual stress reduction has become the focus of many investigations.

Laser based processes such as SLM are known to introduce large amounts of residual stress, due to the large thermal gradients, which are inherently present in the processes (Chou 2013). Mercelis and Kruth describe two mechanisms

that cause residual stress during SLM process, the first mechanism introducing residual stress is called the Temperature Gradient Mechanism (TGM) (Mercelis and Kruth 2006), shown in Figure 2-9. It results from the large thermal gradients that occur around the laser spot. The TGM mechanism is commonly used for laser bending of sheets along straight lines. Owing to the rapid heating of the upper surface by the laser beam and the rather slow heat conduction, a steep temperature gradient develops. The material strength simultaneously reduces due to the temperature rise. Since the expansion of the heated top layer is restricted by the underlying material, elastic compressive strains are induced.

A second mechanism that induces residual stresses is the cool-down phase of the molten top layers which tend to shrink due to the thermal contraction. This deformation is again inhibited by the underlying material, thus introducing tensile stress in the added top layer and compressive stress below (Popovich et al. 2016).
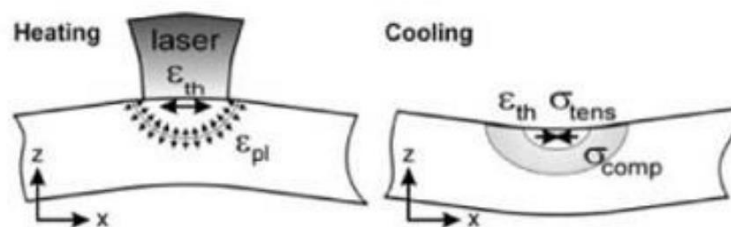
Figure 2-9 Representation of TGM, with thermal strain εth, plastic strain εpl, tensile stress σtens and compressive stress σcomp – (Mercelis and Kruth 2006)

2.2.5.2 Porosity

Porosity in additive manufactured parts is defined by the total void volume over the total solid volume within the produced part and is expressed in % of volume, nevertheless is common for researchers to quote a samples in % density (Kgm-3); the reason is because the voids are features resulting of processing rather than a particular property of the material considered as macroscopic internal defect and is been listed as one of the main reasons that influence the mechanical performance of the material (Louvis et al. 2011).

The achievement of full density for SLM materials is considered the first step before to proceed with mechanical testing and further investigations. Porosity has been the focus for many of the initial research for SLM alloys (Olakanmi 2013). It has been found that porosity in SLM occurs due to several reasons: insufficient or incomplete melting (lack of fusion), insufficient dissipation of laser energy, vapourisation, oxide inclusions, trapped gas, and balling (Olakanmi 2013). Figure 2-10 shows the evolution of voids of SLM aluminium alloyAlSi10Mg using different processing parameters.
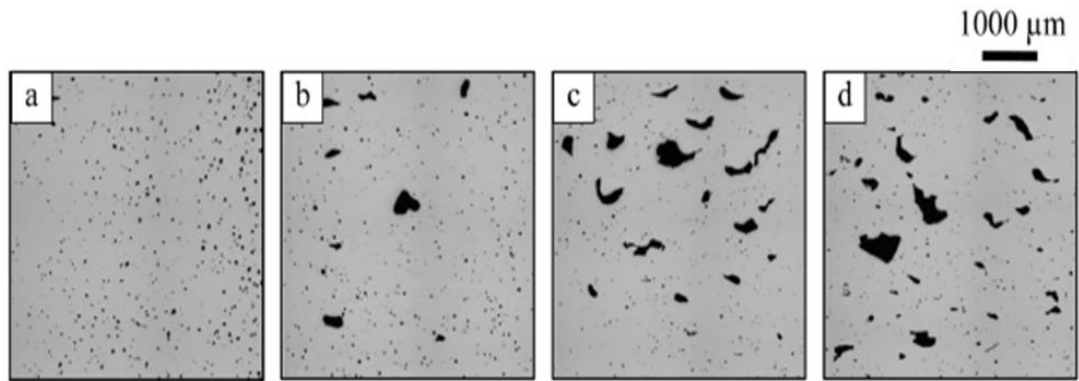
Figure 2-10 Evolution of voids at different scanning processing: (a) 250 mm/s, (b) 500 mm/s, (c) 750 mm/s, and (d) 1000 mm/s. (Nesma et al. 2014)

2.2.5.3 Balling

The balling effect is a complex physical metallurgical process often seen in SLM. Balling affects the deposition of the new layer as entities may rise above the present layer and will obstruct the hopper/coater. Balling can lead to production of porous parts and irregular surface finish (Rombouts et al. 2006). Figure 2-11 shows the balling effects on stainless steel processed by SLM.

Several studies have shown different reason for balling effect. Studies undertaken by researchers Simchi (Simchi et al. 2003) and Tolochko (Tolochko et al. 2004) concluded that high scan speed leads to the balling effect due the insufficient energy input to penetrate and melt the powder. Balling is

also caused due to high surface tension in melt pool leading to poor wetting of substrate (Rombouts et al. 2006).
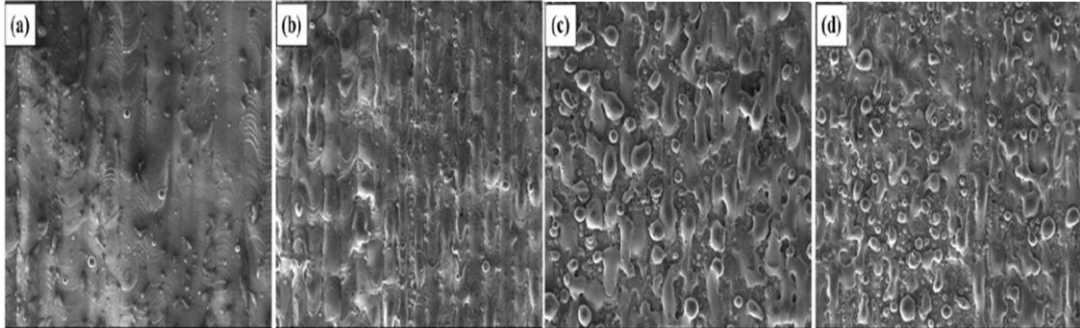
Figure 2-11 Stainless Steel 316L processed samples showing the balling characteristics of SLM layers under different scan speeds: (a) 50 mm/s (b) 400 mm/s (c) 600 mm/s (d) 800 mm/s (Li et al. 2012)

2.2.5.4 Vaporization

High levels of intermolecular kinetic energy causes the liquid to evaporate (Sze 2009). The molecules of a liquid material in the melt pool energised by input of high laser energy causes evaporation. Phase change can cause differences in the chemical composition of the material pre-processing and post-processing under a laser.

Several studies reported that vapours from the vaporisation exert an increased pressure on the melt pool and cause laser irradiation of metals. A plasma plume

can be created due to interaction of the vapours with inward gas particles from the laser affecting the concentration and amount of heat supplied to powder bed (Rombouts et al. 2006).

The dispersed heat due to vapour interaction can generate an internal disturbance wave that moves in radial axis outward from the melt pool. The increase in pressure exerts a recoil pressure on the melt pool (Morgan et al. 2004). Recoil pressure may result in improved part density (Kruth et al. 2004, O'neill et al. 1998), initiate melt pool ejection (Allmen et al. 2002, Fujinaga et al. 2000) improve wetting behaviour of melt pool and can also blow the powder away from the laser-material interaction zone (Mumtaz 2008).

The melt pool ejection due to high recoil pressure is often known as spatter. The force generated by recoil pressure acts like a piston on the melt pool and causing the liquid out (Allmen et al. 2002). Reducing the recoil pressure can reduce the spatter from the melt pool. The recoil pressure can be reduced by suppression of plasma plume. Rombouts suggested the radial pressure gradient must overcome the surface tension force to determine threshold value for avoiding spatter (Rombouts et al. 2006).

The vaporisation of material then leads to spatter formation can be disadvantageous to SLM. Figure 2-12 shows the formation mechanics of

spatter. The spatter forms contamination on the powder bed and cause problems in deposition of powder and may affect the laser beam delivery by solidify directly below the laser trajectory (Mumtaz 2008).
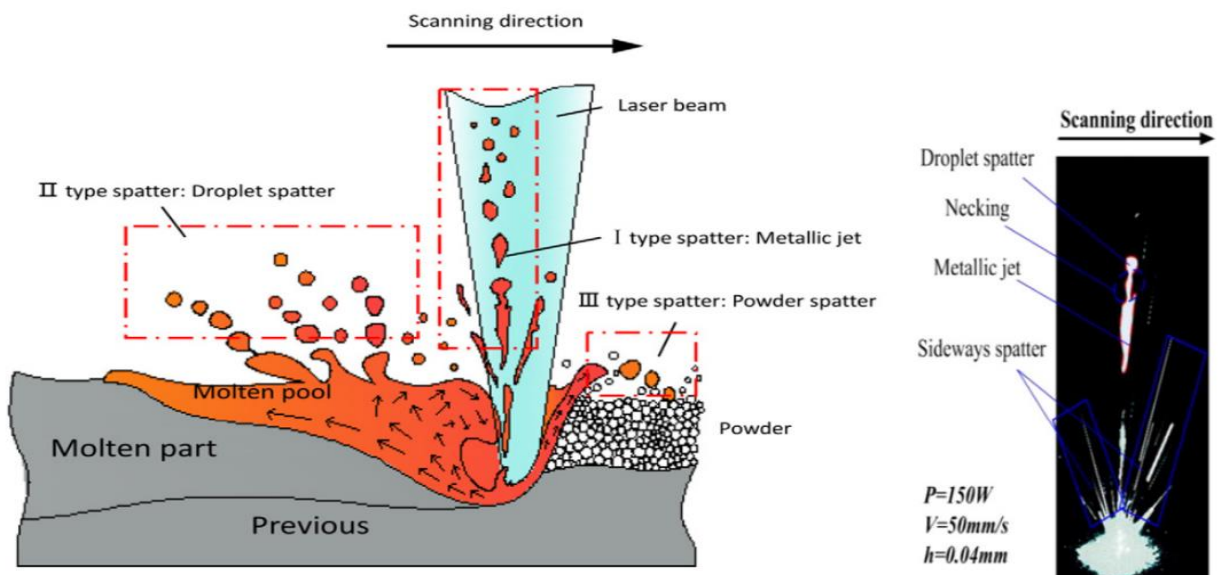
Figure 2-12 Spatter formation mechanisms during SLM processing. Main different types of spatter (Left), spatter behavior during processing (Right) (Wang et al. 2017)

2.2.5.5 Cracking

Micro or macro cracking in SLM parts reduces the densification level and may contribute in potential failures during mechanical performance. It is also known as process induced cracking. For SLM materials, Ni-based superalloys

are characterized by high crack susceptibility and is practically impossible for this alloys not exhibits internal cracking after processing (Marchese et al. 2017).

Findings by Harrison suggested that micro cracking in SLM Ni alloys occurs when internal stress concentration during processing surpass the ultimate tensile stress (UTS) of the material at a precise period and temperature (Harrison et al. 2015). Figure 2-13 shows a micro cracking observed in Hastelloy-X processed by SLM. A key observation in Figure 2-13 (c) is possible to observe that the cracks initiate from internal voids, (Fabregue at al. 2008) demonstrated similar observations.
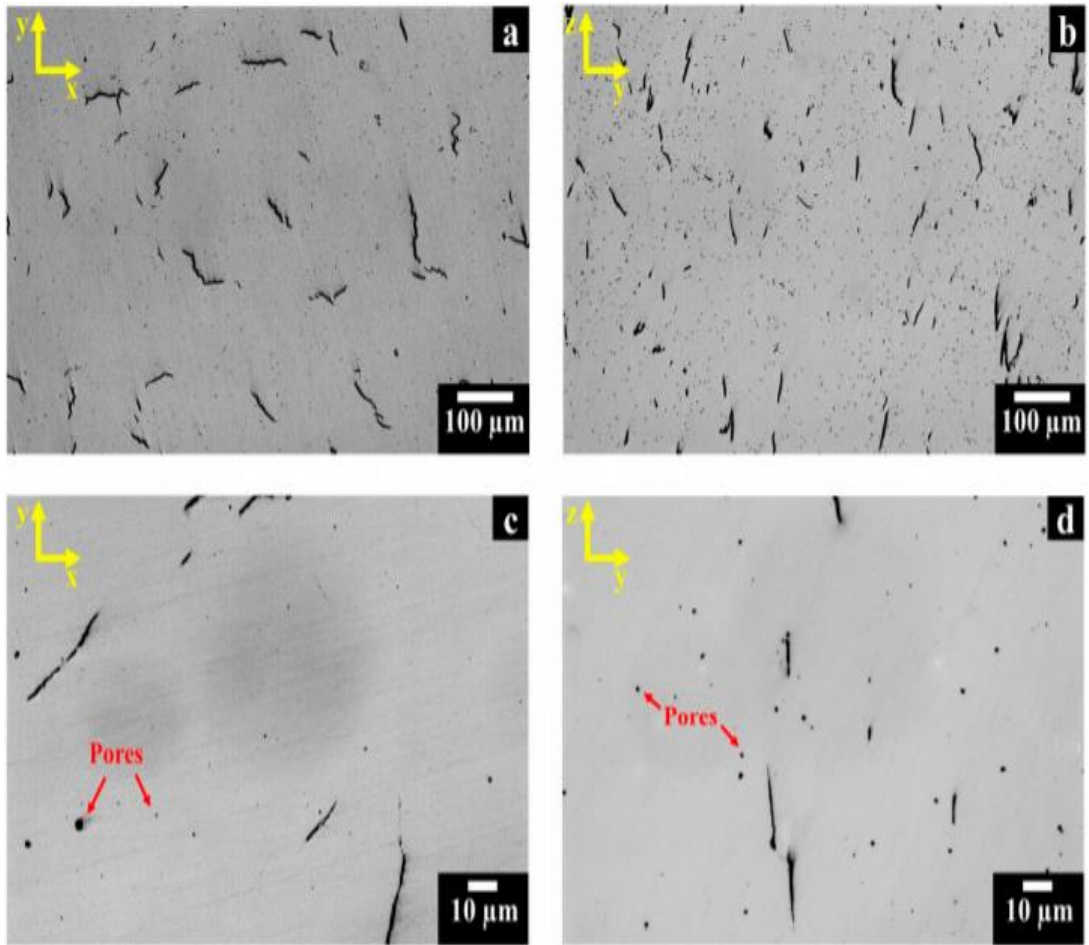
Figure 2-13 Optical micrograph of Hastelloy-X processed by SLM showing micro cracking along different planes at different magnifications. (Marchese et al. 2017).

2.2.6 Controllable parameters

The above-mentioned factors affect selection of process parameters. Processing parameters are the values selected for various functions of the machine to control consolidation and produce a 3D component and represented in Figure 2-14.

Energy density is the energy supplied by a laser per unit area is called the energy density. Sufficient energy density facilitates complete melting of material, higher or lower amount degrades or partially melts the powder.

$$ED = \frac{P_L}{V * Ss * L}$$

Scan spacing or hatch spacing is the distance between the two laser scans. To melt the material fully, the spacing between two scans should be small enough to form an overlap. However too small a spacing increases processing time and may induce material vaporisation.

Scan Speed is the speed at which laser travels across the powder bed. The lower the speed the higher will be the power supplied to the material.

Laser Power is the energy supplied by the laser with respect to time.

Bed Temperature is the preheating of powder reduces the energy required to melt material and reduces the thermal stress induced in component.

Layer Thickness is thickness of material spread over the substrate or consolidated material. Thinner layers can provide better accuracy and minimise the staircase effect. Thinner layer thicknesses can increase processing time.
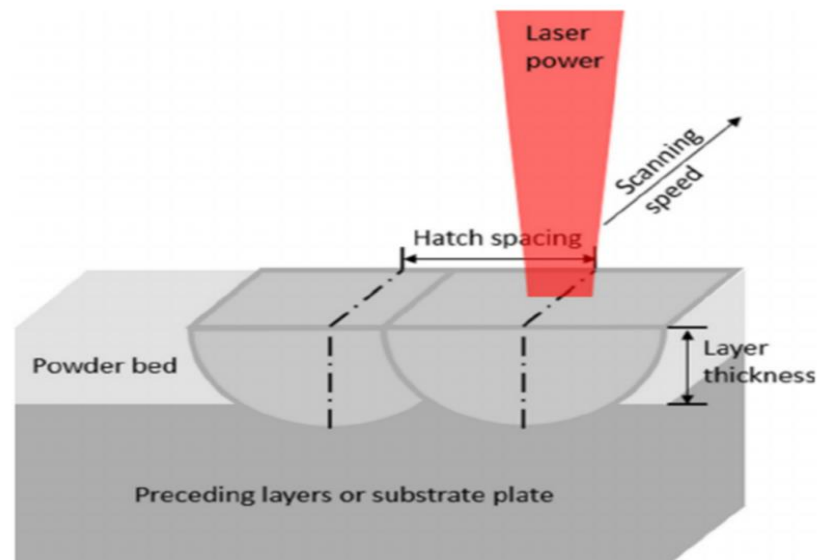
Figure 2-14 Schematic illustration of SLM standard process parameters:

Laser power, hatch spacing, scanning speed laser thickness. (Yap et al. 2015)

2.3 Solidification in SLM

This section details theory and literature of the phenomena of controlled solidification, microstructure growth in general processing and specific to laser process. Followed by a brief description and interpretation of analysis of

microstructure that is often used to understand the effect of processing condition on performance and mechanical properties of SLMed parts.

2.3.1   Metal phase transformation

Metal phase transformation is a key phenomenon to understand in material processing. In traditional and advanced manufacturing processes such as casting, forging, hot rolling, AM and other similar processes; the material is processed by addition of heat inducing a phase transformation in the material that allows shaping the material easy and thus evolve desirable microstructures by controlled cooling.

Phase transformation of a material can involve transformation into solid, semi-solid or liquid phase by the method of addition or subtraction of heat energy. These phase transformations have been an important process in metallic materials and has been subjected to extensive research. As a metal is heated the solid material begins to soften and eventually melts if heat input is continued above the critical point of melting temperature thus making processing easier.

The heat input excites the molecules of the material; reducing contact bond energy at molecular level thus making it soft. This makes the shaping of metals easier. In mechanics of material the mentioned phenomenon can be expressed

as decreasing viscosity of material effectively reducing shear stress by heat input.

2.3.2 Controlled solidification

A controlled solidification is a process of phase transformation that converts liquid or semi-solid state to complete solid state in a controlled technique. Normally in metal processing, as material is melted, a decrease in viscosity is observed in large magnitudes. This helps in processing materials with greater ease. Thus, theory of solidification is an influential factor on microstructure and improving properties of final product. Controlled cooling rate can be characterised as slow, moderate and rapid cooling. Slow cooling rate and large solidification time can lead to coarse microstructure. These structures are often found to have poor mechanical properties. On the other hand, rapid cooling leads to growth of refined microstructure with tighter packing resulting in high strength.

In solidification, the heat energy from the thermodynamic body at high temperature is extracted by introducing a thermodynamic heat sink which changes the energy phases.

The heat sink creates a heat flux by applying cooling to the melt, decreasing the enthalpy, resulting in cooling rate $\dot{T}$ expressed by dT/dt. This process of solidification is governed by an elementary thermodynamic equation of heat transfer. Adding constraints and boundary conditions depending to the application and processes the equation can be modified to calculate precise cooling rates for a given location (z) and time (t). (Kurz and Fisher 1992).

$$\dot{T} = \frac{dT}{dt} = \frac{dT}{dz\prime} \cdot \frac{dz\prime}{dt} = G.V \qquad\qquad \textbf{\textit{Equation 2-4}}$$

Where $\dot{T}$ is the cooling rate, dT/dz' is the temperature gradient G, and dz'/dt is the grow rate of solidification rate V. Benefits in casting process such as better control of properties, absence of macro segregation and more uniform microstructure could achieve by controlling G and V.

2.3.3 Microstructure growth

A metallic microstructure comprise of dendrites, eutectics or combinations of both. The type of microstructure depends on conditions such as solidification rate, alloy composition, processing method etc.

The solidification microstructures of a pure metal or an alloy can be divided into single phase primary crystals and polyphase structures. The single phase primary structures are tree like primary crystal known as dendrites. The polyphase structures are laminar structures generally found for eutectic structures. Such growths have been studied for manufacturing processes such as casting, forging, welding etc. In these processes the material processed typically is in contact with a planar surface i.e. the walls of the mould, die/ punch, or edge of the joint. These site acts as point of nucleation for microstructural growth. Figure 2-15 shows a typical casting where are three distinguished regions during any solidification, solid, solid-liquid (mushy), and liquid.
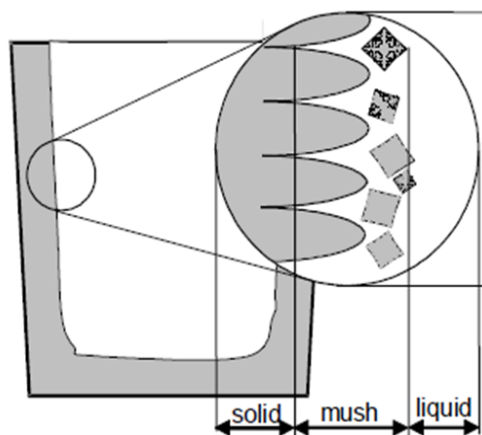
Figure 2-15 Solidification in conventional casting (adapted from Stefanescu 2009)

The solidified material advances inwards from the mould walls and several nucleation sites are form. These grains thus form a constrained columnar structure as seen in Figure 2-16a.

The growth direction for columnar grains is opposite to the heat flux applied/ induced (along the direction of the thermal gradient). In addition often other equiaxed grain regions are formed in the central region of the casting -see Figure 2-16b.

These are fine detached dendrites arm that grow within the remaining undercooled liquid and are characterized by having similar size in all direction. It is possible to obtain a fully equiaxed microstructure during the solidification by adding external nucleation agents enhancing the isotropic properties of the material as seen in figure 2-16c.
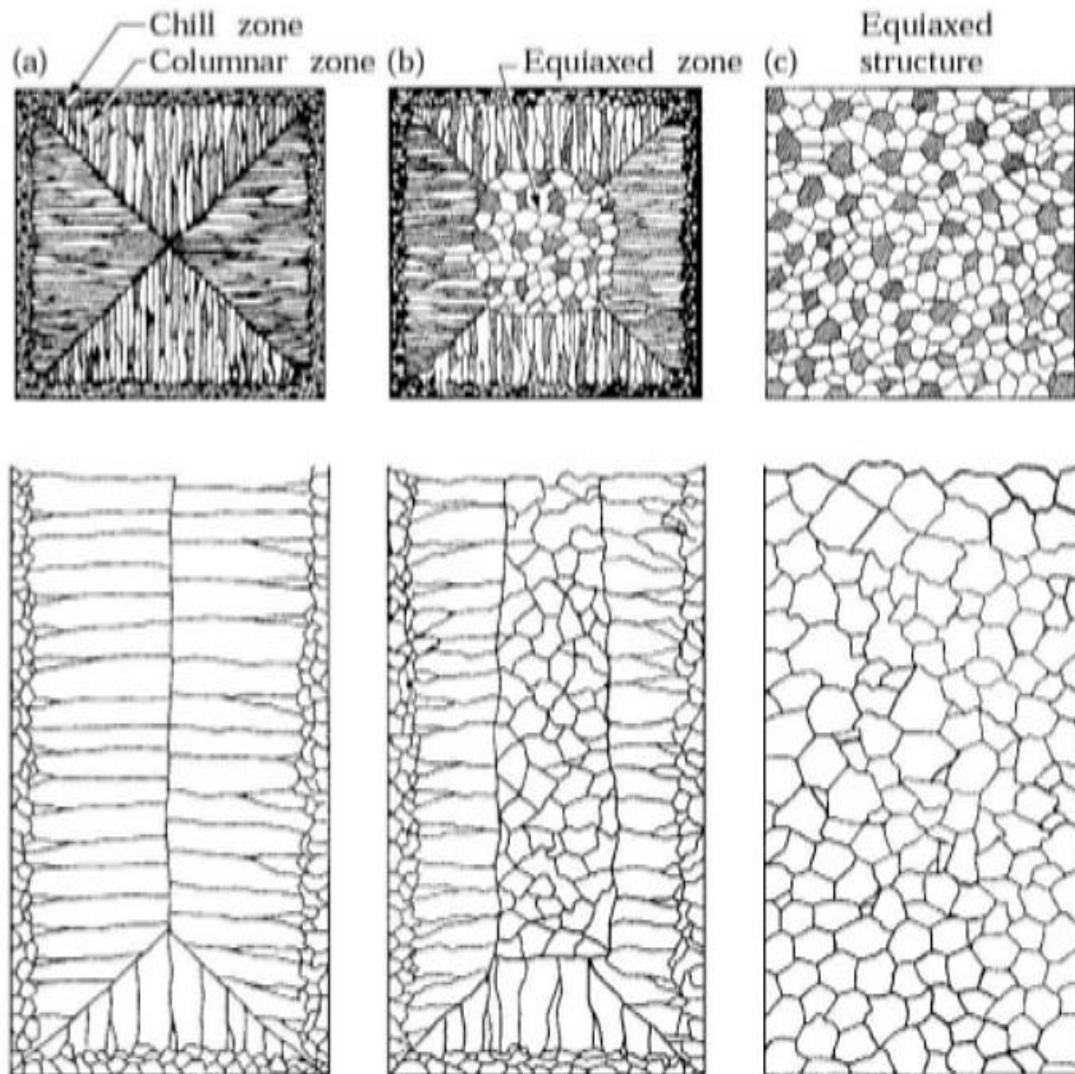
Figure 2-16 Characteristic grain structure in solidification for metals in a square mould: (a) pure metal (b) solid-solution alloys (c) structure obtained by heterogeneous nucleation of grains using nucleating agents. (Cibula et al. 1949)

The columnar structures rapidly grow and form dendrites. These structures have constrained growth, as in case of directional solidification as seen in Figure 2-17. The dendrites are typically arranged with the primary trunk

45

parallel to each other. The space between the primary dendrites is a function of solidification conditions and is called as Primary Dendrite Arm Spacing (λ_1). The primary dendrite arm branch out to secondary arms that grow perpendicular to each other. The spacing between the secondary arms is referred as Secondary Arm Spacing (λ_2) as seen in Figure 2-17. The spacing values are generally used to calculate the cooling rate of the material (Davies 1980).
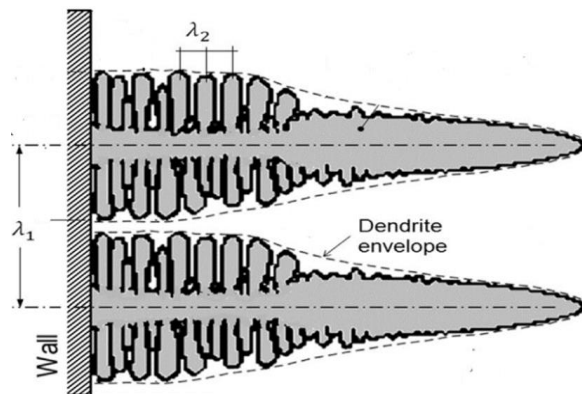
Figure 2-17 Primary and secondary spacing of dendritic structures.

(Ahmadein 2014)

2.3.4   Rapid solidification

Rapid Solidification Processing (RSP) as the name suggest, involves rapid heat extraction/ high cooling rates to produce a faster solidification ($V>1$cm/s) during the transition from high temperature liquid state to room temperature.

Extreme cooling rates greater than 10^4 K/s (i.e from 1400 °C to less than 380 °C in 10^{-3} seconds) are considered for RSP such as Powder atomization, Melt Spinning, Laser Surface Melting. The current nucleation models presented are not affected by RSP only the growth is considered due the fact that rapid heat extraction allows less time for the coarsening of morphological features during the solidification growth process *(Ahmadein 2014).*

The G-V diagram shown in Figure 2-18 shows the development of morphological features during RSP regarding the changes between the temperature gradient G at the solid-liquid interface and the rate of solidification V of the solid-liquid interface.
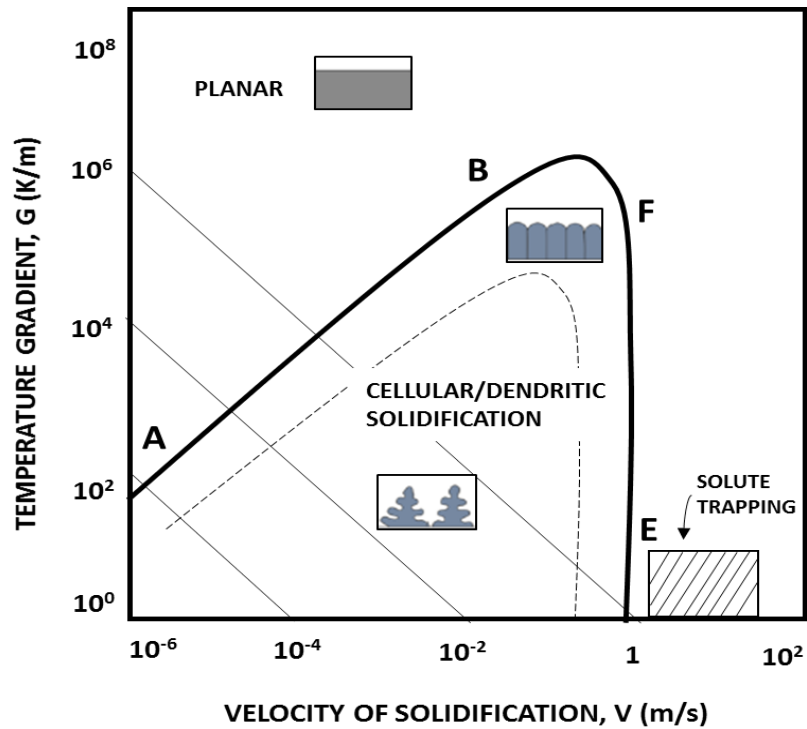
Figure 2-18 Schematic of G vs V showing different morphologies for solidification (Adapted from Ahmadein 2014).

For non-supercooling conditions, the slope of the line AB represent the function of G, and V and is expressed by the following equation:

$$\frac{G}{V} = \frac{m_L C_0 \left(k_E - 1\right)}{D_L k_E}$$ *Equation 2-5*

Where C_0 is the solute concentration in the liquid, D_L, is the Diffusivity of solute in liquid, k_E, is the equilibrium partition ratio, m_L, is the slope of liquidus line. If $\frac{G}{V}$ is greater than the right hand of equation the interface

48

advances on a planar front while the solid phase is under extraction of heat conditions, as result there will be not micro-segregation of solute atoms. If $\frac{G}{V}$ is less, than the right hand of equation, a transition from planar to cellular/dendritic morphology occurs due C_0 is steep enough to induce morphological instability and this leads to cellular or dendritic growth with solute enriched micro-segregations.

For RSP conditions, the equation for the function of G and V should be modified to include very rapid solidification rates:

$$V = \frac{m_L D_L \left(k_E - 1\right) C_0}{K_{E2}\, T_M\, \Gamma} \qquad \textbf{\textit{Equation 2-6}}$$

Where T_M is the melting temperature of the interface without solute and Γ is the ratio of solid/liquid surface energy to the latent heat of fusion per unit volume. If, V is sufficiently large, beyond EF line, the instability is re-established and creates a transition from cellular to planar morphology, which is independent of the imposed temperature gradient. As V advances and reach the limiting interfacial velocity EF the potential perturbations in the growth front turn finer due the influence of surface tension establishing a planar interface (Glicksman 2011). The microstructures under RSP conditions can be predicted using *G-V* diagrams if the values for solidification growth velocity and temperature gradient are known.

RSP leads to high interfacial velocities and, in turn, to solute trapping in the advancing solid-liquid interface and incorporated into solid, as result of this, the solidi-liquid interface is no longer in equilibrium due insufficient time of solute and solvent atoms to diffuse and maintain local equilibrium. The diffusive speed is given by Di/λ; where Di is the solute diffusion coefficient at the interface and λ is the inter-atomic distance (Aziz and Kaplan 1988).

There are two models for solute trapping formulated by Michael Aziz to redistribution of solute atoms during RPS, the two mechanisms are known as: stepwise growth and continuous growth (Aziz and Kaplan 1988). In stepwise model the growth occurs by rapid lateral steps of height λ, then the average time between each step is $\tau = \lambda/V$. The solute is trapped in the solid monolayer interface if the solute atoms does not diffuse back into the liquid during the interval time τ. For continuous growth model the solute atom is being dragged towards its lattice space during the interval time τ, this model has been successfully proved to capture the phenomenology of most RSP effects over stepwise model.

2.3.5   Laser processed microstructure growth

In recent times, laser processing has been often employed in many advanced manufacturing technologies. Commonly used for joining, cutting, surface re-melting, and recently widely used for adding materials in some additive manufacturing processes. The laser beams scan the desired area and the high energy melts the material fusing in welding, additive manufacturing, or surface re-melting. The opposite is true with cutting process; no material fusing takes place.

This section will provide a brief understanding of laser processed microstructure obtained from a material processed under laser. The laser processing method is often considered as rapid solidification processing. The rapid solidification normally takes place either when a material had controlled solidification with lack of heterogeneous nucleation sites or quenching or with moving energy sources. Unless controlled cooling rate is applied, the microstructure obtained by laser processed is similar to a rapid undercooled structure i.e. solid solution with fine precipitated elements.

In contrast to a static casting process, the solidification process occurs in series of small pockets behind the laser. The high energy creates a melt pool that solidifies rapidly. However, there is a difference observed in the cooling rate

of the melt pool. This has been studied using several mathematical simulation models. However due to high complexity most of the simulations are often based on few assumptions (Gremaud et al. 1990).

As described in section 2.3.4 the variation in cooling rate results in range microstructural features. For example, in solidified weld joint, a columnar structure is observed close to the base metal and an equiaxed dendrite often found at the centre of the weld joint as shown in Figure 2-19. The solidification is a function of weld speed, the energy input, weld pool shape, the material thickness.
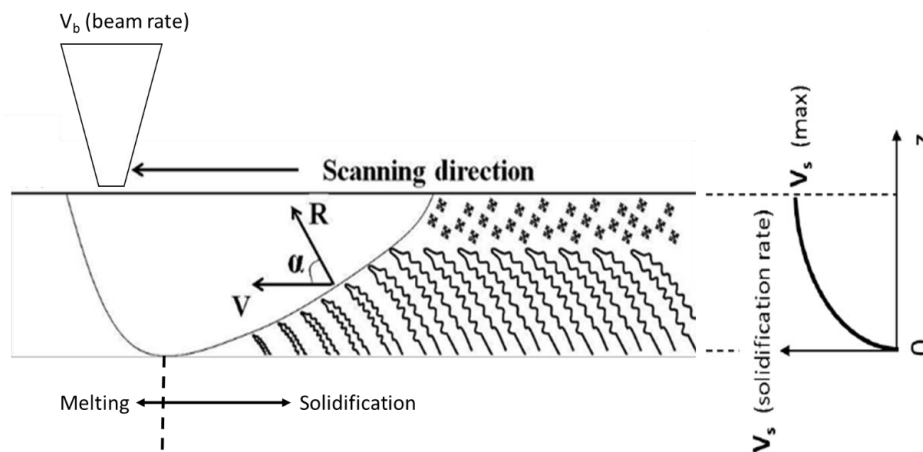
Figure 2-19 Solidification of SLM with a moving laser source. (Adapted from Gremaud et al. 1990)

The Solidification velocity *Vs* increases rapidly from zero at the base of the melt pool to *Vb* (beam velocity) at the surface via the relationship $V = R \cdot cos\theta$, where θ is the angle between the velocities (Gremaud et al. 1990).

2.4   Research in Selective Laser Melting

The effects of process parameters, development of new commercial materials, opportunities of laser melting for different applications and modelling laser melting process using tools such as FEA, dimensionless equations, etc. have been undertaken by various researchers. Hauser studied the geometries resulting from the different processing parameters and scanning strategies similar used by Kruth to study the thermal stress effects (Hauser 2003 , Kruth et al. 2004). Hauser reported different scan speed resulted in changes of laser absorptivity of materials affecting melt pool dynamics of stainless steel (Hauser 2003).

The physical phenomenon such as wettability, evaporation of melt pool, instability and cracking of consolidated material was studied and effects of varying machine parameters to obtain the highest possible density was studied by Das and Over C. (Das 2003, Over 2003).

Several new materials have been studied for use within AM. SLM is capable of using different powder systems such as single component powder, pre-alloyed powder and multi-component powder systems. Titanium alloys are being widely used for medical implants (as a replacement for bones) and lightweight applications for aerospace industry have been studied intensively by several researchers. Van Elsen studied possibilities of building overhanging structure with titanium and showed that fibre lasers often had better performance compared to Nd: YAG laser for processing titanium (Van Elsen M. 2007).

Yadroitsev studied new materials such as copper alloys, stainless steel 316L and tool steel H13 (Yadroitsev et al. 2010). In single-track analysis it was found that lower scanning speeds resulted in distortion and irregularities and excessive high speed caused the balling effect. Gold is widely used for dental crowns, Khan carried out an extensive study using 24 carat gold and processed using SLM. It was found gold had cohesive and non-flowing behaviour for spreading thin layers. Optimising the method of gold powder spreading in SLM, optimum processing parameters were identified (Khan 2010).

Superalloys such as Inconel[TM] have been difficult to shape, machine or weld using traditional processes due to work hardening and was studied by Mumtaz (Mumtaz 2008). Research studied the effects of pulse shaping on the properties

of laser melted Inconel^{TM} and evaluated the possibilities of minimising wall thickness and lower the surface roughness of components. Rombouts studied the effects of alloying elements on the mechanical properties and melt pool of iron based powders (Rombouts et al. 2006).

2.4.1   Research in Aluminium Alloys

2.4.1.1 Aluminium and its alloys

Al-alloys have been used widely for applications within automobile, aerospace and medical industries due to their physical properties such strength to weight ratio, good machinability and corrosion resistance for some of the Aluminium series. However, the effectiveness of SLM processing is a challenge due to the following factors: poor laser beam absorption, poor flow ability susceptibility to oxidation, cracking sensitivity, high thermal conductivity. Figure 2-20 shows the number of papers published related new SLMed Al-alloys.
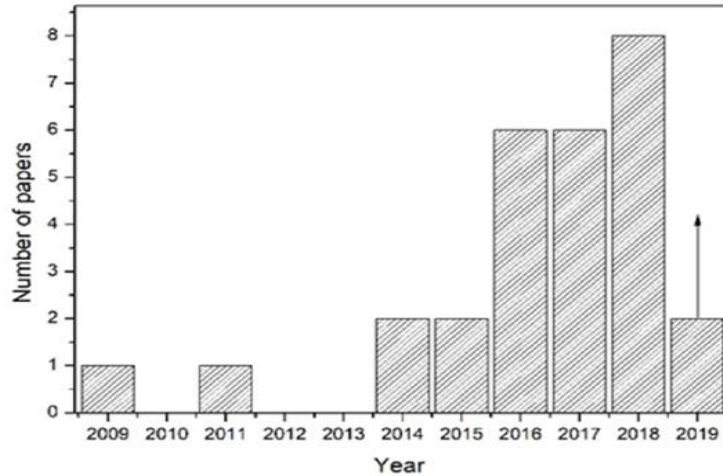
igure 2-20 Number of papers published in during 2009-2019 on new aluminium alloys for SLM (Aversa et al. 2019)

Among all commercial aluminum alloys, Al-Si series alloys, such as AlSi10Mg, Al-12Si, A356 and A357, are generally used in SLM process and in particular, AlSi10Mg is the alloy most studied to date (Aversa et al. 2017).

It was found that the addition to Si to Aluminium alloys improves the fluidity of molten and it plays an important role to reduce the solidification shrinkage due to its laser absorption properties (Sercombe et al. 2016). The excellent performance of AlSi10Mg is attributed to the content of Si and the formation of Mg_2Si compound related with the grain boundary straightening mechanism.

High strength Al- alloys such as 2xxx, 6xxx and 7xxx series are hardly processable by SLM due its susceptibility to solidification cracking, most of these alloys contains elements such as Li, Zn and Mg that are well known by

its evaporation during laser processing (Manduit 2017). Zhang observed crack formation in Al-2024 for a wide range of processing parameters (Zhang et al. 2016), Kaufman successfully build nearly dense Al-7075 using a high power (300W) however the reports showed long cracks oriented along the building direction, Kaufman studies also reported the solidification cracking decrease by using pre-heating platforms (Kaufman et al. 2016). Al-6061 shows delamination issues during laser melting and poor consolidation due solidification cracking (Louvis et al. 2011).

Jia and Schmidke investigated the effects in solidification cracking of Al-alloys by adding different elements such Zr and Sc resulting in high degrees of grain refinement improving mechanical behavior (Jia et al. 2018, Schmidke et al. 2011). Table 2-2 shows mechanical properties reported by different authors for new Al-alloys processed by SLM.

Table 2-2 Mechanical properties of Aluminium alloys processed by SLM.

(Aboulkair et al. 2019)

Material	Heat Treatment	Details	As-built (HV)	Heat-treated (HV)
AlSi7	AA	300 °C − (0.1–168 h)	94	45
AlSi7Mg	T2	300 °C − 3 h	124-133	76-78
	AA	165 °C − 0.01–60 h	-	115-150
	SHT + AA	535 °C − 1–8 h	-	60-115
		165 °C − 0.01–60 h	-	
	SHT + AA	535 °C − 1–8 h		63-115
		180 °C − (0.01–60) h		
AlSi10Mg	-	-	140-150	-
	-	-	127	-
	-	-	106-112	-
	Annealing	300 °C − 2 h	132	88
	SHT	530 °C − 6 h	132	60
	SHT	520 °C − (1–4) h	110	62-68
	SHT + AA	520 °C − 1 h	110	75-79
		160 °C − (6–12) h		
	SHT + AA	520 °C − 4 h	110	94-96
		160 °C − (6–12) h		
	SHT + AA	520 °C − 1 h	125	100-103
		160 °C − (6–7) h		
AlSi12	-	-	135	-
	-	-	110	-
	Annealing	300 °C − 3 h	145-150	105-115
	Annealing	450 °C − 6 h	135	65
	-	-	119	-
AlSi12/TiB2	-	-	142	-
AA-2024	-	-	111	-
AA-7075	AA	150 °C − 6 h	160	170
	SHT	470 °C − 2 h	160	100
	SHT + AA	470 °C − 2 h	160	115
	-	150 °C − 6 h	-	
	SHT + AA+AA	470 °C − 1 h	80	150-170
	-	110 °C − 5 h	-	-
	-	150 °C − 14 h	-	-
ScalmalloyRP	AA	325 °C − 4 h	105	177
Al-Sc-Zr	AA	300 °C − (0.1–168 h)	40	115
Al-Mg-Sc-Zr	AA	300 °C − 12 h	110-135	160-170
	-	-	86-94	-
Al-3.60Mg-1.18Zr	AA	400 °C − 0.5–144 h	275	320-410
Al-3.66Mg-1.57Zr	AA	400 °C − 0.5–144 h	300	360-420

2.4.2 Research in in-situ SLM alloys

As mentioned in section 1.1.2, there is a lack of research investigating in-situ alloying processing, and its potential is yet not assessed with full understanding. Research studies of in-situ processing using SLM from researchers (Vora et al. 2017, Kang et al. 2017, Sistiaga et al. 2016, Yadroitsev et al. 2017) had been identified with positive preliminary findings showing that the development of tailored in-situ alloys has strong potential in development of new material properties.

Bartkowiak demonstrated the use of in-situ allying of Al-Cu powder as feedstock material for the SLM process however it was limited only to produce a few single track lines onto the substrate (Bartkowiak et al. 2011). The utilisation of elemental mixtures may represent a cost-effective approach towards the designing of powder feedstock prior to committing to manufacture new customised powders for research study (Vora et al. 2017). In-situ allying process was found to be an efficient way to create Ti-Mo binary alloy by SLM (Yadroitsev et al. 2017).

2.5 Eliminating supports from additive manufacturing technologies

SLM of metals requires additional melting of metal powder to create supports or anchors to build parts. Anchors/Supports in SLM are key to avoid process failure due to internal stresses leading to warping. In polymer sintering, the material's unique super-cooling properties allows parts to be built without anchors. However metals do not have the 'super-cooling feature' seen in Laser Sinter polymers like nylon.

2.5.1 Super cooling effect

Laser sinter (LS) polymers are synthesised to have a window within which the LS process can be carried out to avoid warping of laser sintered layers by careful control of temperature. LS materials such as nylon-12 have recrystallisation temperatures of (138-143°C) that are lower than their melting temperature (185-189°C) (Dickens et al. 1994, Rietzel et al. 2008, Salmoria et al. 2009). This phenomenon of slow re-crystallisation at lower temperatures compared to their melting temperatures is a characteristic of super-cooling polymers. The difference between the melting and re-crystallisation temperatures of LS polymers is called the process window (PW) (see Figure 2-21, PW of 17°C).

During LS process, the part bed temperature is set to a temperature above the re-crystallisation temperature (see Figure 2-21, region in green). The laser scans the material adding sufficient heat energy to melt the material, on completion of scan another layer is spread and the process is continued till the part is completely built.

The bed temperature ensures the melted material to remain in molten state throughout the build process and the unsintered material will remain solid. On completion of the build, the part is allowed to cool and therefore avoids warping of consolidated layers in LS due to shrinkage during solidification (Goodridge et al. 2012, Tontowi et al. 2001).

The elevated bed temperature also reduces the temperature gradient between the consolidated layer and new layer spread, thus reducing internal thermal stress. Delaying the re-solidification process of melted polymer material, in-process warping of layers resulting in build failure and distortion of parts are avoided.
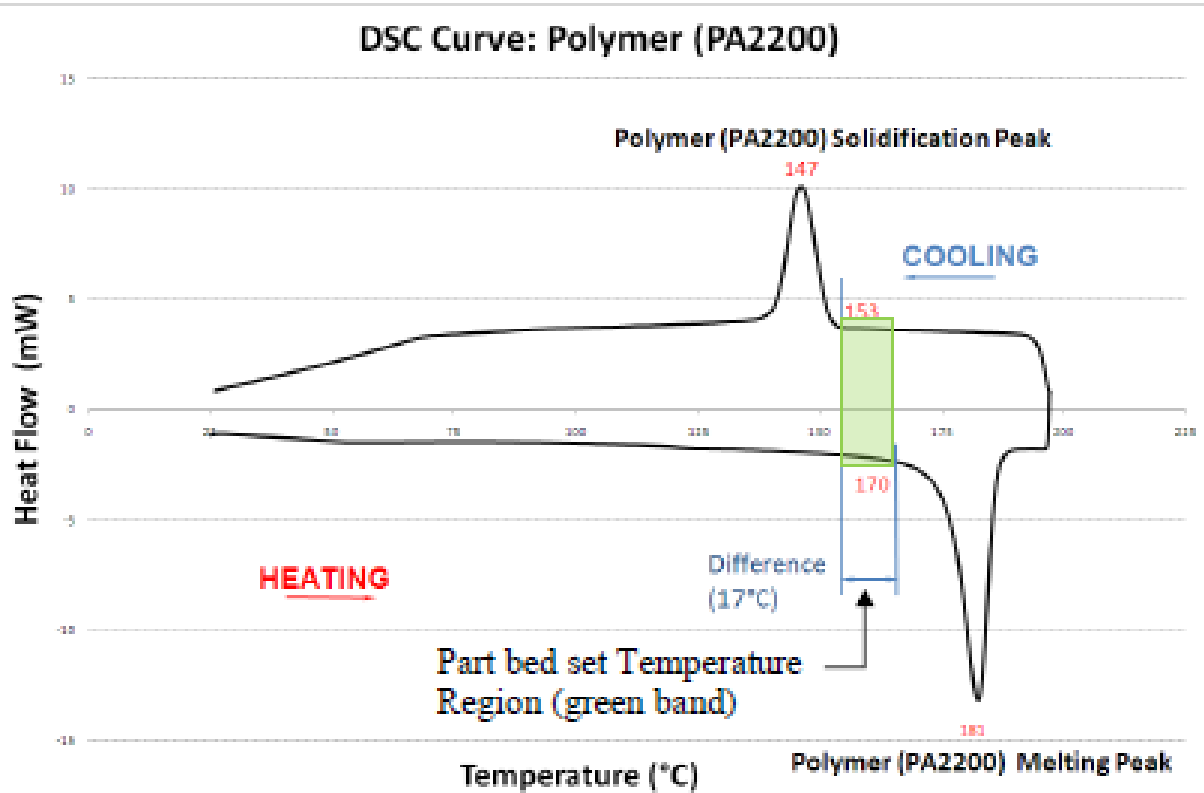
Figure 2-21 Relative volumes of Amorphous and Semicrystalline polymers at

melting temperature (Beaman et al. 1996)

2.5.2 Anchorless Selective Laser Melting

ASLM is a novel method using a eutectic alloy powder mix, at controlled operation high temperatures and maintaining the consolidated material in processing SLM machine to temperatures (similar to LS) near the re-solidification temperature.

2.5.2.1 Origin

Researchers at the Additive Manufacturing Research Group (AMRG), Loughborough University have developed and patented a process to eliminate the requirement for anchors in conventional SLM (Furlong et al. 2011) by introducing the 'super-cooling feature' in metals. Therefore, this method is known as ASLM. The process involves use of eutectic alloy system the key to the 'super-cooling feature' in metals.

2.5.2.2 Eutectic Composition

A eutectic composition is defined as a mixture of two or more materials at a composition that has the lowest melting point and the materials simultaneously crystallise from molten solution at the same temperature. A phase diagram is a thermal curve often plotted between temperature and weight percentage (wt %) of a component material from the mixture. Various key points and phases of material at respective temperature region such as melting point, mixture proportion, chemical reactions etc. can be identified from phase diagram.

Figure 2-22 shows a phase diagram marking the phase transformations of an alloy at eutectic composition. The eutectic composition is marked at the intersection of materials' liquidus line that is 'V' shape in a phase diagram.
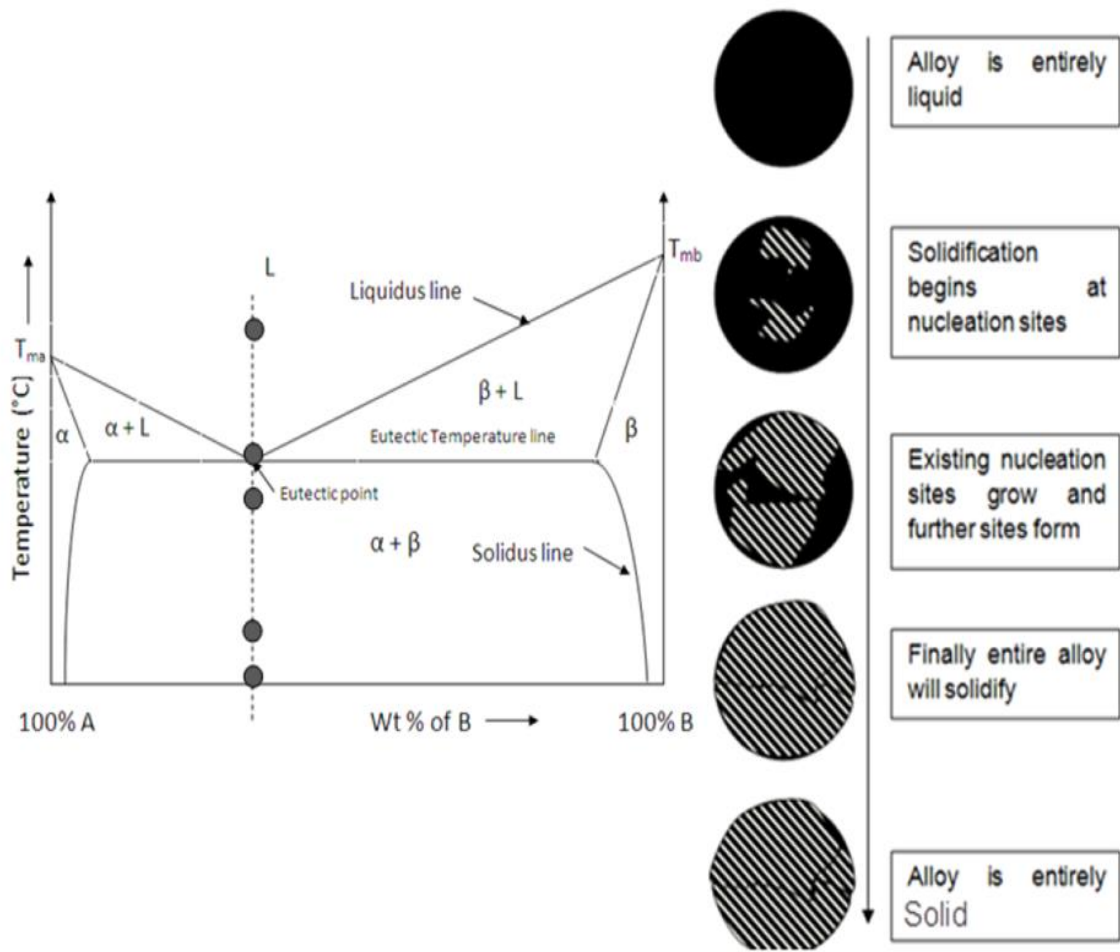
Figure 2-22 Phase diagram of eutectic composition (A-B) showing

solidification at different temperatures. (Askeland 1998)

2.5.2.3 ASLM Process

The ASLM process for building components is similar to conventional SLM.

The process uses a metal powder mix to create a eutectic alloy system and

employs specific pre-heating of the powder bed such that parts do not require

support/anchors during a build. At least two metal powders are mixed in eutectic system proportions to create the feedstock material for ASLM process.

The feedstock material is not completely alloyed at this stage; the feedstock powders finally form the eutectic alloy when fused by the laser. Mixing can be done using appropriate powder mixing methods such as mechanical mixing, vibratory mixing etc.

The eutectic feedstock powder mixture is spread over the substrate using an appropriate spreading method such as a hopper/wiper or roller. The powder layer spread is pre-heated to a temperature above the re-freezing temperature of the eutectic alloy system. Like conventional SLM, the feedstock powder is spread over the substrate and is melted and alloyed under the laser. The alloy formed produces a lower re-crystallisation temperature than the parent materials.

The processing bed temperature throughout the build is held near or above the re-crystallisation temperature of the eutectic alloy. This laser melted material remains in a liquid/semi liquid form and is allowed to cool uniformly at the end of a build thus avoiding internal thermal stresses and interlayer shrinkage leading to warping of consolidated layers. Figure 2-23 compares conventional SLM with ASLM.

Conventional SLM

Metal C

Anchors are melted in place

Laser melts layer of powder. Powder behind laser start to freeze as laser moves ahead.

Laser

Laser melts next layer over previous. Anchors prevent the previous layer from warping

Part is allowed to cool down in the bed

Melted layers warp upwards without anchors in SLM

Anchors are removed and rough surface due to anchors on parts is obtained

Anchorless SLM

Metal A and Metal B mixed at eutectic system composition (hypo/at eutectic/ hyper)

Bed Temp T

Pre-heated feedstock powder spread over preheated powder bed at temperature T

Bed Temp T

Laser melts first layer forming alloy with freezing temperature below bed temp T

Laser

Bed Temp T

Laser melts next layer (red) over previous layer (orange) and builds the part

Melted layers freezes completely as bed temp T falls below freezing temperature of eutectic system alloy forming part ASLM part

Flat surface part is produced with ASLM requires less post processing

Figure 2-23 Comparison processing schematics of Conventional SLM vs.

ASLM (Mumtaz 2011)

2.5.2.4 Parameters

ASLM parameters are similar to those used in standard SLM processing. However, additional control of the bed temperature is required with ASLM and different parameters (low energy density) would be beneficial to avoid additional melting of loose powder below the first layer of un-supported geometry.

To produce parts without anchors processed material needs to remain in liquid/semi-liquid condition throughout the part build (Furlong et al. 2011). This is achieved by maintaining the processing chamber temperature above or near the re-freezing temperature. Allowing the material to be in molten or semi-molten state prevents the previously melted layer from re-freezing and thus avoids the shrinkage of material during re-freezing. The bed temperature should be in the region (marked in green) as shown in Figure 2-24.The temperature can be selected from the results obtained from thermal analysis (DSC) of the powder mix pre-laser melting. Some material would not require the bed temperature as mentioned above.
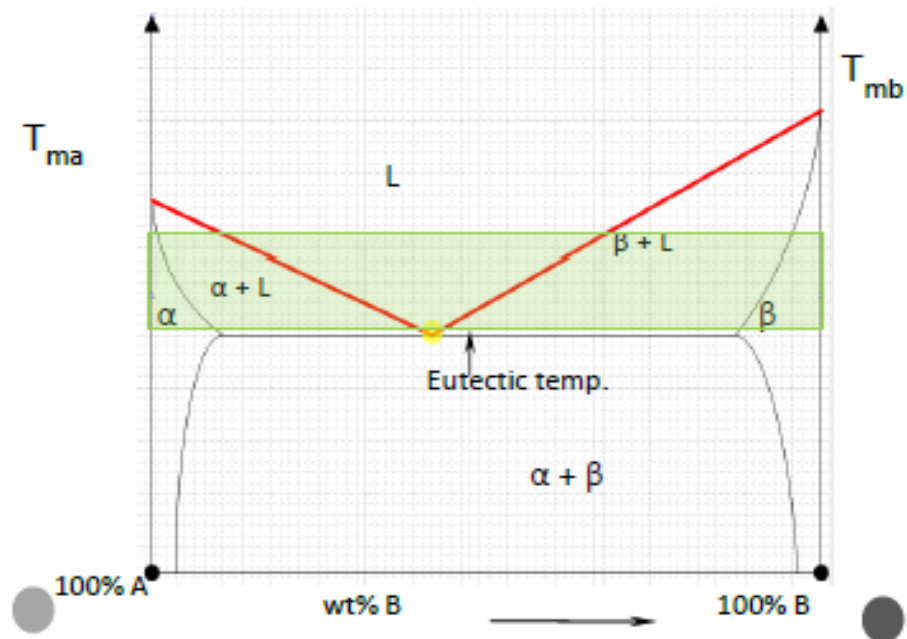
Figure 2-24 ASLM bed temperature (Tb) range (Author's image)

2.5.2.5 Initial Research

Researchers at Loughborough University were successfully able to build SLM

parts without anchors. These geometries were typically large flat geometries

that were the most prone to warpage/stress build up during processing. The

material used in the research were low melting materials such as bismuth (Bi),

zinc (Zn) and tin (Sn). The machine used was a Realizer SLM 100 machine

and was capable of pre-heating bed temperatures up to a maximum 250°C.

These materials when mixed in their specific eutectic alloy compositions

created a new melting point near 250°C and therefore would not warp when

pre-heating was applied. The eutectic phase diagram is shown in Figure 2-25

marking the eutectic composition.
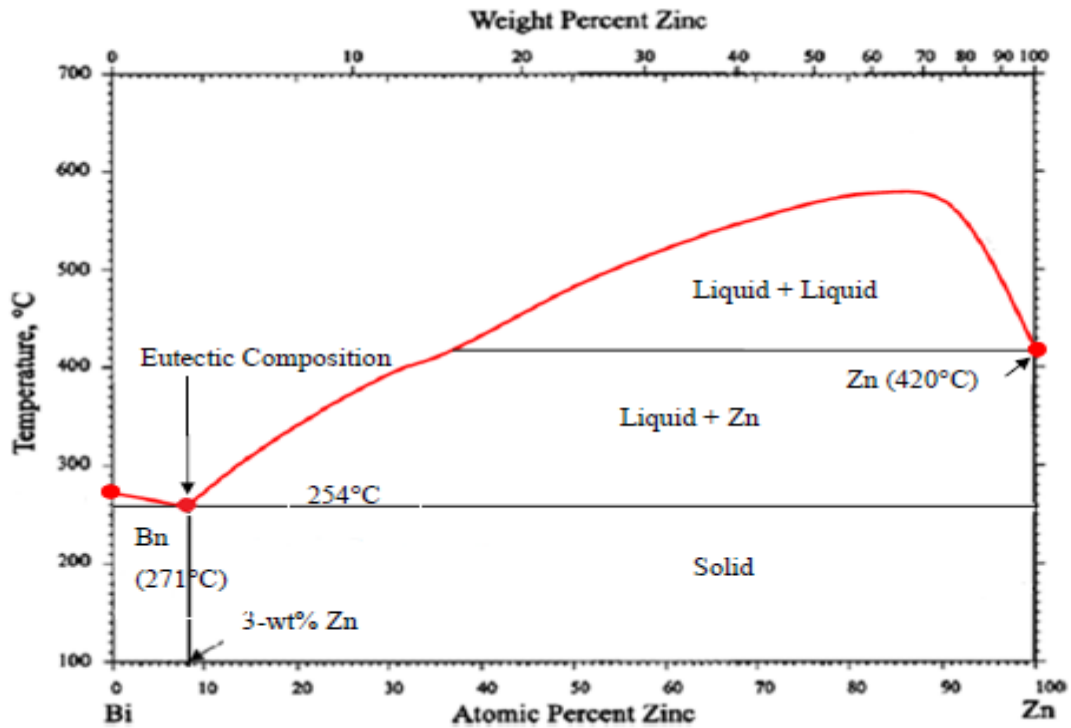
Figure 2-25 Bi-Zn phase diagram (Bi-3Zn, eutectic composition from

Okamoto 1997)

For initial trials, geometries with overhanging and unsupported features (see

Figure 2-26) were built without anchors. The parts produced demonstrated

poor mechanical properties compared with SLM alloys such as AlSi12 or

SS316, thus the alloy have limited engineering applications for SLM materials.

The produced components were cross-sectioned and examined under a microscope. The microstructure showed presence of a eutectic structure and proved the alloying of materials in their correct eutectic composition was achieved during laser processing.
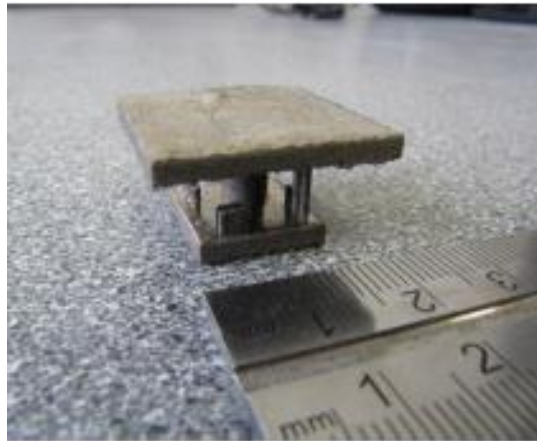
Figure 2-26 Bi3Zn eutectic part fabricated using ASLM (Mumtaz et al. 2011)

During analysis of the microstructure zones with laminar structure (typical eutectic microstructure) and spaces with no zinc were observed. This was suspected as a result of improper mixing of powder or due to small proportion of zinc. Thus resulting formation of eutectic structure only in areas with zinc presence under laser. Performing DSC analysis on the parts build by laser confirmed (single melting peak) the Bi3Zn was completely alloyed under laser processing. A thermal lag was observed in cooling peak. The difference between the melting and solidification peak (~ 25°C) could be due to thermal lag and/or undercooling of metal. Figure 2-27 shows the DSC plot confirming the alloy formation.
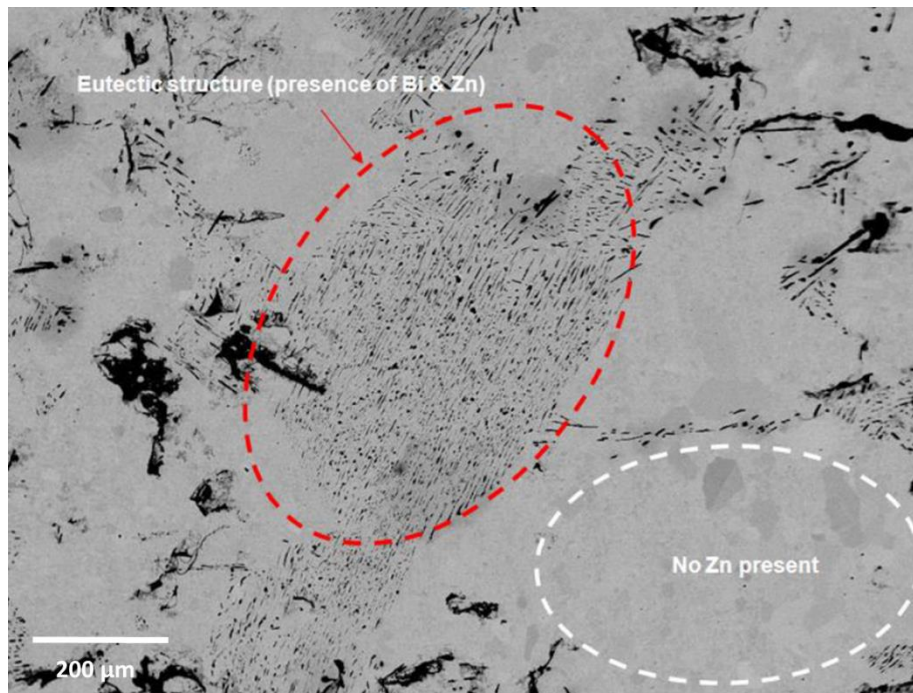
Figure 2-27 SEM image for laser processed Bi3Zn material. (Mumtaz et al.

2011)

2.6 Summary of literature review

The literature review has summarized the following:

- The SLM process and the factors affecting the process ability of metals (e.g. environment, laser, powder, energy density, solidification, etc).

- Current status of in-situ SLM alloys has only been applied to a few alloys with variable microstructure and significantly improvement in mechanical properties.

- A potential approach to create support-less geometries using SLM.

2.6.1 Knowledge Gap

From literature review the following knowledge gap has been identified and will be addressed by the research contained in this study:

- Lack of research in processing in-situ SLM alloys from elemental mixing and its potential to create tailored microstructures and mechanical properties that may be beneficial for new applications and does not requires expensive production methods.

- Lack of research on Al-Cu alloys due its cracking sensitivity compared with most common SLM Al materials such as Al-Si alloys.

- Lack of research investigating the influence of in-situ heat treatment on the microstructure and mechanical properties of SLM parts.

- Lack of research addressing, Room and High processing temperature mechanical properties (hardness, tensile) for Al alloys.

- Lack of research in the novel method ASLM and its potential to create SLM parts without supports as sacrificial structures.

Even though the use of different elements such as Zr and Sc have been successfully proved to increase mechanical properties and potential use for aerospace components, the use of these elements does not represent a cost-effective solution to develop in-situ new alloys for SLM due their price in the market.

Chapter 3: Experimental Methodology and System configuration

This chapter details the material and experimental methodology used in sample production, sample preparation and characterization of material investigation as well as a detailed description of the design and development of the controllable pre-heating bed system to enabling the ASLM process.

3.1　In-situ Aluminium Alloy Powder

The powder used in these trials was a elemental blend of pure argon gas atomized Aluminium and Copper powder, with a size range of 20-45µm for Aluminium and 5-25µm for Copper with a Gaussian distribution. The aluminium powder was manufactured and supplied by ALPOCO powders and the copper powder was supplied by LPW. The test certificate for the powder is shown in Appendix A, indicating the material composition and percentage powder by volume within each size range.

The powder complies with international standards (ISO) for Al and Cu powders. The composition of the elemental blended powder is shown in Table 3-1. Both powders were mixed by weight percent (wt. %) using a mixing ratio of Al: Cu =88:12 % as shown in Figure 3-1, in order to achieve a eutectic composition, and were blended using a tumbling speed mixer DAC-800 at 950

rpm for 10 minutes using 600 gr. The tumbler time was selected to avoid pre-sintering of powder during the blending process. The average particle size of the Al and Cu powder was 20-45µm and 5-25µm respectively, it was noted that for initial trial using the same powders size for both elements had not shown promising results for achieving high density. The Al-Cu binary composition phase diagram is shown in Figure 3-2. The use of smaller size Cu powders is to improve packing density.

Table 3-1 Composition of Al-Cu12 powder

Element	Al	Cu
Composition (%)	88.00	12.00
Particle size (µm)	20-45	5-25
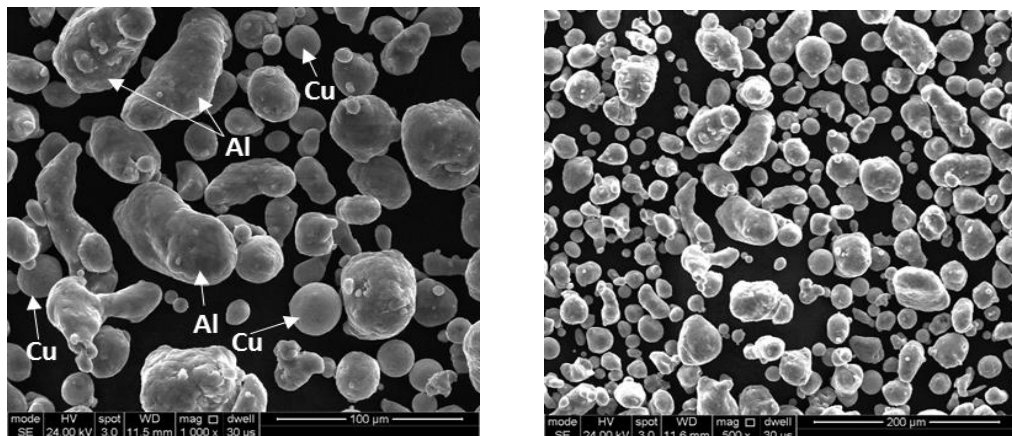
Figure 3-1 Morphologies of blended Aluminium and Copper powders at different magnifications.
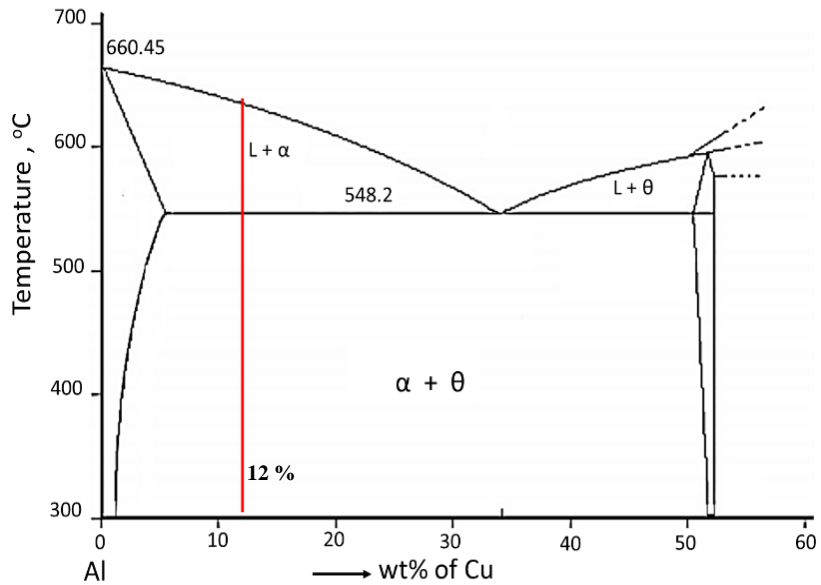
Figure 3-2. Binary phase diagram Aluminium-Copper (Adapted from Martinez 2019)

3.2   Selective Laser Melting Commercial System

The SLM system used in the investigation was the Renishaw AM125 SLM sited in the Mercury centre in the University of Sheffield shown in Figure 3-3. The system build volume is 125mm x 125mm x 120mm. A consolidating process was performed under continuously recirculating Argon at 1.03bar (atmospheric pressure) thus reducing oxygen content in the build chamber and preventing oxidation of the melt pool at elevated temperatures. The system uses a modulated laser scan, point to point, to control scan velocity.

75

The machine has the option to pre-heat temperature of up to approximately 140°C. This machine, was modified to increase the bed pre-heat temperature resulting in a reduction of the build volume to 65mm x 65mm x 100mm. These modifications enabled insulation material to be added preventing damage to the inner chamber and peripheral mechanisms. The full details of the modifications are described in Section 3.6.3.

This SLM system was used for manufacturing all of the test components to develop high dense processing parameters for in-situ Al-Cu12 alloy and the study of the effects of high temperatures on mechanical properties.

Figure 3-3 Renishaw AM125 Selective Laser Melting Machine (Renishaw SLM 2013)

3.3 Optimization parameters

There are seven processing parameters that are programmable using the Autofab Software from Renishaw AM125. These include:

- Laser Power (P)

- Layer Thickness (LT)

- Hatch Spacing (HS)

- Exposure Time (ET)

- Point of Distance (PD)

- Scanning Strategy

- Focus Offset (FO)

The laser power is the input power required to melt the processing material. The system used in this research has a range of 0-200W. The effect of using a different laser power will be discussed in section 3.4. With the combination of these parameters it is possible to calculate the energy density (*ED*) expressed in (J/mm³) as shown in Equation 3-1 establishing the process window for the SLM process detailed in section 3.4. The variation of these parameters will affect the melt pool size which has a significant effect to produce high dense parts.

$$Scanning\ Speed = \frac{1}{\frac{ET}{PD} + \frac{1}{v_{idle}}}$$
Equation 3-1

The Exposure time is the length of time when laser spots a series of multiple points. The point of distance is the distance between these spots, the combination of the exposure time and point of distance results in scanning speed expressed in (mm/s) as shown in Figure 3-4.
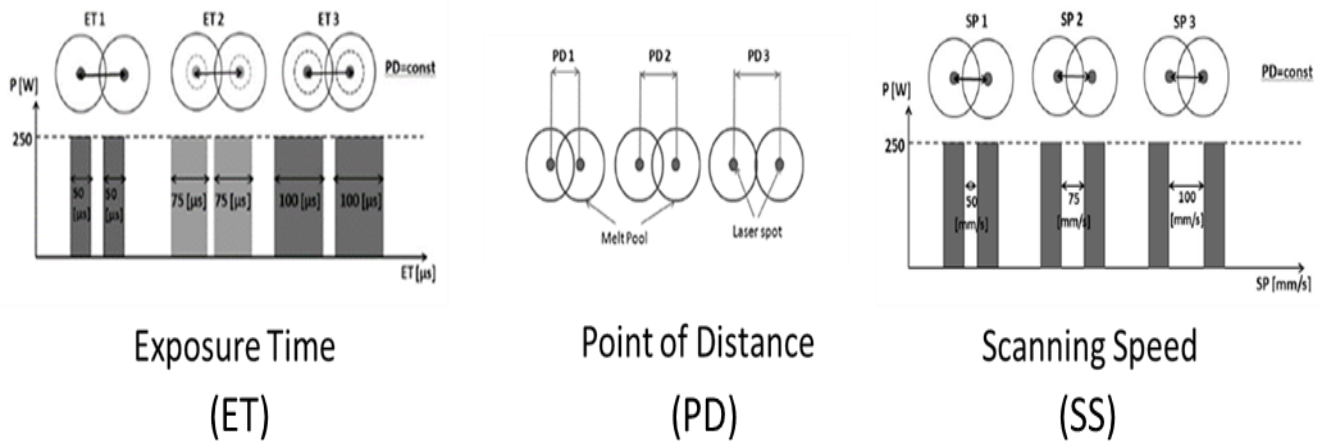
Figure 3-4 Renishaw AM125 Selective Laser Melting Machine (Adapted from

Stwora, 2013)

Scan strategy is the pattern the laser follows for the melting tracks based on the two dimensional sliced shaped from the CAD file. There are different scan strategies, the most common being Meander hatching, Stripe hatching and Chessboard hatching pattern, these patterns may be used for different purposes, whether it be to speed up the build time or get an homogenous distribution of residual stress. For this research the scan strategy used was meander with a laser rotation of 67° degrees for each layer. This rotational angle is used to ensure the scanning direction is not repeated until twenty layers have been completed.

A set of build parameters were developed and optimized to produce a fully dense (>99.5%) SLM-built test sample cubes. These were carried out using the elemental blend Al-12Cu test powder and the Renishaw AM125 SLM machine to be used in all future test cubes. A design of experiments (DOE) was produced with the assistance of Minitab statistical software using factorial design to optimise parameters for density. Levels and factors for factorial design are discussed in section 4.4. All sample cubes were checked for density, using optical microscopy for porosity analysis. The operation of the machine was followed by the internal Renishaw standard operation procedure (SOP).

3.4   Density optimization trials

Since there are 7 controllable parameters, a number of trials had to be conducted to evaluate the effect of porosity for each sample.

As Al-Cu12 is not exist in pre-alloy for SLM, previous experience in processing AlSi12 pre-alloy, melt pool size analysis and literature parameter values for processing aluminium alloys indicated the use of low scan speed, small scan spacing, and relatively high laser power promotes higher densification (Olakanmi 2015). As most of the results published in literature

are expressed using scanning speed, rather than point of distance and exposure time (Renishaw laser regime) it is possible to calculate using the Equation 3-1.

Where *ET* is exposure time, *PD* is point of distance and *vidle* is the velocity of laser when this travels between spot to spot. (For Renishaw AM125 machine is 2.5 m/s)

Using the Renishaw AM125 machine, 5 x 5 x 5mm^3 cubes were manufactured at a normal bed temperature for density optimisation trials as shown in Figure 3-5. A process parameter optimisation trial was carried out using the SLM parameters shown in Table-3.2.

Table 3-2 SLM processing parameters

Power (W)	Exposure (μs)	Hatch Spacing (mm)	Point distance (μm)	Layer Thickness (μm)	Bed Temperature (°C)
160,170,180	130-160	0.05, 0.07, 0.09	20-40	40	Room T, 400°C
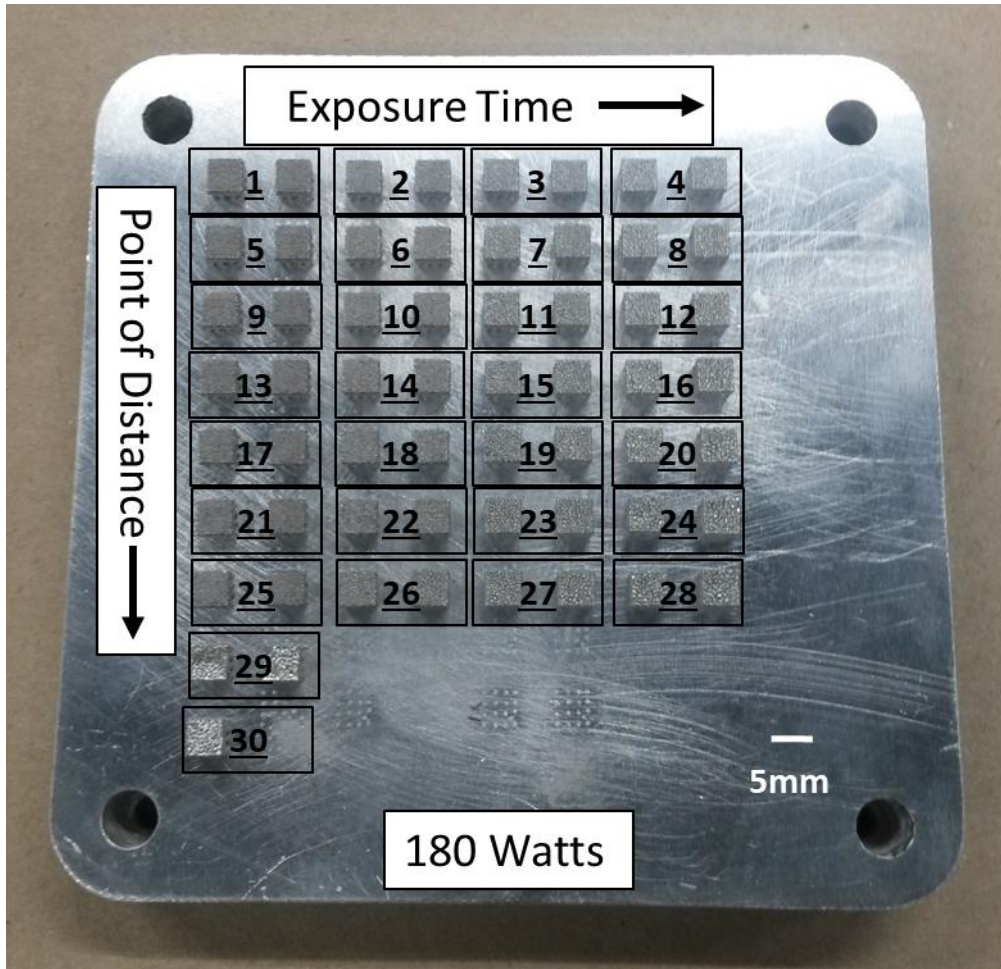
Figure 3-5 Density optimization trial arrangement built for SLM using

Renishaw 125AM

Table 3-3 and Table 3-4 shows the full factorial design with the combination of parameters with density results used for this research for room and high temperature. The purpose is to analyse the parameter trends and the impact in density with variation of different controllable parameters.

Table 3-3 Factorial design table with density values for room temperature

samples

Sample	Point of Distance (μm)	Exposure Time (μm)	Hatch Spacing (mm)	150 W	170 W	180 W
				Porosity % per sample		
1	20	130	0.05	9.08	8.95	7.2
2	20	130	0.09	12.04	9.72	5.86
3	20	140	0.07	7.45	9.56	13.94
4	20	150	0.05	8.83	11.67	12.06
5	20	150	0.09	6.47	12.93	6.49
6	20	160	0.07	9.56	5.43	0.32
7	25	130	0.05	8.64	6.14	4.59
8	25	130	0.09	5.89	4.24	1.7
9	25	140	0.07	5.29	7.68	2.4
10	25	150	0.05	6.31	10.45	6.55
11	25	150	0.09	7.49	6.29	2.08
12	25	160	0.07	11.03	5.1	0.96
13	30	130	0.05	12.04	8.29	5.2
14	30	130	0.09	10.49	7.95	4.3
15	30	140	0.07	9.93	6.34	6.23
16	30	150	0.05	14.93	5.03	6.91
17	30	150	0.09	12.83	12.45	4.66
18	30	160	0.07	11.09	6.93	6.6
19	35	130	0.05	8.43	7.05	7.59
20	35	130	0.09	6.03	4.98	5.96
21	35	140	0.07	8.19	5.89	4.4
22	35	150	0.05	7.4	7.94	5.47
23	35	150	0.09	11.84	5.86	4.82
24	35	160	0.07	13.02	5.29	3.6
25	40	130	0.05	12.98	7.34	7.89
26	40	130	0.09	9.47	7.24	5.8
27	40	140	0.07	10.34	6.48	7.26
28	40	150	0.05	9.67	9.46	3.7
29	40	150	0.09	8.19	8.18	5.53
30	40	160	0.07	8.34	6.39	6.38

Table 3-4 Factorial design table with density values for heated bed

processing samples

				High Temperature (400°C)		
Sample	Point of Distance (µm)	Exposure Time (µm)	Hatch Spacing (mm)	160 W	165 W	170 W
				Porosity % per sample		
1	20	130	0.05	4.77	7.226	4.85
2	20	130	0.09	4.86	3.98	2.88
3	20	140	0.07	7.21	1.58	1.15
4	20	150	0.05	4.6	5.44	3.55
5	20	150	0.09	3.55	3.72	2.66
6	20	160	0.07	6.22	1.54	0.58
7	25	130	0.05	5.65	7.89	5.66
8	25	130	0.09	4.55	6.73	3.42
9	25	140	0.07	9.76	3.52	1.8
10	25	150	0.05	5.85	7.87	5.44
11	25	150	0.09	4.37	4.82	2.08
12	25	160	0.07	8.55	2.25	1.44
13	30	130	0.05	9.67	8.29	5.85
14	30	130	0.09	7.85	7.95	4.3
15	30	140	0.07	8.56	4.88	4.21
16	30	150	0.05	7.22	8.65	6.91
17	30	150	0.09	5.64	7.57	3.55
18	30	160	0.07	8.56	4.29	2.58
19	35	130	0.05	11.86	8.33	7.59
20	35	130	0.09	9.85	7.834	4.32
21	35	140	0.07	9.93	6.9	4.4
22	35	150	0.05	8.83	7.94	5.47
23	35	150	0.09	7.26	7.8	4.82
24	35	160	0.07	8.34	6.6	3.99
25	40	130	0.05	11.77	8.12	7.89
26	40	130	0.09	9.7	7.74	5.2
27	40	140	0.07	13.02	6.48	5.77
28	40	150	0.05	11.98	8.15	6.75
29	40	150	0.09	8.19	8.18	4.77
30	40	160	0.07	9.93	6.9	4.4

3.5 Sample preparation

In order to study the porosity and microstructure of Al-Cu12 produced by SLM, samples were mounted perpendicular to the build direction in bakelite using Buehler SimpliMet 3000 automatic mounting press. Once mounted all samples were then grinded and polished on a Buehler EcoMet 250 Grinder-Polisher. The procedure was as follows: general grinding using silicon carbide pad of 800, 1200,2500,4500 grit size following by Diamet diamond suspension of 1µm and the final step with 0.05µm silica suspension. A number of selected samples were mounted with conductive bakelite to be analysed with electron microscope in order to analyse microstructure more in depth.

Once the mounted samples were polished, an optical analysis for density were performed using a Nikon Eclipse LV150 optical microscope fitted with Buehler Omnimet 9.5 software. The micrographs were taken at 50X magnification with a pixel size of 10.2µm. Four micrographs of 2 x 2.5 mm^2 were enough to cover the 5 x 5 mm^2 sample size. The open source software Image-J was used for porosity analysis using the threshold method, which converts the images into binary (red and white) to measure the porosity ratio between these colours as shown in Figure 3-6.

The polished samples were etched with 5% HF reagent (100 ml distilled water, 5 ml Hydrofluoric Acid) by 15-20 seconds in order to perform microstructural analysis. A scanning electron microscope (SEM) JEOL6610LV fitted with a tungsten filament, with optional magnifications between 5X to 300,000X (on 128 mm × 96 mm image size) and accelerating voltage of 20KeV was used to perform the microstructure analysis once the samples were etched.
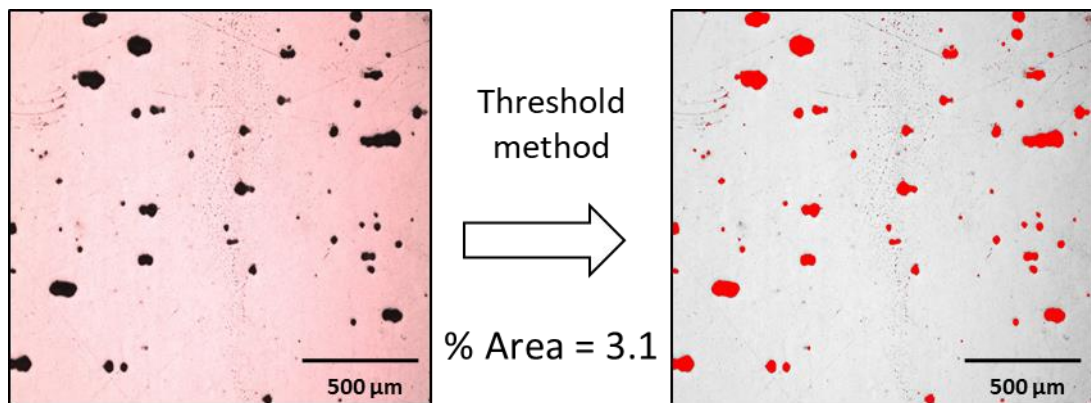
Figure 3-6 Representation of how the micrograph is turned into binary using threshold method in micrographs taken at 50X magnification.

3.6   Development of heated bed platform for selective laser melting

In order to reduce residual stress on build materials and eliminate supports from the powder bed. The ASLM process requires materials to be processed at elevated temperatures as explained in section 3. The Renishaw AM125 SLM system in its default configuration was capable of elevating the powder bed temperature to 140°C. The temperature recorded by temperature sensor is

located approximately 35mm deep in "Z" axis from the top surface of substrate plate. Commercial materials with wide industry interest such as aluminium alloys, titanium alloys, ceramics and few other materials for specialised applications required higher powder bed temperature. Thus it was necessary to design a powder bed capable of obtaining a high temperature that would enable production of samples with low residual stress and eliminate supports from metal powder bed.

Several concepts were developed, accessed and the model that suited with the design requirements was taken further for development and manufactured. A modular heated bed with available build volume of 66 x 66 x 110 mm was developed that would fit on the existing elevator system replacing the actual one. This enabled use of the machine in its default condition for commercial purposes and for special purpose research applications whenever required. In addition, a new scaled down powder hopper and deposition was made to suit the powder requirements small heated powder bed.

The new design minimises the use of special powder feedstock mixed with elemental powders for research and thus reduced wastage due to contamination by spatters and overheated particles. AISI 310 stainless steel refractory grade was selected for the assembly to assure a good performance under high temperatures and minimize deformations within the entire structure.

The original wiper was found to be unsuitable for high temperatures and was replaced for a new stainless steel 316 wiper to assure no deformation under high temperature. The silicon lined wiper from the machine was replaced to sustain high temperatures over the heated build face plate. A detailed description of the design and commissioning of heated bed is provided in section 3.61.

3.6.1 Heated platform

The function of the heated platform in ASLM was to maintain material in a stress free relaxation state, close to solidification temperature of in-situ alloy formed and reduce thermal shock by preheating the powder layer during laser melting. The heated platform is a cube packed arrangement with an enclosed heating system. Blueprints and engineering drawings are added in Appendix B.

The heated platform assembly consists of three main bodies of stainless steel SS310 and one part of ceramic alumina-zirconia with a square shape to be adjusted perfectly into the machine chamber. Inside the assembly of these four bodies exists an internal pocket cavity where the heated pad is located and securely assembled with the help of M4 tighten screws to assure no movement and good heat transfer during operation.

All the internal area surrounded the heated pad is filled with high temperature insulation material to minimize the heat transfer and secure outer temperature. The alumina zirconia is used as an outer insulation ring to protect heat transfer to the rest of the body and machine platform. The assembly is fitted with a silicon gasket to avoid powder leakage. The assembled heated bed into the main chamber is shown in Figure 3-7 and a detailed illustration of the heated bed platform is illustrated in Figure 3-8.

Cross sectioned
heated bed

Renishaw AM125
internal chamber

Cross sectioned
internal chamber
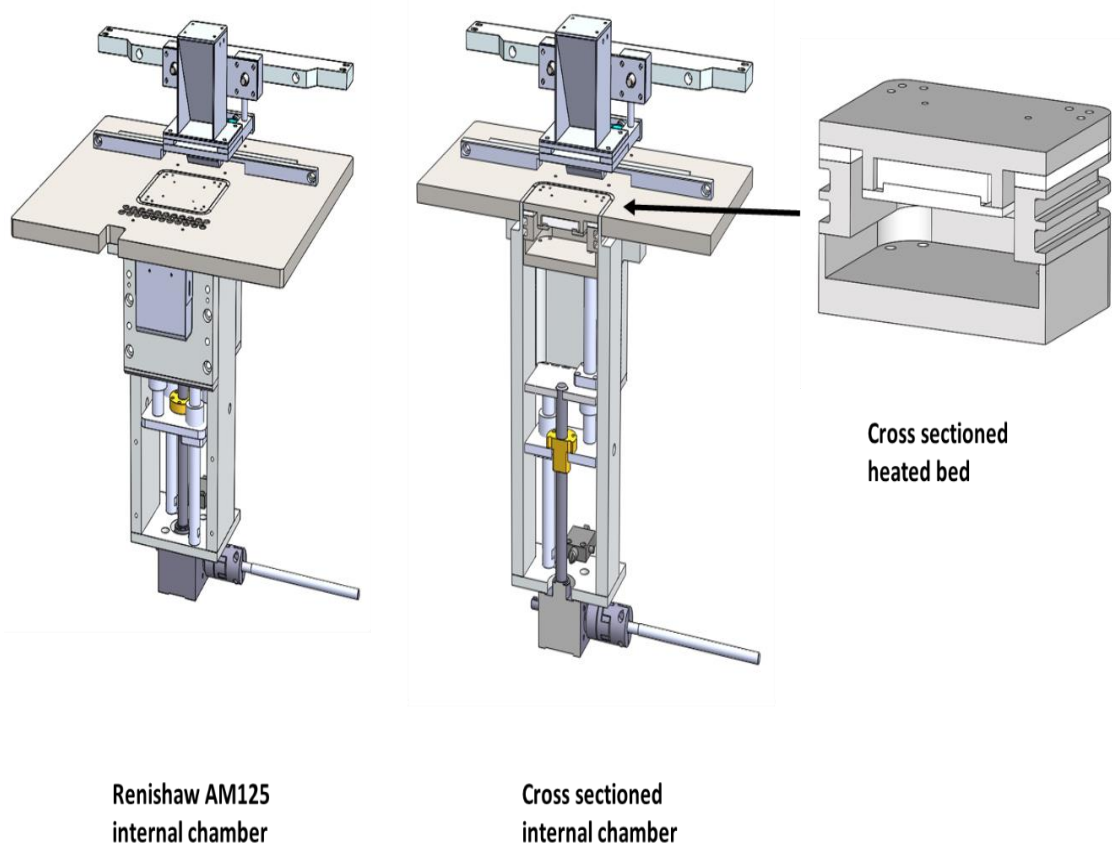
Figure 3-7 Schematic of heated bed assembly inside the Renishaw AM125.

Designed and manufactured for ASLM processing

SS-310
Zirconia ring
Silicon gasket
SS-310
SS-310
Heating Pad
Insulation   material
Power cable
Thermocouple
Transformer
Controller
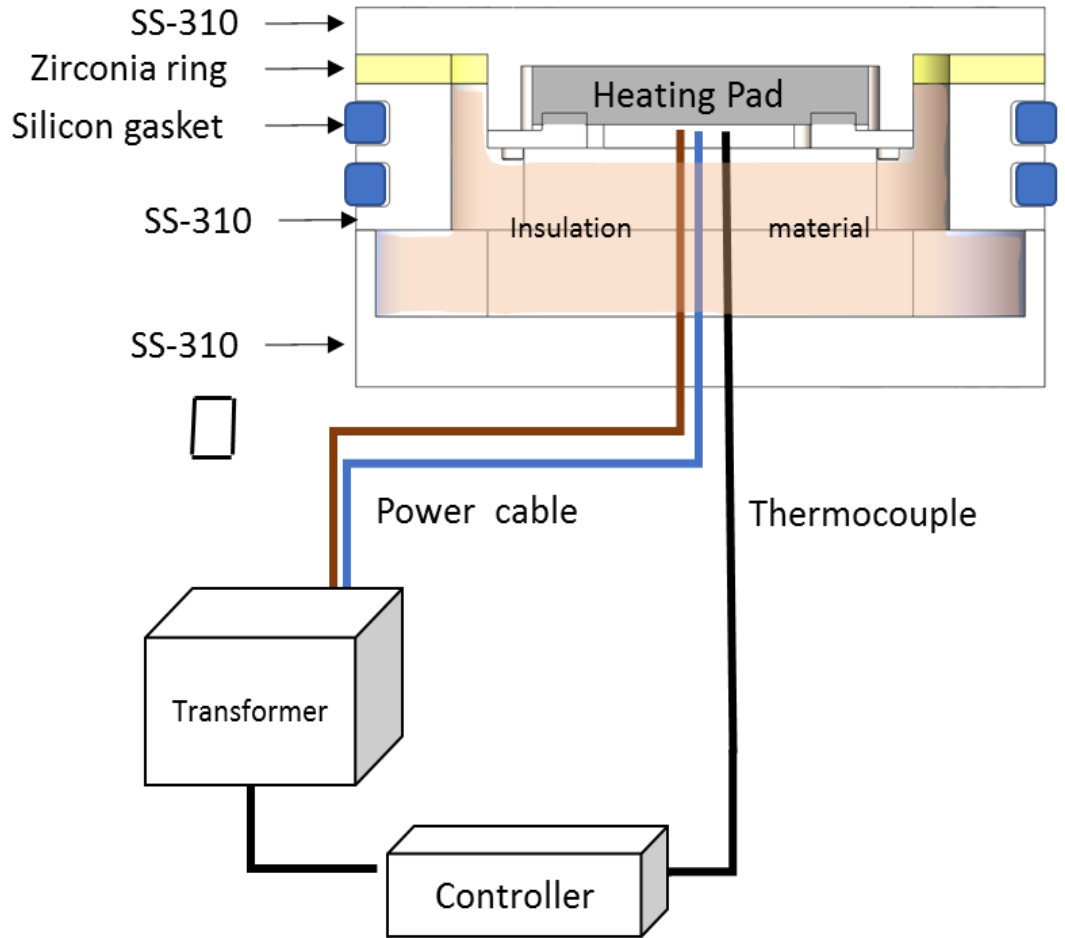
Figure 3-8 Detailed diagram of heated bed internal assembly and control

schematic assembly

3.6.2 Temperature control and monitoring

An integrated system was developed to monitoring temperatures. The heated

bed is fitted with a 40V internal heating resistant so it was necessary to connect

a transformer unit to step down power supply from 240V to 40V. The system was designed with a built in safety feature for the SLM machine.

Additional thermocouples were installed in the machine and set point temperature for each was configured based on location thus providing alarm signals to disconnect power supply to the heater in case of overheating. The integrating system included an Elmatic control box to adjust temperature in a range of 0-999 $^\circ$C.

3.6.3 Machine modifications

The Renishaw AM125 SLM machine required few modifications to fit in the heated bed assemblies. Modifications such as additional tapped holes to attach external power supply from transformer. Two M5 holes were drilled and tapped on the machine side panel in order to hold the thermocouple plugs. A 38 x 38 mm notch was machined of the machine face plate to allow leads to enter bottom chamber. Additional adjustments and proper sealing was done to protect wiring.

3.6.4 Installation and commissioning

Commissioning of the heated bed was done in two phases. Phase one included mechanical testing of the assemblies outside the machine by conducting bench tests to assess the maximum temperature the system could achieve. The distribution of temperature on the top surface substrate area as well as the external faces of the assembly were tested. In order to perform the test, a set of thermocouples were attached to the heated bed assembly to record the temperature readings through thermocouple Data Logger model TC-08 made by Pico Technology with a sample rate up to 10 measurements per second.

The measurements were made at the top were the substrate is located and two additional to the side and base of the assembly. Figure 3-9 shows the outside testing trials. Once the trials were successful, phase two included testing the assembly inside the build chamber. With modifications mentioned in Section 4.6.3, the assemblies were installed in the machine and a conventional SLM build was performed using the maximum temperature achieved during the outside trials. To ascertain the temperature at key locations on the Renishaw AM125 build chamber, a testing rig was developed and numbers of thermocouples were installed to monitor increase in temperatures. All sensitive temperature areas were found to within safe working limit conditions and the internal temperature sensors did not alarm during a continuous build test of 26 hours using preheating system at 840 ºC degrees.
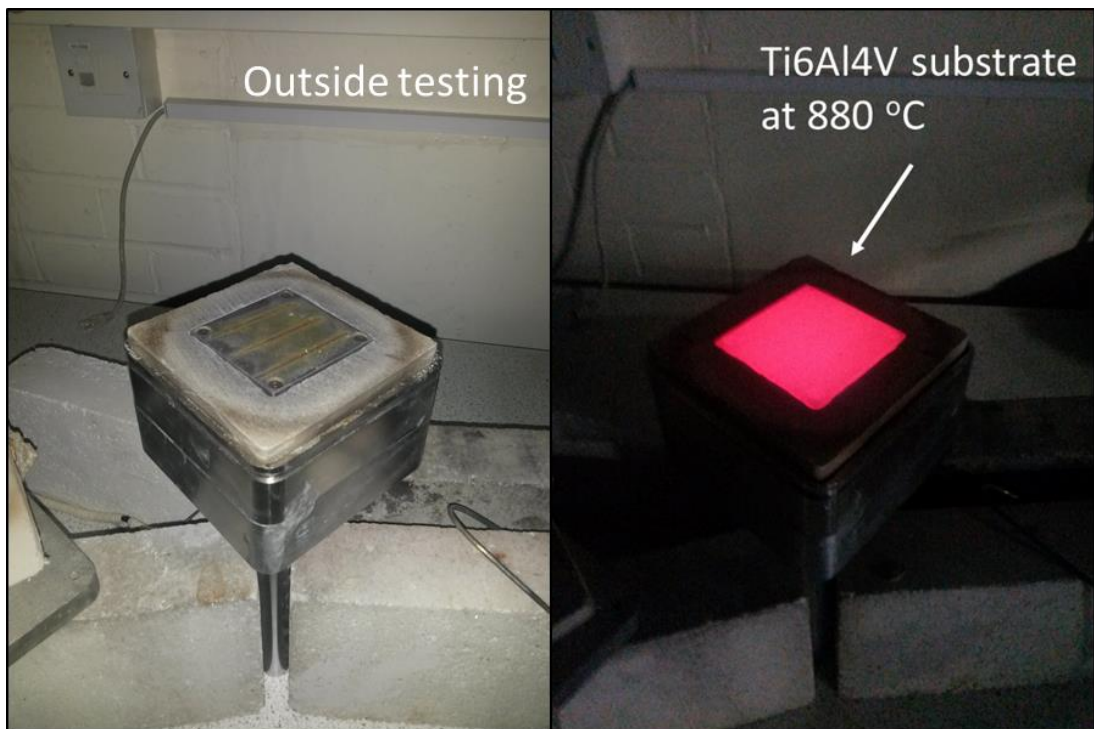
Figure 3-9 Heated bed testing trials outside the chamber and measurements of temperature distribution on the substrate

3.7 Powder mixing

The powder mixing was performed to obtain a homogeneous distribution of two elemental powders in a bulk material to be use for SLM processing. In powder mixing no material conversation takes place in terms of physical or chemical particle properties. The method of solid to solid mixing under controlled parameters such as temperature, atmosphere, rotational speed etc. is used for synthesising new experimental alloys. Table 3-5 shows the parameters used for powder mixing. It was found that speeds higher than 1000 rpms are

not suitable for this mixture alloy due sintering of the material creating lumps that interrupt the flowability during the recoating operation for SLM. Figure 3-10 shows the schematics of powder mixing.

Table 3-5 Speed Mixing parameters

Material	Velocity (rpm)	Time (min)	Quantity/Container (gr)	Mixing Ration	Total time (min)
Aluminium-Copper	950(V1) 500(V2)	3(V1) and 1(V2)	600	88:12	10
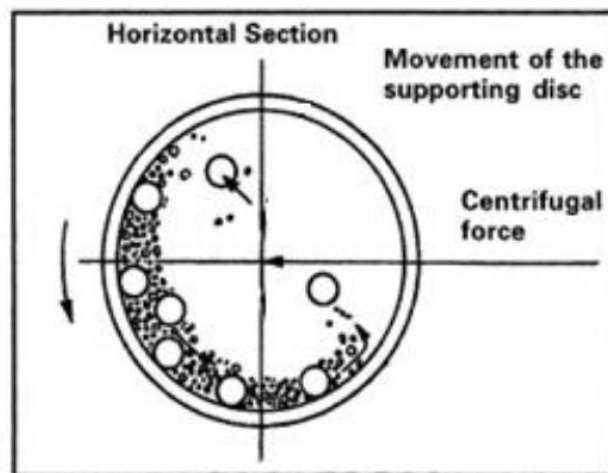
Figure 3-10 Schematic of centrifugal powder mixing for in-situ alloying

(Suryanarayana 2001)

3.8   Mechanical testing

Tensile testing samples were manufactured according to the cylindrical shape specimen 3 from ASTM E8/E8M Standard as shown in Figure 3-11(ASTM, E8 Standard, 2013) using Renishaw AM250 SLM. All samples were produced using the highest density optimized parameters (180W, 119 mm/s). The tensile tests were carried out at room temperature using a Shimadzu (AG-X) machine according to ASTM E8-16a Method B with a free-running crosshead speed of 2 mm/min fitted with extensometers using ISO6892-1 standards. The values displayed in table 3-6 correspond to the ASTM E8-16a parameters. The results of the test are presented in section 6.1.

Table 3-6 Dimensions for tensile specimens ASTM E8-16a Specimen 3

Nominal diameter (mm)	D	6
Gauge length (mm)	G	24
Minimum parallel length (mm)	A	30
Minimum transition radius (mm)	R	6
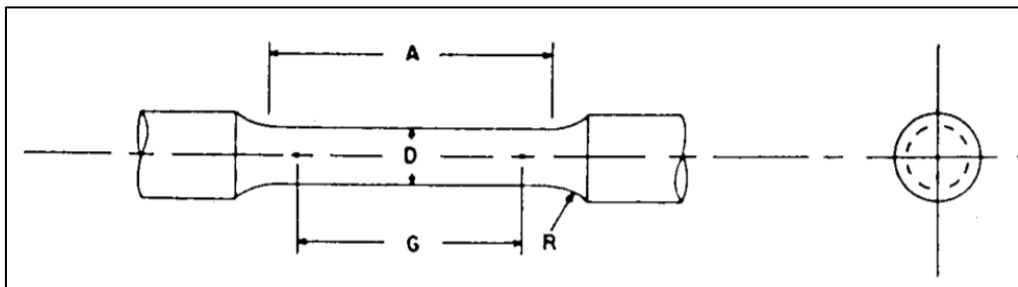
Figure 3-11 ASTM E8-16a Specimen #3 for tension test. All dimension in mm.

(ASTM, E8 Standard, 2013)

3.8.1 Hardness

Micro-hardness Vickers test were conducted according ISO6507-1:2005. Vickers hardness was measured with a load of 25g for 15 seconds with a total of 10 indentations per sample in different regions to obtain the average value using a Zwick Micro-hardness tester.

3.9 XRD analysis

X-ray Diffraction (XRD) phase analysis was performed using Siemens- D500 XRD system equipped with a Cu anode x-ray tube. The system operates at room temperature to identify the phases and operates using a voltage of 2700 watts with a scanning angle is from 20° to 120°. the peaks for different phase and orientation were determined according (Wang et al. 2017)

3.10 Warping measurements

Distortion warping measurements were performed using micrograph analysis, Omnimet v9 software to measure warping in samples build using ASLM processing produced using Renishaw AM125 machine. Optical images were taken using Olympus optical microscope. The images as a general practice

were calibrated using scale bars. These images were re-calibrated in Omnimet v9 software and warp distortion was measured. Warp measurement was expressed in linear distance between horizontal baselines to extreme most point of a warp surface.

3.11 Residual stress

Residual stress was measured in selected samples with three different conditions (room temperature, 300ºC and 400ºC) using X-ray residual stress analyser Pulstec μ-X360s portable x-ray analyser fitted with a Cu exchangeable x-ray tube. The system operates under a safety cabinet at room temperature using a low power input x-ray of 30 Kv. The measurements were performed using an angle of incidence of 35º and a sample distance of 60.0mm.

Chapter 4: SLM Process optimisation

This chapter assess the utility of Design of Experiments (DoE) in optimising the process parameters for in-situ mixture alloy Al-Cu12 from elemental powders. Initial experimentation was performed to assess the defects and internal voids using different layer thickness and scan strategies. Finally this section highlights the impact of final porosity with a variation of processing parameters. Finite Element Analysis (FEA) modelling simulation was used as tool for prediction of powder procesability.

4.1 Initial trials for effect on SLM process parameters on porosity optimisation

Initial trials were perform with different aluminium alloys such as Al-339, AlSi12 and Al2024 as a benchmark analysis in order to establish a processing window to find the optimum combination of parameters to achieve nearly fully dense parts (99.6%). The previous trials were used to assess porosity optimization for in-situ Al-Cu12. As the scan strategy and layer thickness are parameters that remain fixed during the building process, initial trials were perform to analyse their impact in porosity.

4.1.1 Effect of hatching scanning strategy

There are many scanning strategies that could be employed for SLM processing, and their use is mainly geometrically dependant. However there are three which have become predominant for SLM processing. The meander hatching pattern which is suitable for small parts and thin features, the chessboard hatching pattern which is used mainly for large parts, and stripe hatching pattern which is also common for large parts and high build rates.

The Renishaw Autofab software has pre-loaded these three scanning strategies and had been used to assess the effect in density. The pattern used for this study consisted in a 67° rotating meander hatching due the size of specimens used to perform porosity analysis as well to optimize residual stress by rotating each layer in a different position during the build-up, this method is well known for the positive impact in the residual stress. It was found that the use of chessboard or stripe hatching pattern strategies has not significant impact in density as shown in Figure 4-1.

Initial 5 mm x 5 mm x 5mm cubes size were built in order to perform a porosity analysis using optimized parameters for previous alloys, Table 4-1 shows the scanning strategy used for each sample case. All the samples were built on the same platform at room temperature.
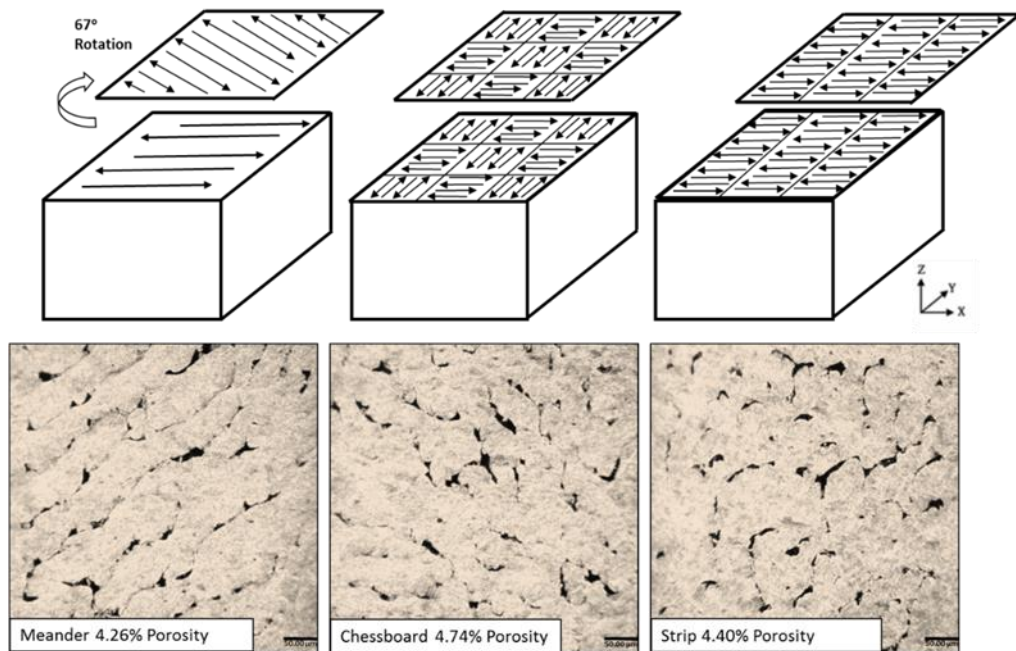
Figure 4-1 Porosity variation of processed samples with different scanning

strategies: Meander Chessboard and Strip

Table 4-1 Different scanning strategies experimental test cases

Test case	Sample 1	Sample 2	Sample 3
Scanning Strategy	Meander 67°	Chessboard 2x2mm	Strip 67°

4.1.2 Effect of layer thickness

A complementary set of trials were carried out using two different layer thickness. Literature and previous experimentation with aluminium alloys concludes better density performance with thinner layer thickness. For these initial trials the layer thickness was 40μm and 50μm and were build using meander strategy using same laser power and scanning speed as shown in Table 4-2. As 40μm is the standard layer thickness for Aluminium alloys in Renishaw AM125 machines, two different layer thickness were selected; 40μm and 50μm, using the latter to reduce processing time.

Table 4-2 Layer thicknesses experimental test cases

Test case	Layer thickness	Layer thickness
Layer Thickness (μm)	1	2

For each layer thickness, a series of block samples were built using previous optimized parameters. Figure 4-2 shows the different density values for each experiment carried it out for this experimental test. For this experiment a layer thickness of 40μm was set and the implications of increase or decrease the thickness will be discussed in section 4.3. After the result analysis of the initial trials it was concluded that the use of 40μm for layer thickness and 67° rotating

meander hatching strategy were the most promising combination to develop further studies of porosity optimization for in-situ Al-Cu12 mixture powders.
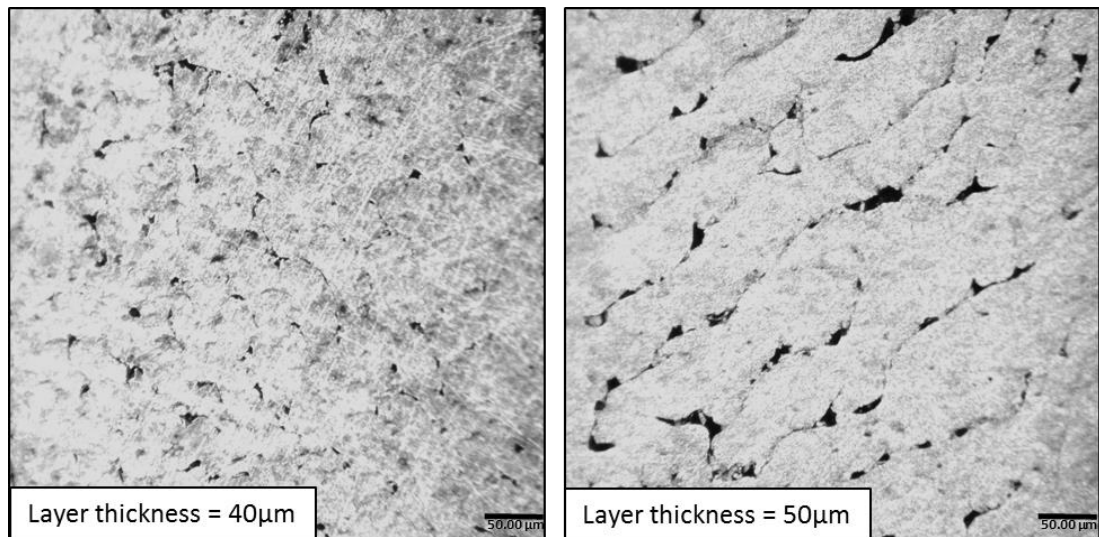
Figure 4-2 Porosity variations using different layer thickness for processed samples: 40μm and 50μm

4.1.3 Effect of different powder size

Initial trials were performed using the same particle powder size of 20-45 μm for Al and Cu powders. It was found that the density of processed samples improved using different size of Cu powder as shown in Figure 4-3. An improvement in relative density resulted in using a powder size smaller than initial trials. It was demonstrated by Linger that the packing density in blended powders has a strong influence of sintering process. The difference of size ratio

for both elements helps the distribution and packing of particles minimizing gaps between particles to improve laser absorptivity (Linger and Raj, 1987).
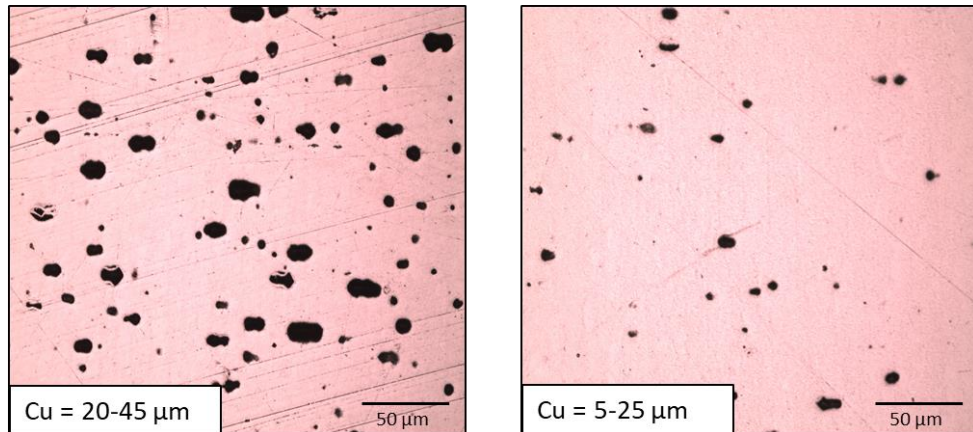
Figure 4-3 Porosity variations using different powder size for samples processed using same process parameters conditions (180W, 140 mm/s of SS, and 40µm layer thickness).

After these findings, it was suggested to use the smaller powder particle size of Cu powder for further parameter optimization trials.

4.2 Layer processing modelling

Finite element analysis (FEA) is a tool that can provide a good understanding about the melt pool dynamics and the residual stress build up on SLM

processing. FEA provides a good direction prior to experimental work by predicting the thermal history presented in the SLM process, reducing a number of experiments needed to find the optimum processing window parameters.

FEA was used to provide a better understanding of the melt pool dynamics and thermal history in the SLM process and understanding the effects of a single layer processing for further parameter optimisation in the development of ASLM alloys.

4.2.1 Thermal model

A SLM moving laser beam heat source and the induced fusion of metal powders and the substrate platform was modelled to predict the thermal history of the process. Ali in 2017 (Ali et al. 2018) developed an elastic model to predict melt pool formation for SLM parametric variation. As the work of Ali was conducted along the same project timeframe, as this project it allowed for close collaboration (see subroutine for Aluminium alloy in Appendix C). This model simulates the melt pool behaviour for a single scan track containing 14 laser spots. As Ali model was developed for titanium powder, further modifications were needed to adjust layer thickness and material properties.

As shown in Figure 4-4(a) a 1.0X0.33mm sheet layer of 40µm thickness was applied on to a substrate base of .5mm thickness. An element type DC3D8 8-node linear heat transfer brick was used for mesh. DC3D8 requires less computational time for converged results (Yilbas et al. 2012). A mesh size of 32 x 32 x40 µm was used for powder layer as shown in Figure 4-4(b).
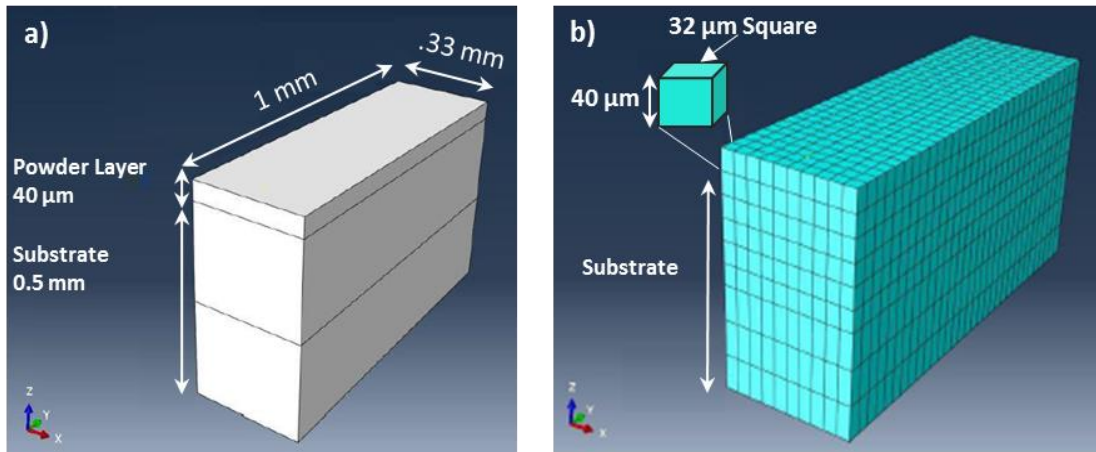
Figure 4-4 (a) substrate and power layer model (b) mesh model

The solution for the thermal distribution of the temperature is governed by the heat conduction equation 4-1.

$$pCp\frac{\partial T}{\partial t} = kxx\frac{\partial^2 T}{dx^2} + kyy\frac{\partial^2 T}{dy^2} + kzz\frac{\partial^2 T}{dz^2} + q \qquad \textit{Equation 4-1}$$

Where *p* is density, Cp is the specific heat, q is the heat source, *T* is temperature, *t* is the time, *x, y*, and *z* are spatial coordinates; *kxx, kyy* and *kzz* are thermal conductivities.

4.2.2 Material properties

The primary material used for the development of this research is Aluminium in-situ alloy Al-Cu12. During the SLM process, the powder material experienced phase transformations from solid (in powders state) to liquid then back to solid (as alloy state) by the beam power source. Thermophysical properties of the material are needed in order to perform an accurate modelling of this phase transformations. ABAQUS USDFLD subroutine of Ali's model that was used to simulate the melt pool size and temperature using a modified cylindrical laser heat flux MCHF model (Ali et al. 2018) as shown in equation 4-2.

$$q_{mod\ cyl.} = .18\eta\,\frac{P}{\Pi r_{las}2} \qquad\qquad \textit{Equation 4-2}$$

Where P is the laser power, $\Pi r_{las}2$ is the radius of laser spot taken from Renishaw AM125 machine as 50 µm, and η is the laser absorptivity for Aluminium .Thermophysical properties of solid and liquid Al-Cu12 used in this model are presented in Table 4.3 to 4-5.

Table 4-3 Thermophysical properties of solid Al-Cu12 (from Kurochkin 2013)

Temperature (°C)	Density (kg/m3)	Specific Heat (J/g C)	Thermal Conductivity (W/m K)
25	3374	0.85	59
100	3358	0.9	116
200	3334	0.95	134
300	3312	0.97	149
400	3289	1	158
500	3267	1.08	162
548	3184	1.1	162.9
550	3181	1.106	162.9
570	3146	1.1072	162.9
580	3129	1.108	163.6
600	3095	1.11	164
620	3060	1.116	164.04
630	3043	1.14	164.04
700	3009	1.14	164
800	2994	1.14	162

Table 4-4 Thermophysical properties of powder Al-Cu12 (from Kurochkin 2013)

Temperature (°C)	Density (kg/m3)	Specific Heat (J/g C)	Thermal Conductivity (W/m K)
25	1603.2	0.85	100.75
100	1981.22	0.9	109.16
200	2067.08	0.95	119.67
300	2152.8	0.97	125.46
400	2302.3	1	133.01
500	2940.3	1.08	169.20
548	2674	1.1	188.00
550	2647.9	1.106	172.63
570	2642.68	1.1072	169.55
580	2639.2	1.108	167.50
600	2630.5	1.11	162.38
620	2604.4	1.116	147.00
630	2500	1.14	85.50
700	2480	1.14	85.00
800	2452	1.14	84.00

Table 4-5 Thermal properties of solid Al-Cu12

Latent Heat (kJ/kg)	Solidus Temp ($^\circ$C)	Liquidus Temp ($^\circ$C)
553.660	553.66	568.89

4.2.3 Initial conditions and considerations

A temperature of 25 °C was set as the initial condition for modelling and is attributed to the metallic powders. The same temperature of 25 °C was used for substrate base plate. The packing density of powder was not considered for this model, the layer is considered as dense. Note that, a high temperature preheating substrate was not used for modelling Al-Cu12 processing powders.

Figure 4-5 shows the schematic diagram of SLM process, during the laser processing a fraction of heat is not absorbed and is considered a heat lost due convection and radiation at the top surface of layer bed. Meanwhile at the bottom of layer powder there are heat losses by conduction absorbed by the substrate base plate.
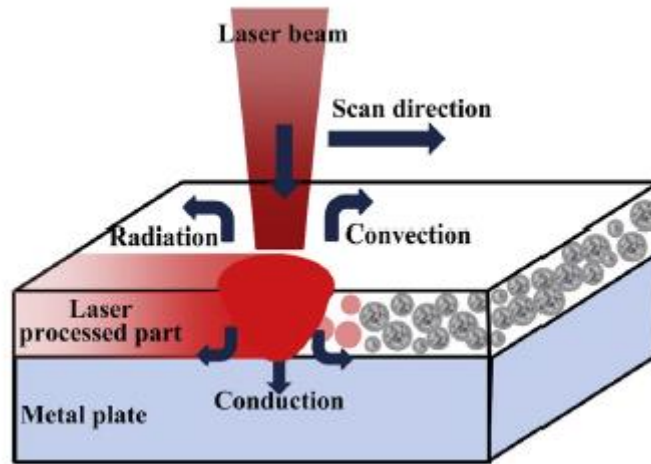
Figure 4-5 Schematics of thermal behavior for powder bed under laser

processing (directed from Yali et al. 2014)

A convective coefficient of 10 $\frac{W}{(m^2 \,^\circ C)}$ was used for this FEM model. A surface film condition was defined on the five external surfaces of the substrate in order to simulate the conductive loss. Radiation heat losses were not considered for this model also in agreement with Polivnikova the radiation heat losses are negligible (Polivnikova T. 2015). Temperature-dependent conductivity of Aluminium powders was used, as a convective heat transfer on the surfaces expressed in the equation 4-3.

$$h_2 = k_{powder}(T) \qquad\qquad \textbf{\textit{Equation 4-3}}$$

Where h_2 is the convective heat transfer applied on the surfaces of the modelled layer, k_{powder} is the temperature-dependent conductivity of aluminium powder adapted from Kurochin (Kurochin 2013).

4.2.4 Thermal model validation

Thermal FEA model was validated by comparing a processed single track dimensions with model simulated melt pool.

Experimental single scanned track were measured using the Renishaw AM125 machine. A 40µm layer of in-situ Al-Cu12 was deposited onto substrate base plate. A single track line was processed using parameters shown in Table 4-6.

Table 4-6 Experimental parameters for single scan track

Power (W)	Point of Distance (µm)	Exposure Time (µm)	Substrate Temperature (^{O}C)
180	20	160	25

After processing, the plate base was cross sectioned for sample preparation procedures, the sample was mounted, polished and etched to reveal microstructure melt pool following the procedure explained in section 4 for sample preparation. The melt pool were measured from the micrographs taken from SEM microscopy.

4.2.5 Melt pool dimensions

Figure 4-6 shows a comparison of dimensions (width and depth) from experimental melt pool processed with optimum processing parameters versus a predicted modelled melt pool created by Ali's Model. For the dimensional analysis. Three melt pools were measured from cross-sectioned processed samples.

The average dimension for experimental melt pool width and depth measurements are 132µm for width and 60µm for depth meanwhile the predicted modelled melt pool dimensions are 124µm width and 57 for depth. Nevertheless is well know that using

A melt pool schematics using the thermal model are shown in Figure 4-7, where it is possible to observe different features during laser processing such as thermal distribution across the processed layer, the nodal temperature (NT11) and prediction of melting pool size for in-situ Al-Cu12 alloy.
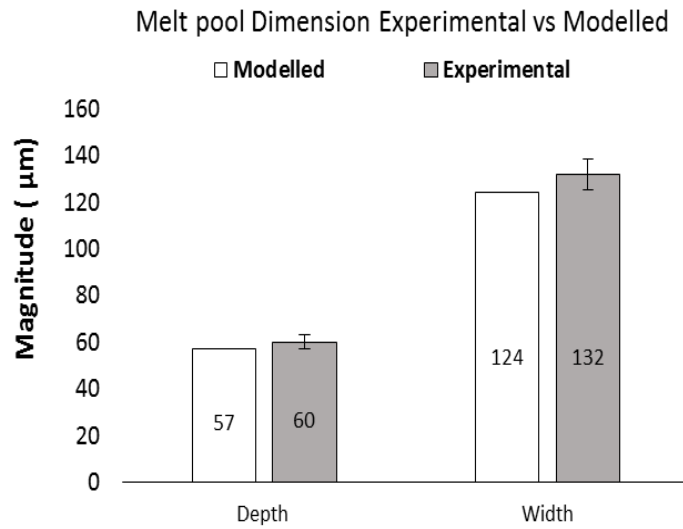
Figure 4-6 Melt pool dimension comparison: Modelled vs Experimental
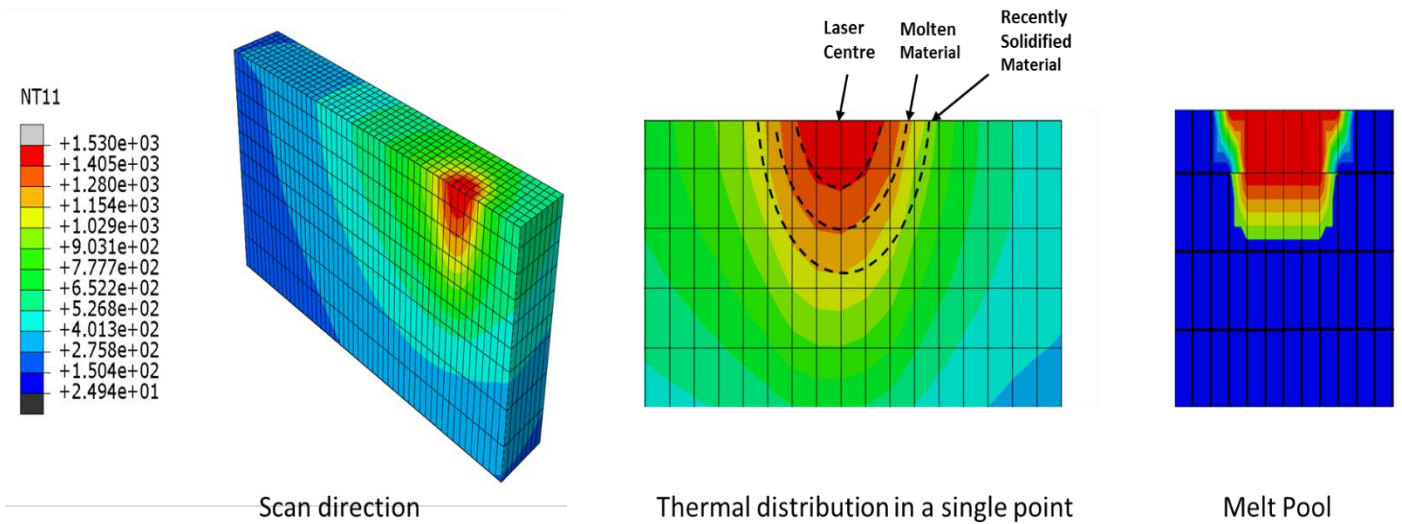
Figure 4-7 ABAQUS FEM Melt pool prediction model for SLM optimum

processing parameters showing the nodal temperature (NT11) in Celsius using

laser single pulse mode.

A comparison of SEM micrograph of experimental melt pool cross-sectioned sample with the average dimensions and the image from ABAQUS FEM software are shown in the Figure 4-8. This results provide a good direction for experimental work by reducing the number of experimental trials needed for density optimisation providing a narrow processing window.
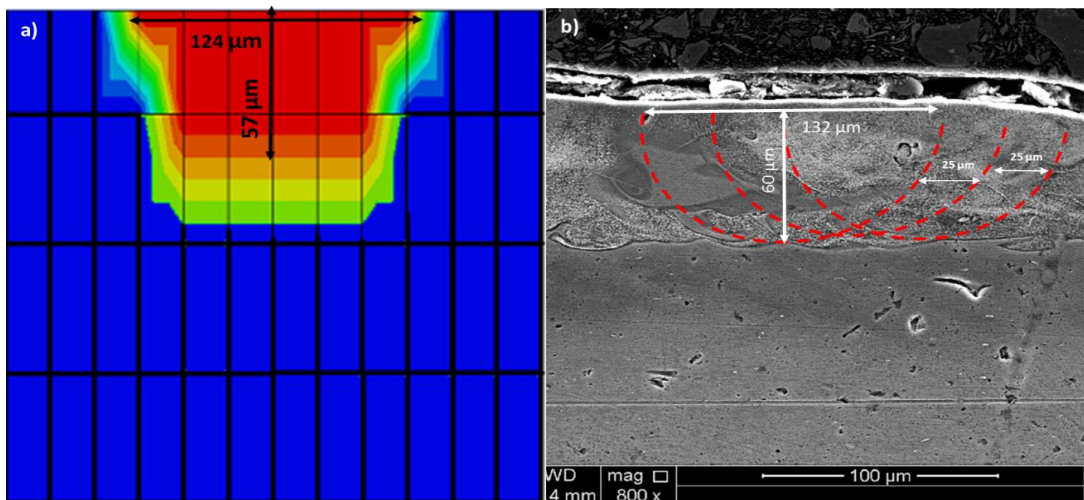
Figure 4-8 (a) Predicted melt pool by ABAQUS FEA model (b) Experimentally measured melt pool dimension

Figure 4-8(a) shows predicted melt pool dimensions from FEA model, using optimised SLM parameters for in-situ Al-Cu12 (99% density). The model results predicted a melt pool depth of 57µm which represents 5% less than the average experimental melt pool sample depth of 61µm. It can be observe from Figure 4-8(b) that the FEA model image indicates a melt pool width of 124µm and the average experimental melt pool width dimension is 132µm. Based in this comparison the results for width variation are 5% less for the predicted

FEA model. It can be concluded that FEA model predictions of melting behaviour of in-situ Al-Cu12 when fuses by laser beam correlates well with experimentation.

Figure 4-9, shows the melt pool instabilities in a single track line using fixed processing parameters of exposure time (ET) and point of distance(PD) while laser power input vary in a range of 160W to 200W. This experiment provided a better understanding of the instabilities of the melt pool and how the input energy affect the solidified surface morphology and how this may impact the next layer during processing. The laser power and laser profile were tested prior the trials showing a variability of 8-10 % for laser power, the results of the profilometer are included in Appendix D.

The surface morphology also had an impact in the powder deposition leaving an uneven surface that may affect the quality of the parts generating porosity. The combination of 180W laser power and 160µs exposure time with a point of distance of 20µm resulted with less variation at top surface.
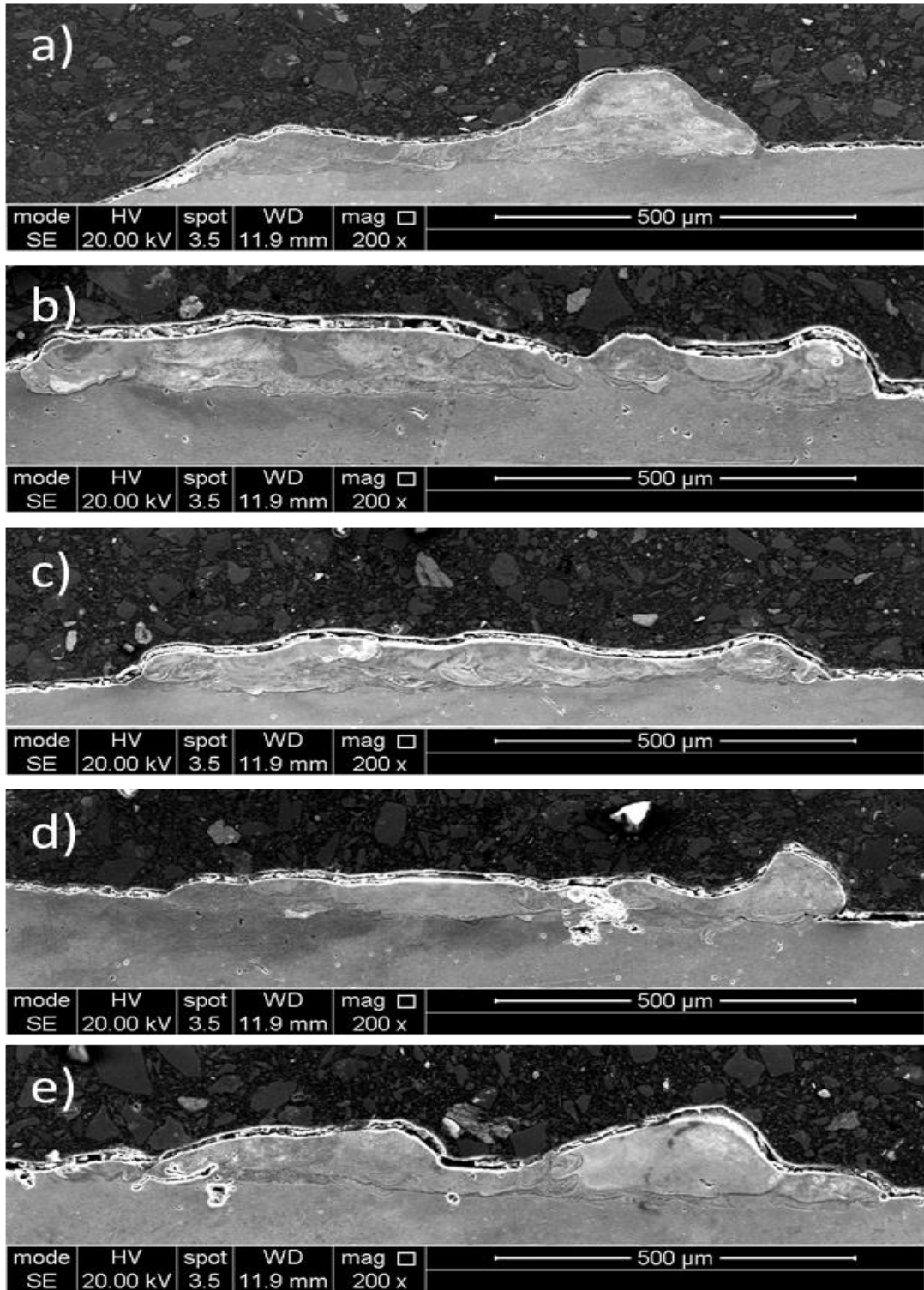
Figure 4-9 Single track variation with Exposure time and Point of distance fixed with variation in power (a) 160W (b) 170W (c) 180W (d) 190W (e) 200W

4.3 Parameter optimization

Different approaches have been used for researchers to optimize processing parameters in SLM such as Analysis of variance (ANOVA), Response surface method (RFM) and Factorial design, however the main goal for this statistical methods are always to determine which variables are the most influential on the response of a process.

This section is solely on experimental data gathered in the scientific paper named; in-situ alloying of elemental Al-Cu12 feedstock using selective laser melting published by the author of this thesis. Using factorial design approach for experiments, a total of 180 samples were created from the Al-Cu12 elemental blends and analysed for density optimization, chemical composition and microstructure for room temperature and high temperature conditions in order to achieve near full density samples. A total of 30 test cubes 5mm x 5mm x 5mm size were built per substrate with laser power fixed per trial.

The processing parameters such as point of distance, hatch space and exposure time varied in different levels as shown in section 3.4. A good example to understand how the selection of parameters may affect the density of the part is with a P-V diagram for laser processing showed in Figure 4.10. The main

116

objective of parameter optimization is determine the right window processing to achieve good part density.
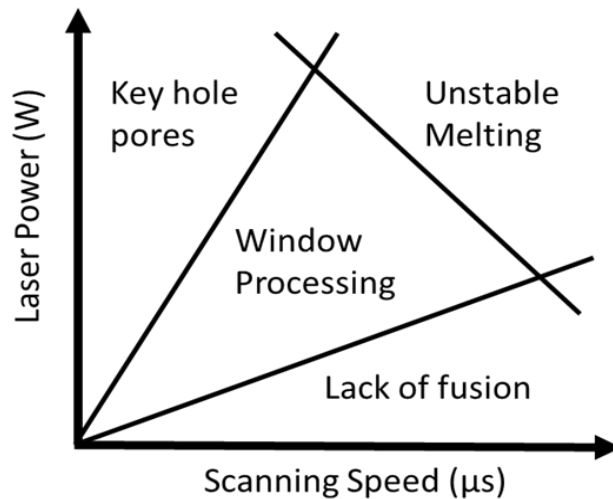
Figure 4-10 Laser power vs scanning speed window processing to maximize density (P-V Diagram Adapted from Suter, 2017)

4.4 Powder characterization

Figure 4-11 shows the particle size distribution for pure Al and Cu powders as received by Alpoco and LPW. It can be seen that the particle size distribution of pure Cu are slightly smaller than pure Al. As mentioned in section 2.2.3, the ideal powder particle size for SLM processing is between 15-63 μm. Powders bigger than 63 μm are unfavorable due the thin layer thickness used for SLM. The bigger particles may sweep across the surface when the recoater is

spreading the new layer resulting in very rough and irregular surface finish and poor bonding to the previous deposited layer.
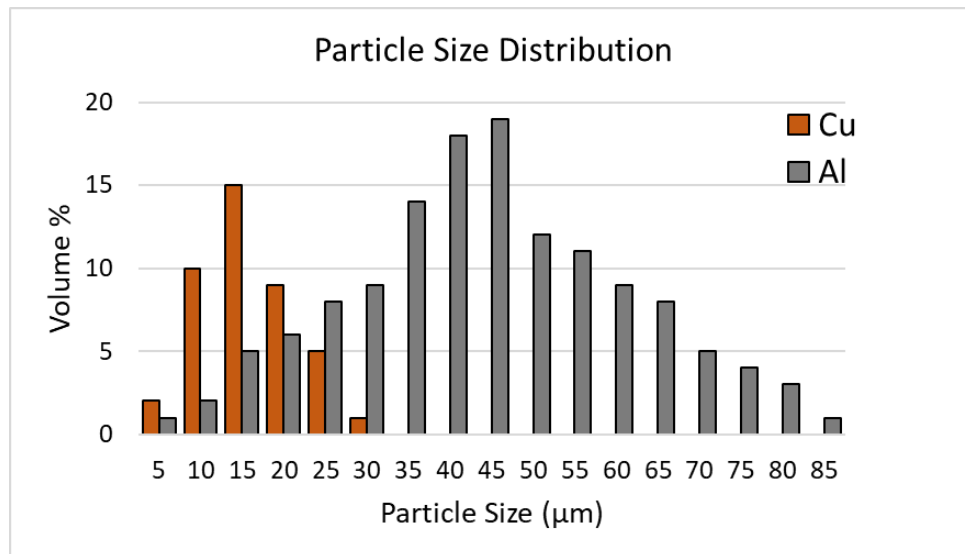
Figure 4-11 Powder size distribution for Aluminium and Copper as received supplied by Alpoco and LPW

Figure 4-12 shows the difference in powder morphology between Cu and Aluminium powders as received by suppliers. Is possible to observe that pure Cu powders are spherical shape, which is preferred for SLM processing due their good flowability during layer deposition. Aluminium powders are a more longitudinal shape and not spherical as preferred.

The use of different particle size distribution helps the pack density minimizing the possibility of entrapped gas pores during processing, a similar approach

was used by (Bartkowiak et al. 2011) while mixing in-situ Al-Zn powders to process high dense melted tracks using SLM.
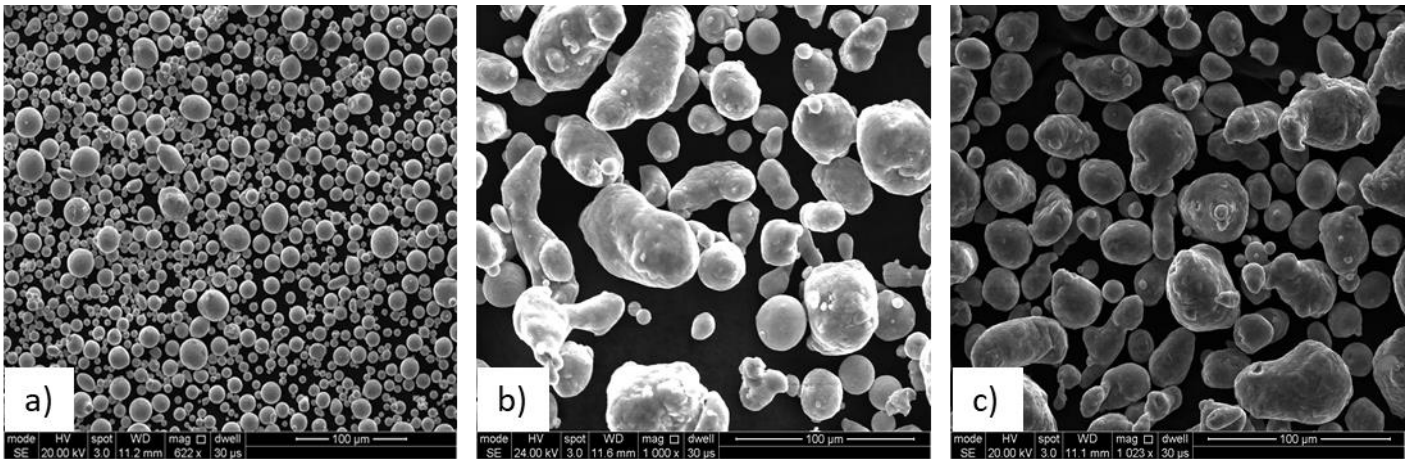
Figure 4-12 SEM micrographs of as received (a) Copper and (b) Aluminum powder supplied by Alpoco and LPW and (c) Al-Cu12 in-situ blended composition

4.5   Porosity results and discussion

4.5.1   Room temperature porosity results

A relative density of 96-99.5% was achieved in samples with the combination of lowest scan speed and highest laser power of 180W, a similar trend could be observed in the test samples processed with 160W and 170W in combination with low scan speed. As expected it was found that due to the high reflectively

and thick oxides presented on the surface of aluminium alloy, higher energy densities were required to reduce lack of fusion porosity.

Olakanmi and Louvis, reported similar affirmations in the processing of different aluminium alloys proving that the densification was improved as the laser power increased while the scan speed and scan spacing decreased (Olakanmi 2015, Louvis et al. 2011). Moreover, the less dense test samples with a relative density of 86-92% were found with those samples produced using higher scanning speeds, this may be a consequence of using insufficient energy density to melt particles or by instabilities in the melt pool.

In addition, it was found that using a hatch spacing of 0.07 mm and scanning speeds between 119-147 mm/s achieved the highest relative density values. This may be attributed that both elements requires higher energy density due lower laser absorption of aluminium and their reflective properties for each element, forcing the use of slower scanning speeds. Figures 4-13 to 4-15 shows the relative density of fabricated samples as a function of Scanning Speed (SS) in mm/s for three of (160,170,180 Watts).
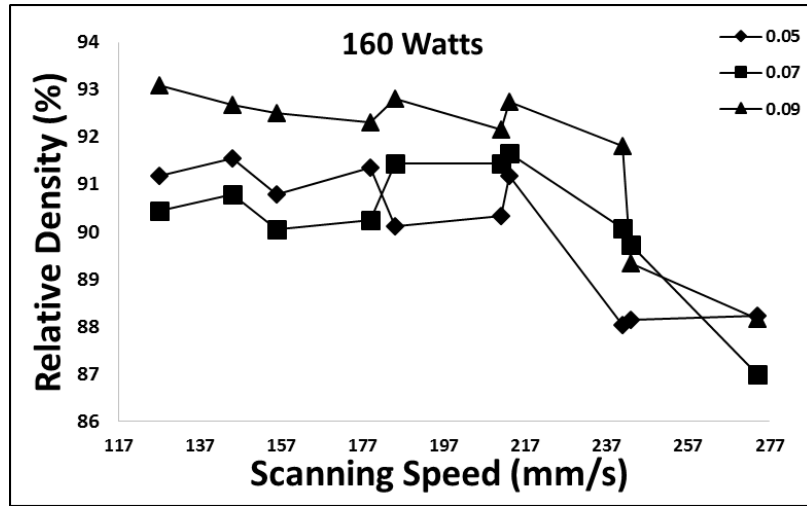
Figure 4-13 Relative density of SLM processed elemental Al-Cu12 (room temperature), hatch space of 0.05-0.09mm and laser power of 160W.
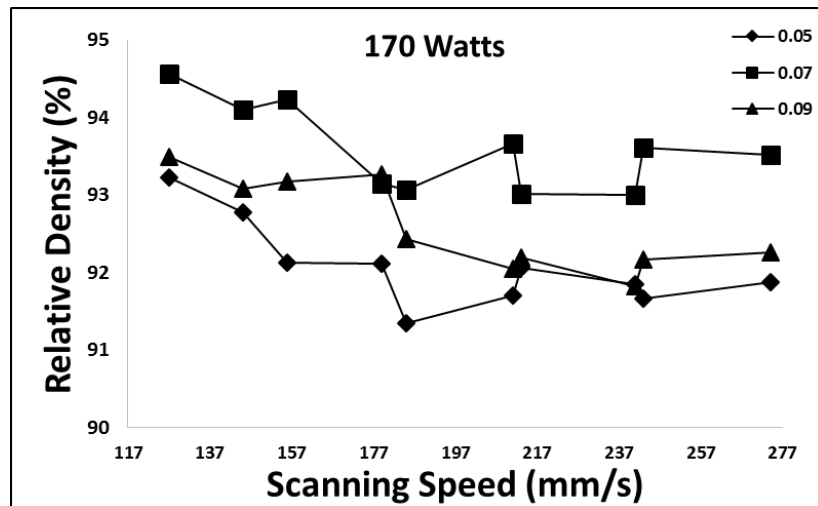
Figure 4-14 Relative density of SLM processed elemental Al-Cu12 (room temperature), hatch space of 0.05-0.09mm and laser power of 170W.
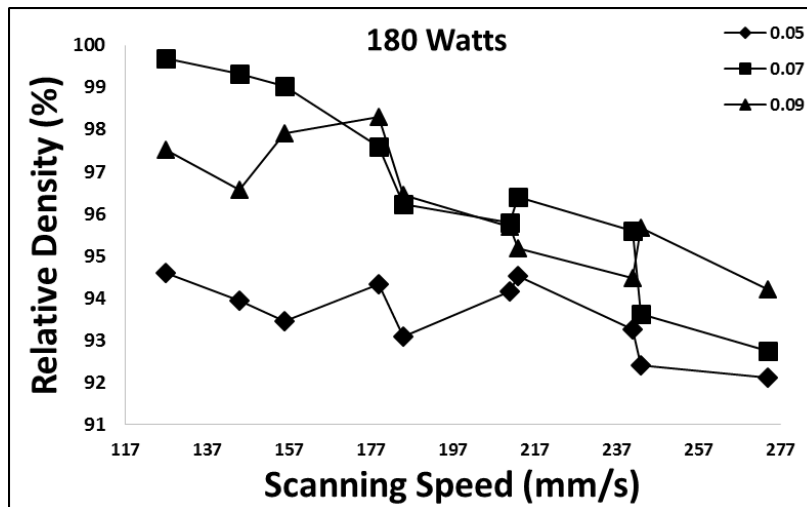
Figure 4-15 Relative density of SLM processed elemental Al-Cu12 (room temperature), hatch space of 0.05-0.09mm and laser power of 180W

Table 4-7 shows the optical micrographs of Al-Cu12 SLM samples produced to density optimization. The highest and lowest sample porosity attained are represented in function of laser power and exposure time. A combination of 180W and 160µs exposure time produced samples with the highest density value of 99.6% can be seen at the bottom right of the Table 4-7, moreover the combination of 160W and 130 µs exposure time produced samples with lowest density value. Is possible to observe a clear variation of porosity morphology in Al-Cu12 samples with different parameter combinations.

For micrographs samples obtained at 160W processing condition, it was observed that irregular shaped voids were present on the sample. These irregular voids are possibly caused by insufficient energy input resulting in a

partial melting of powder as seen in Table 4-7, this could also be attributed to rapid solidification of aluminium alloy without completely filling the gaps created in the melting pool due velocity of laser processing (Rayleigh instability).

There is a notable difference in porosity morphology for samples processed using 170W, it can be observed by the spherical shape, which is a typical characteristic of metallurgical pores. This may be caused by the presence of oxygen or gases trapped during the melting process caused by excess of energy.

After the analysis of the Porosity-Process parameters comparison map shown in table 4-7 it can be assumed that, the higher the energy input in combination with higher exposure time, the higher the density of the produced sample.

Figure 4-17 illustrate a better explanation of the porosity formation for SLM in processed samples when there is an insufficient laser power input and the opposite scenario when there is an excess of input energy processing the powder bed top layer.
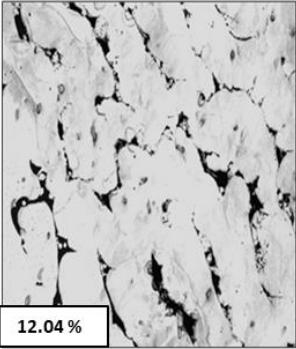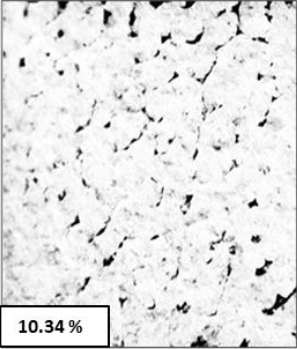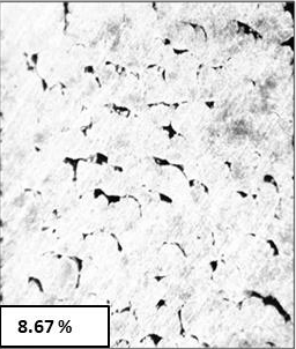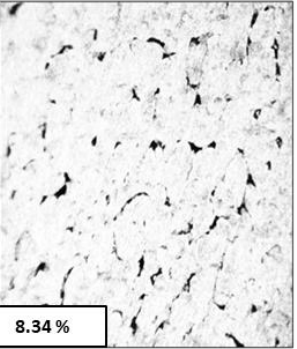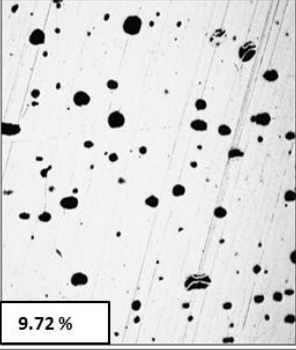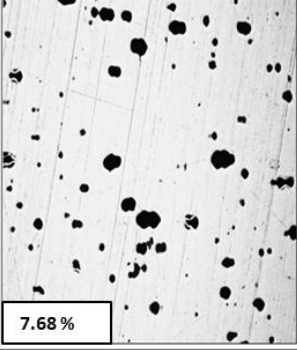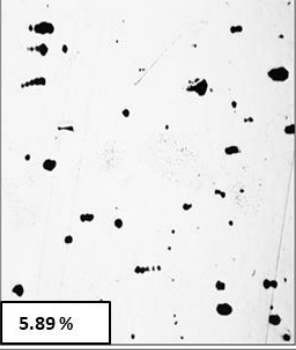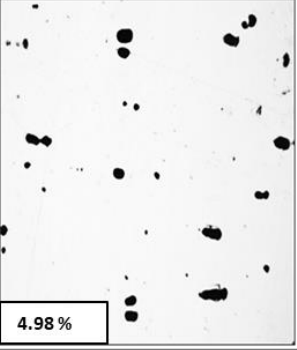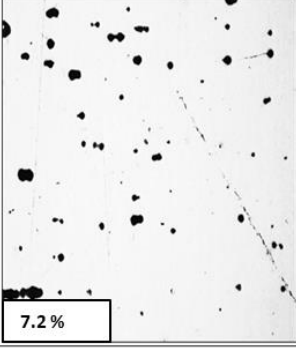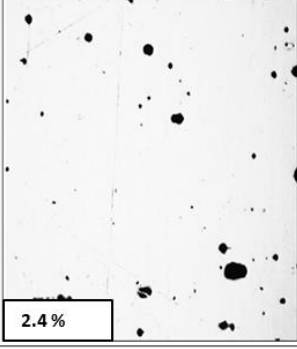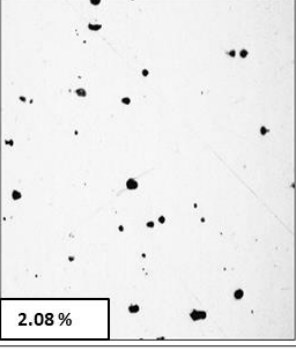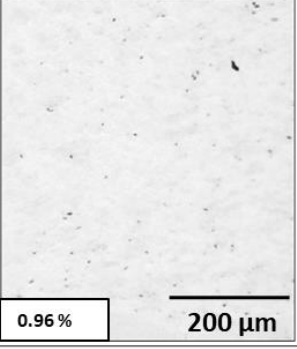
P(W)/ET(µs)	130	140	150	160
160	12.04 %	10.34 %	8.67 %	8.34 %
170	9.72 %	7.68 %	5.89 %	4.98 %
180	7.2 %	2.4 %	2.08 %	0.96 %

200 µm

Figure 4-16(a) shows a density comparison from table 3-3 results where test sample 8 (180W), represents the optimum combination SLM process parameters for Al-Cu12. This combination resulted in maximizing density achieving 99.6 %, with a few metallurgical voids, meanwhile Figure 4-16(b)

shows test sample 24 (160W), which shows numerous irregular shaped porosity caused by lack of fusion resulting in sample density of 87%.
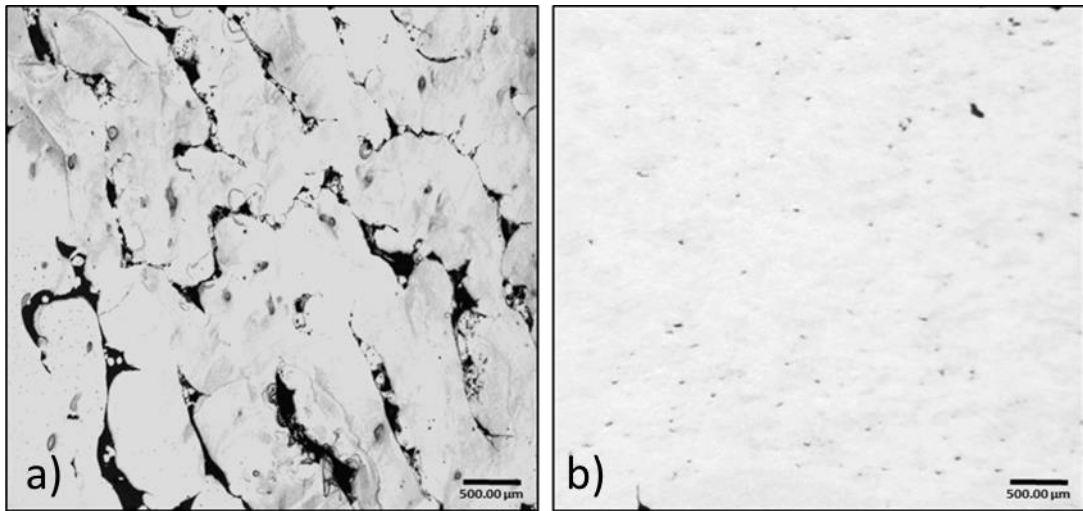
Figure 4-16 Density comparison from room temperature density optimization trials: (a) Sample 24(160W) with 87% of relative density and (b) Sample 8(180W) with 99.6% of relative density
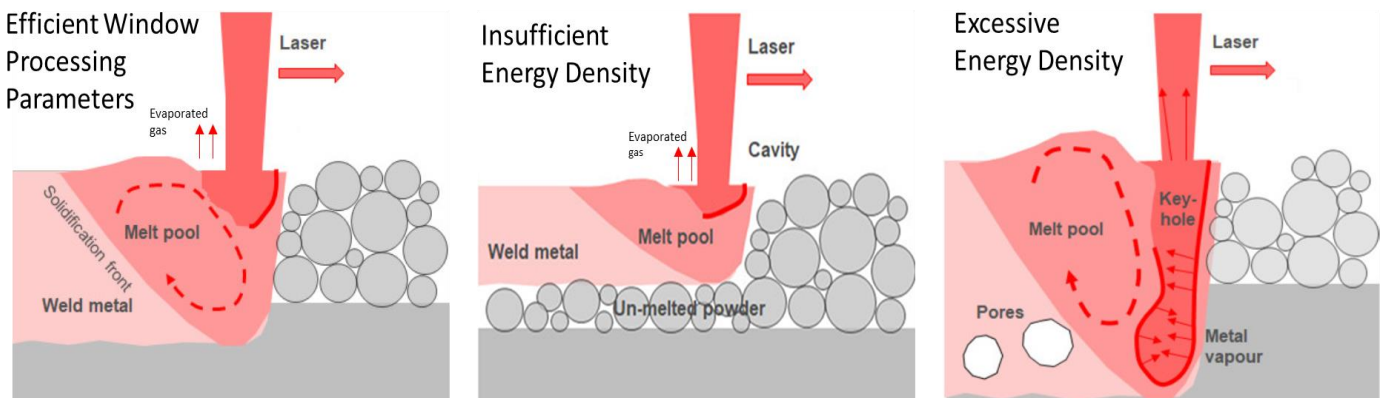
Figure 4-17 Explanation schematics for porosity formation due lack of fusion and excessive energy compared with an efficient window processing (Adapted from Saunders 2018)

4.5.2 Heated bed processing porosity results

A temperature of 400º C degrees (with -5 +10 degrees, for system variation)was selected for the high temperature trials representing the 0.7 of melting point temperature of Al-Cu12 aluminium alloy, this temperature is required for ASLM processing to maintain a stress reduced state. It was necessary to optimize the SLM processing parameters at high temperature to assure high-density parts and good mechanical behaviour of future ASLM parts created by this method.

At the beginning of experimentation, optimized process parameters for room temperature was used for the high temperature trials and it was found that optimization parameters for elevated pre-heating substrate conditions are slightly different from room temperature parameters. For a powder bed pre-heat temperature of 400°C a combination of 170W and 160 µs exposure time produced test samples with the minimum internal voids resulted in a relative density of 99.2%.

It was found that the best combination parameters for room temperature (180W and 160µs) failed many times during processing using a pre-heating substrate at 400 ºC. The elevated powder bed generated excessive heat input causing evaporation of material, increased porosity and generated an irregular surface

(balling) within the processed material this create some layer distortions and eventually coalition with the recoating system creating the failure of the test sample.

Figures 4-18 to 4-20 shows the porosity results of high temperature in situ Al-Cu12 SLM samples produced for density optimization. Table 4-8 shows the porosity comparison map (Laser- Scanning speed) results for the high temperature trials.

Nevertheless, Al-Cu alloys are susceptible to solidification cracking (Manduit 2017). There was no evidence of micro-cracking for samples processed using optimized parameters.

Table 4-8 Heated bed processing porosity comparison of SLM processed elemental Al-Cu12, plotted against laser power and exposure time

P(W)/ET(µs)	130	140	150	160
160	7.26 %	9.85 %	5.64 %	3.55 %
165	8.15 %	6.6 %	3.98 %	1.58 %
170	7.89 %	5.77 %	2.66 %	0.58 %
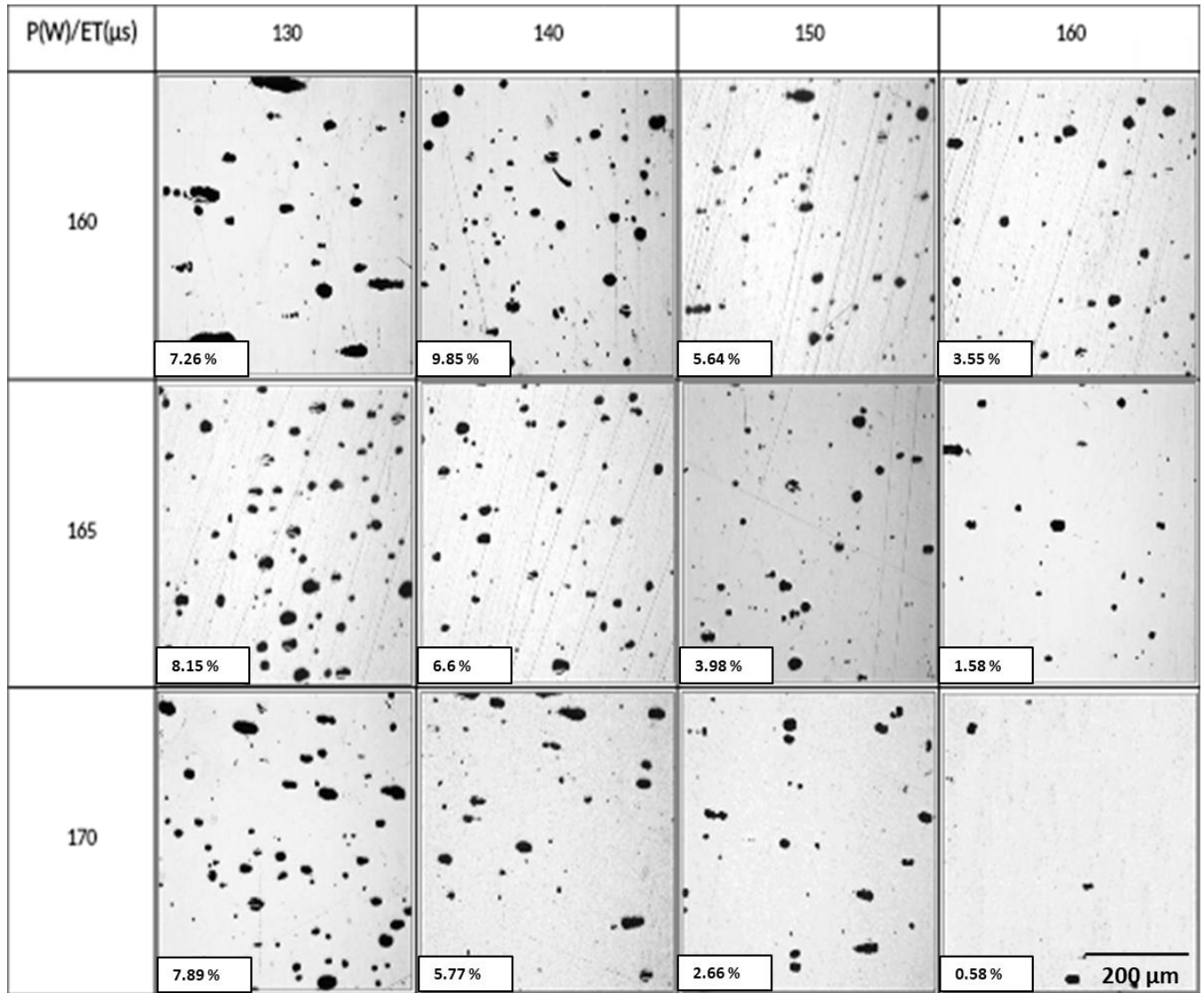
A similar trend can be observed for samples processed at high temperatures in comparison with room temperature samples in Table 4-7 where the resulted dense part is a combination of higher exposure time while using a higher laser power- see Figure 4-22.
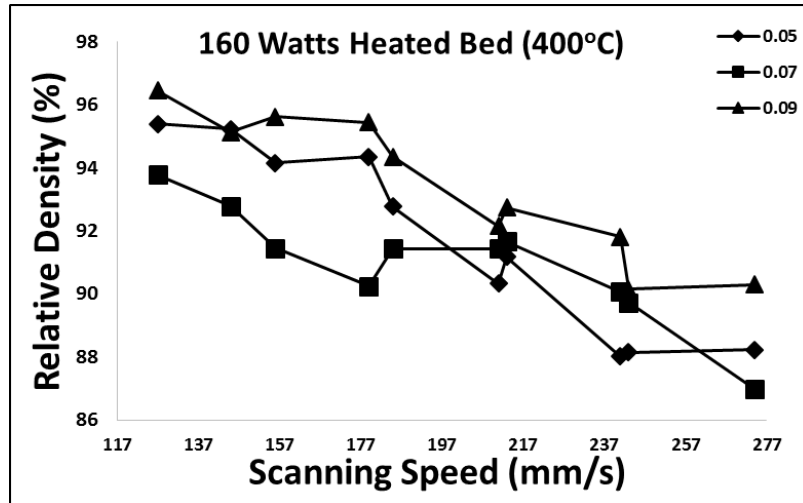
Figure 4-18 Relative density of SLM processed elemental Al-Cu12 (High Temperature), hatch space of 0.05-0.09mm and laser power of 160W
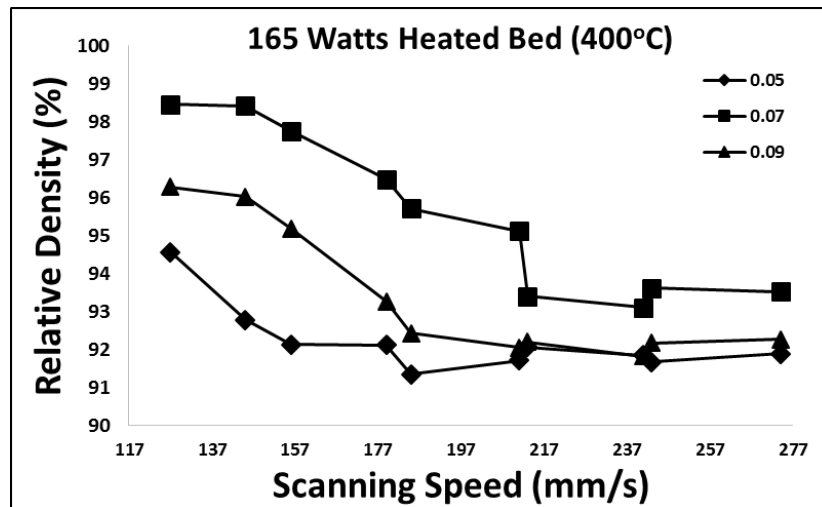
Figure 4-19 Relative density of SLM processed elemental Al-Cu12 (High Temperature), hatch space of 0.05-0.09mm and laser power of 165W

129
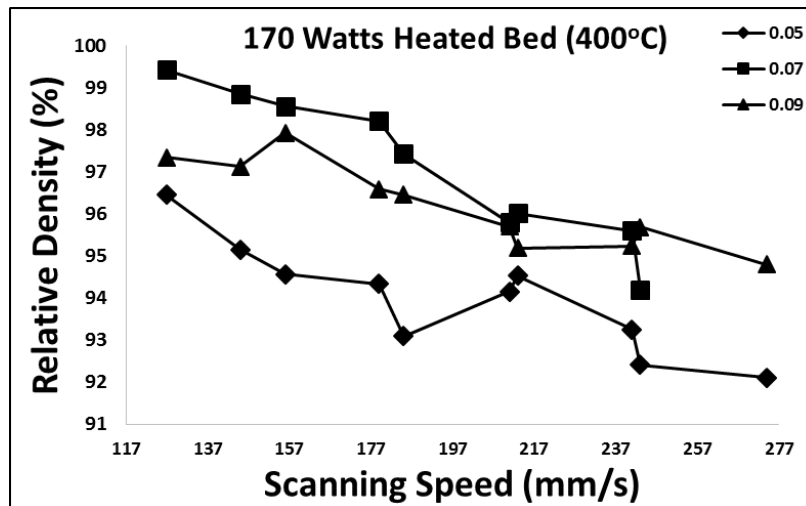
Figure 4-20 Relative density of SLM processed elemental Al-Cu12 (High Temperature), hatch space of 0.05-0.09mm and laser power of 170W

Figures 4-18 to 4-20 shows similar density behaviour trends compared to room temperature processing parameters, the low density attained corresponds to test samples with short exposure time resulting in insufficient input energy creating partial melting or instabilities in the melt pool formation generating poor densification as final result. These instabilities are generated by Marangoni forces creating differential surface tension between the centre and the edge of the melt pool as the laser move forward through the scan track.

As a result of use of heated bed the processing window becomes narrow due the fact that the material required less energy input to create a similar melting effect without heated assistance. Figure 4-21 shows how the process outcomes vary using high temperature substrate.
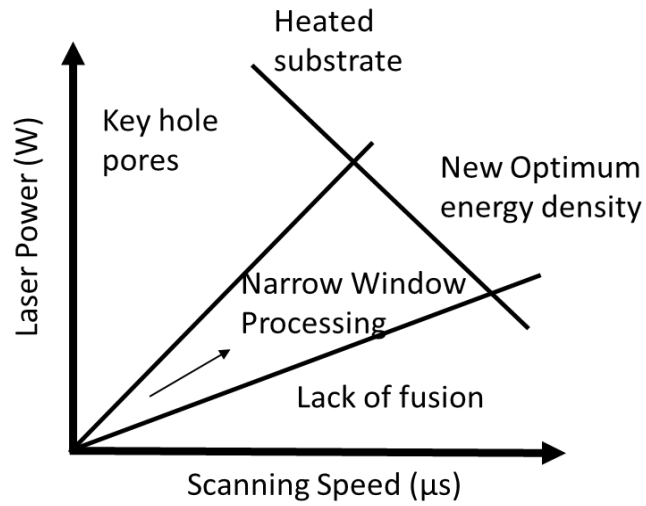
Figure 4-21 Adapted Laser power vs scanning speed (P-V Diagram) for high

temperature substrate. (Adapted from Suter 2017)
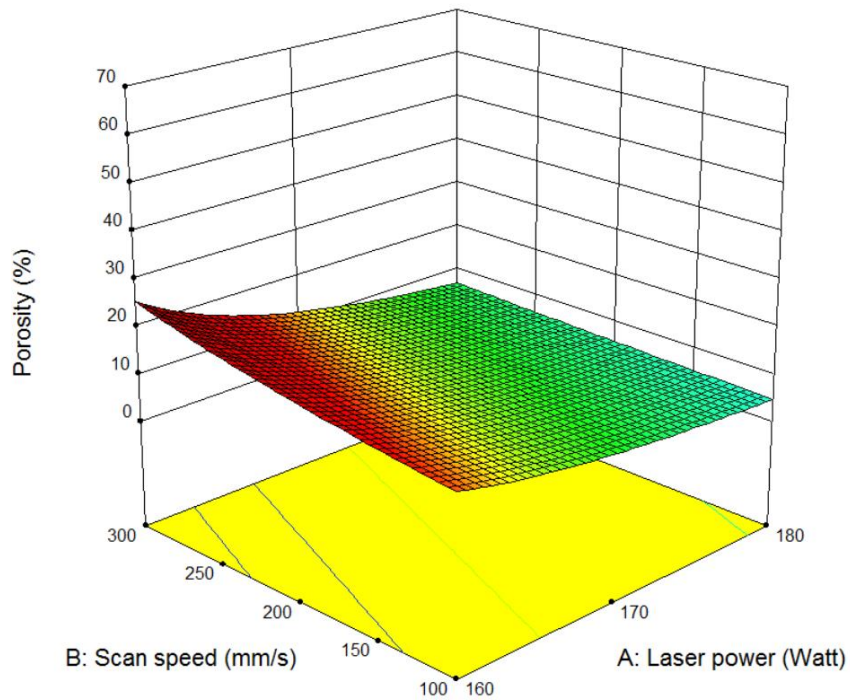
Figure 4-22 Plotted porosity trend for all processed samples of in-situ Al-Cu12

form elemental powder (room temperature and high temperature 400ºC)

4.6 Influence of processing parameters

4.6.1 Laser energy density

Laser energy density vs relative density chart is shown in Figure 4-23. Samples processed using 180W exhibited a relative density >96%. The lowest relative density in produced samples resulted of the combination of 160W and low energy density input. It was found that using an energy density of above 230 J/mm^3 resulting in a poor consolidation for in-situ Al-Cu12 alloy processed samples. Based on the presented densification results in section 4.5.1, a relative density of 99.5 % was achieved using an energy density input of 540 J/mm^3 while using a fixed laser power of 180W.
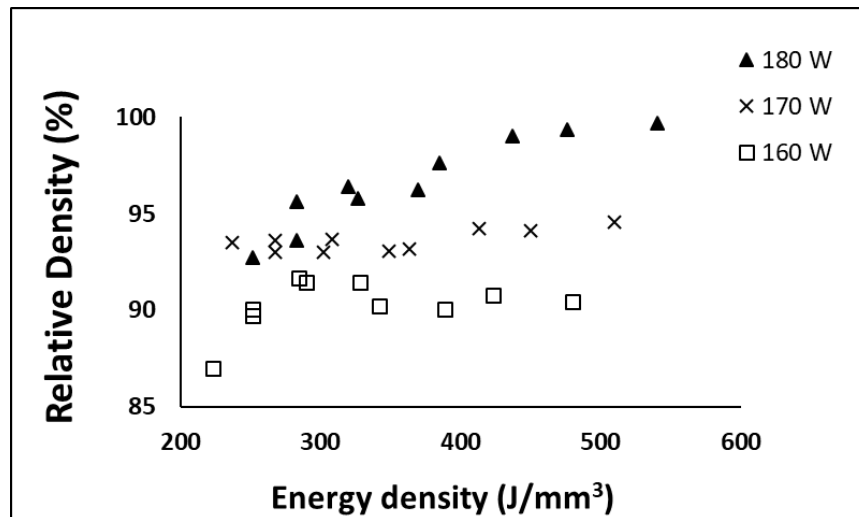
Figure 4-23 Energy density vs relative density for processed samples using different laser power

4.6.2 Variation of laser power

Figure 4-24 shows the highest relative density achieved for processed samples using three different levels of variation of laser power using the same layer thickness. It was found that, most of the porosity morphology resulted using 160W is irregular shape due the lack of fusion and insufficient energy input to break the oxide film formed at the surface of every new layer. The presence of internal voids decreased by increasing the laser power to 180W resulting in a very small spherical voids possible resulted by residual inert gas chamber trapped during the melt pool turbulence effect.

Larger voids typically larger than 20 µm are the result of inadequate laser penetration (Aboulkhair 2014), this macro-voids are much larger than pores resulting of gas trapped and can be distinguished by larger irregular morphology with sharp edges. This sharp edges act as stress concentration zones that trigger mechanical failures during applied loads. The expression to understand the lack of fusion can be described as the following:

Lack of Fusion = Melt pool depth / Layer thickness
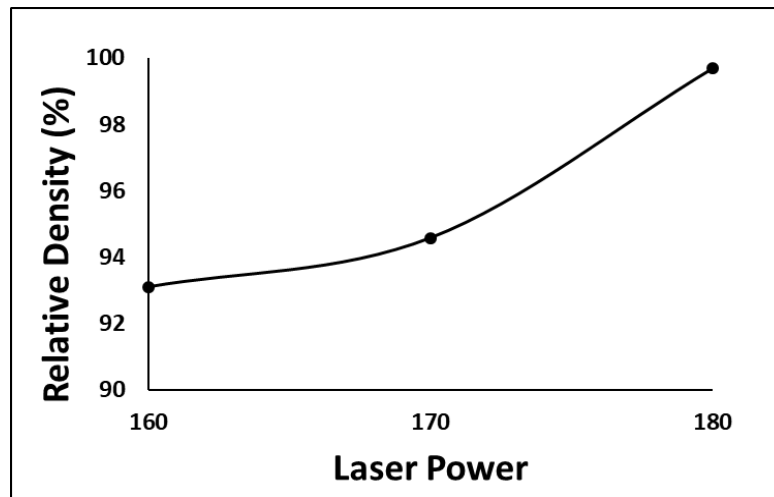
Figure 4-24 highest relative density achieved for processed samples using the best combination of parameters for different laser power

4.6.3 Variation of Scanning Speed

Figure 4-25 shows relative density against the variation of scanning speed for processed samples using different laser power values. The highest density for all processed samples were produced using 119 mm/s and a laser power of 180W, which also produced small spherical shaped pores in comparison with the large irregular voids, resulted from the parameter combination of higher speed and low laser power. It was found that for standard SLM process for in-situ Al-Cu12 the influence of scanning speed on pore size and shape has a negative impact when the velocity is faster, this may be attributed to the low laser absorptivity of Al and the high laser reflectivity of both elements.

134
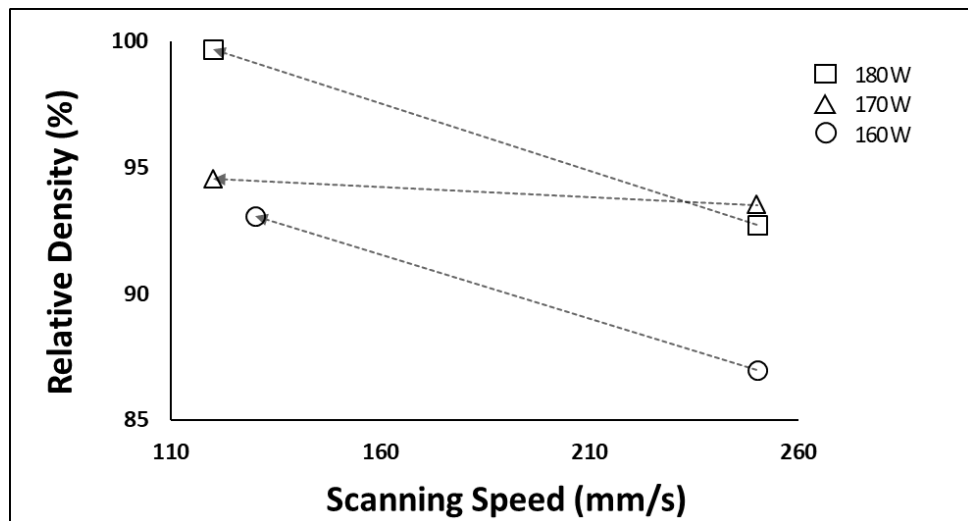
Figure 4-25 Influence of scanning speed on porosity optimization for different laser power conditions; 160W, 170W and 180W

4.6.4 Variation of hatch spacing

Figure 4-26 shows the variation effect of using three different levels of hatch space for processed samples using optimum combination parameters of exposure time and point of distance (scanning speed). 70 µm was the optimum hatch spacing for samples processed using a laser power of 170W and 180W meanwhile for samples processed using lower energy input required a shorter hatch space to maximize densification, this may be attributed to insufficient energy density to cover the large distance of overlapping scanning during laser processing. Conversely, for samples processed using higher energy density found it well to cover the overlapping scanning using a hatch space of 70 µm.
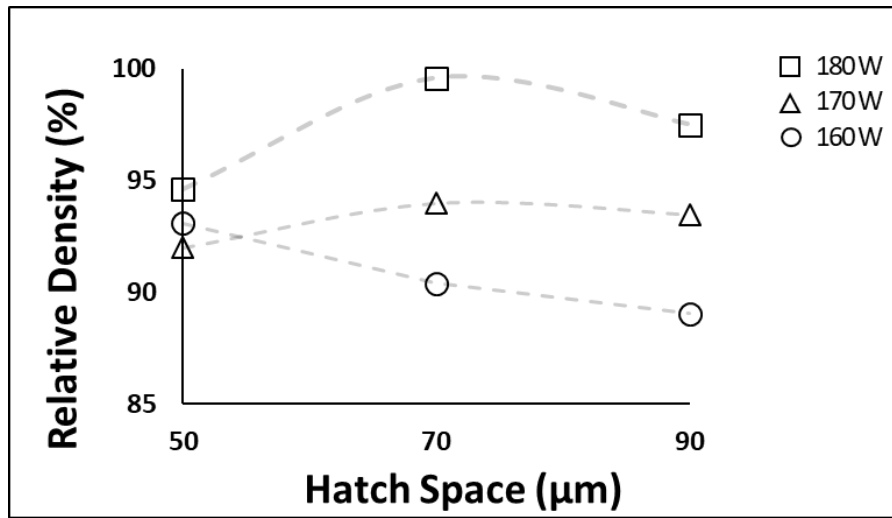
Figure 4-26 Influence of scanning speed on porosity optimization for different laser power conditions; 160W, 170W and 180W

4.6.5 Effects of in-situ heated bed processing

Figure 4-27 shows the variation in porosity for in-situ Al-Cu12 processed samples using a preheating substrate with a temperature close to maximum annealing range (400°C) and standard built conditions. It was found that, the use of high temperature substrate are beneficial for samples processed with 160W and 170W. Samples processed using preheating substrate with a laser power of 160W increased 3% for overall relative density and for samples processed using 170W the increment was in 5% in densification, this increment in density is related to the low thermal energy required for wettability of material while using the preheating system as external energy input. It was

observed the porosity morphology also changed for samples using 160w from irregular shapes to spherical as shown in table 4-7.
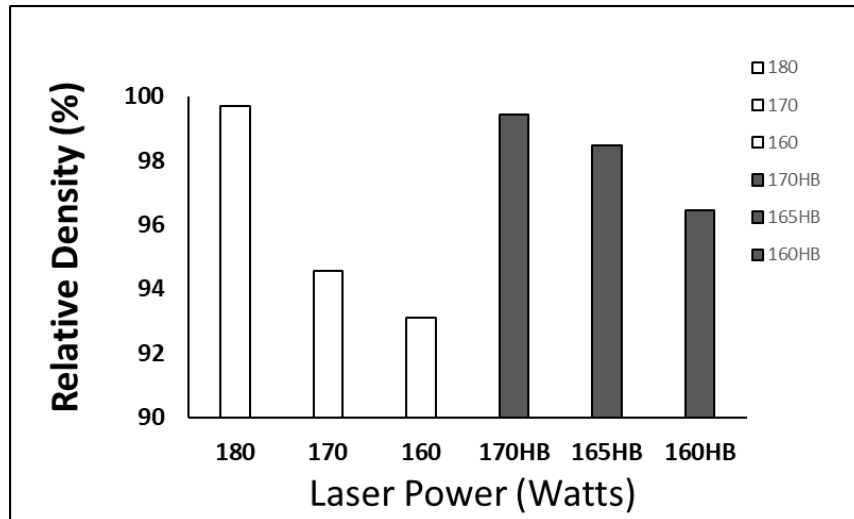
Figure 4-27 Influence of high temperature pre heating substrate on porosity optimization for different laser power conditions; 160W, 170W and 180W

4.6.6 Effects of natural properties of elements

Aluminium and Copper powders are well known for their poor laser absorptivity properties incrementing the difficulty to be processed by SLM. Table 4-9 shows the absorptivity values for powder processed under SLM wavelength range compared with other popular feedstock powders processed via AM. The poor absorptivity of Al and Cu has a negative impact in the interaction of heat source-energy absorption of the blended material as feedstock for SLM processing. The heat source for SLM process with a Gaussian distribution laser source is represented with the following formula:

$$Pd \;=\; \frac{fP}{\pi r_b^2\, t_1}\,[\eta_p + (1\text{-}\eta_p)\,\eta_1]\exp\left(-f\,\frac{r^2}{r_b^2}\right) \qquad \textbf{\textit{Equation 3-2}}$$

Where f is the Gaussian distribution factor, P is the total energy input, r_b is the radius of the heat source η_p is the fraction of energy absorbed by the powder during processing η_1 is the coefficient of absorptivity, r, is the radial distance from any axis point of heat source and t_1 is the layer thickness. The heat absorption by the particles in SLM depends of materials properties, packing density and particle size.

Table 4-9 Material absorptivity coefficient for AM powder materials under

SLM laser wavelength (Palik 1981)

Material Powder	Powder absorptivity coeficient for Gaussian distribution laser source
Al	0.18
Cu	0.12
Ni	0.51
SS	0.58
Ti	0.62

In SLM processes when laser source is in contact with powder, part of the energy is absorbed and other part of the energy is reflected. The low absorptivity of the feedstock material demands high energy density to process this aluminium alloy, this high energy may cause that some molten powder

particles fly out the melt pool resulting in spatter formation on the processed layer. Figure 4-28 shows the schematics of powder reflection during SLM process.
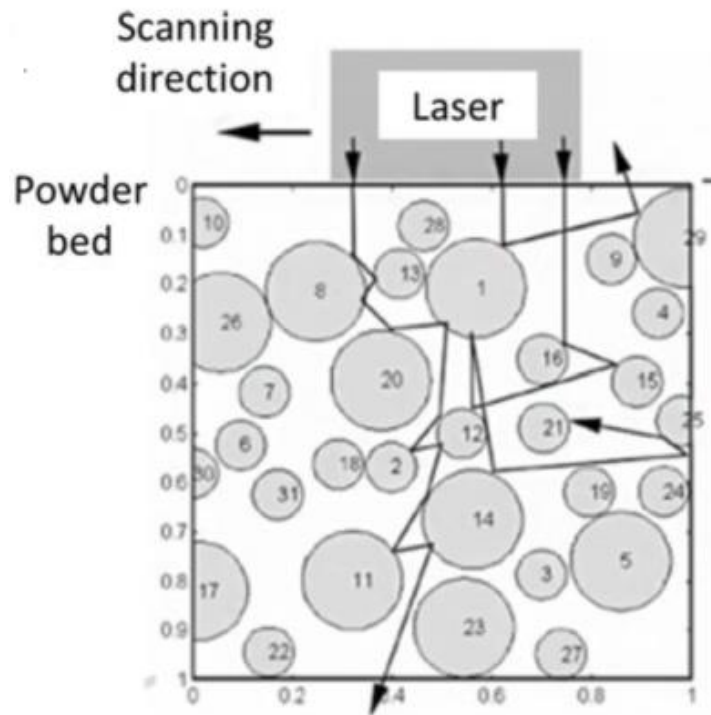
Figure 4-28 Schematics of inter-reflection of laser beam and heat absorption by powder particles during SLM (Wang 2002)

4.7 Conclusions and summary

The main conclusions of the SLM process optimisation parameters for in-situ AlCu-12 alloy are:

The meander scanning strategy and a layer thickness of 40 µm showed the minimum porosity for initial trials using benchmark parameters from aluminium alloys. The use of different size of powder particles improved the packing density therefore a positive impact on density.

The thermal model developed for this study provided a good direction for experimental work by reducing the number of experimental trials needed for density optimisation providing a narrow processing window.

The laser power required to optimization parameters for elevated pre-heating substrate conditions are slightly different from room temperature parameters due the excessive energy input that create evaporation.

The DoE made a significant contribution to in-situ AlCu-12 processing parameter optimisation for room temperature and elevated temperature of 400ºC. The study shows that:

- A statistical approach has been used to evaluate the influence of processing parameters on the porosity of in-situ AlCu-12, showing trends for porosity in processed samples using different laser power.

- A critical energy density value was found to achieve a minimum porosity for processed samples. For in-situ AlCu-12 an energy density of 540 J/mm^3 founded the best resulted in the combination of optimum parameters: Laser power of 180w, Point of distance of 20 µm and Exposure time of 160 µm.

Chapter 5: Microstructure analysis and influence of In-situ high temperature processing

This chapter focuses on the microstructure analysis and the influence of high temperature processing on the microstructure, precipitation and composition of samples fabricated via SLM at room temperature and high temperature. The results shown in this section are from samples built using optimized parameters identified in chapter 4.

5.1 Microstructure analysis

5.1.1 Room temperature microstructure

Selected samples undertaken at room temperature using optimised parameters revealed a hypo-eutectic microstructure produced as a result of in-situ alloying of mixture of Al and Cu powders. The melt pool variable sizes shown in Figure 5-1 are due to the multiple laser scan rotation used by scan strategy Meander 67° degrees and is believed during these overlaps the reheating increased the diffusion of Cu particles into the α-Al matrix.

Figure 5-2(a) and (b) shows an optical microscope image of an etched sample at different magnifications revealed a rich aluminium α matrix microstructure

with dendritic arms for Al-Cu12 characteristic of hypo-eutectic aluminium alloys. Figure 5-2(b) shows the revealed microstructure for selected etched samples consisting in a rich α-Al matrix (in light colour) surrounded by a finely Al-Cu eutectic mixture α and θ, all samples shown a directional solidification caused by the melting pool direction normally presented in SLM microstructures. A transition from a finer microstructure to coarser dendrite microstructure from the core of the melt pool due to the heat source (thermal flow) moving forward to continue processing could be observed, this phenomena is explained with the schematics shown in figure 5-3.
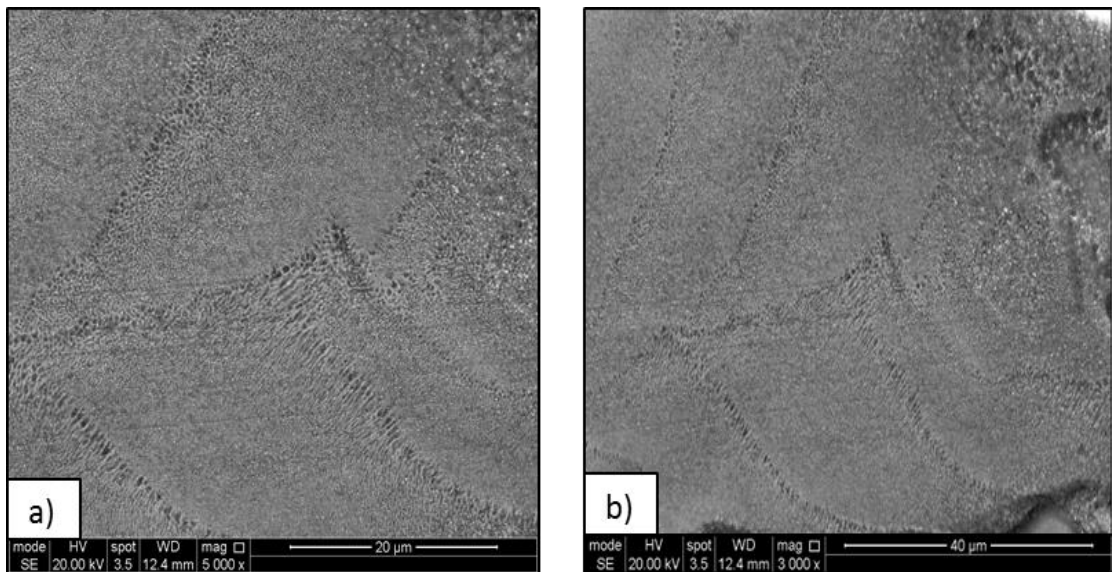
Figure 5-1 Optical microscope images of etched Al-Cu12 sample showing variable melt pool at different magnifications (a) 20 µm (b) 40 µm.
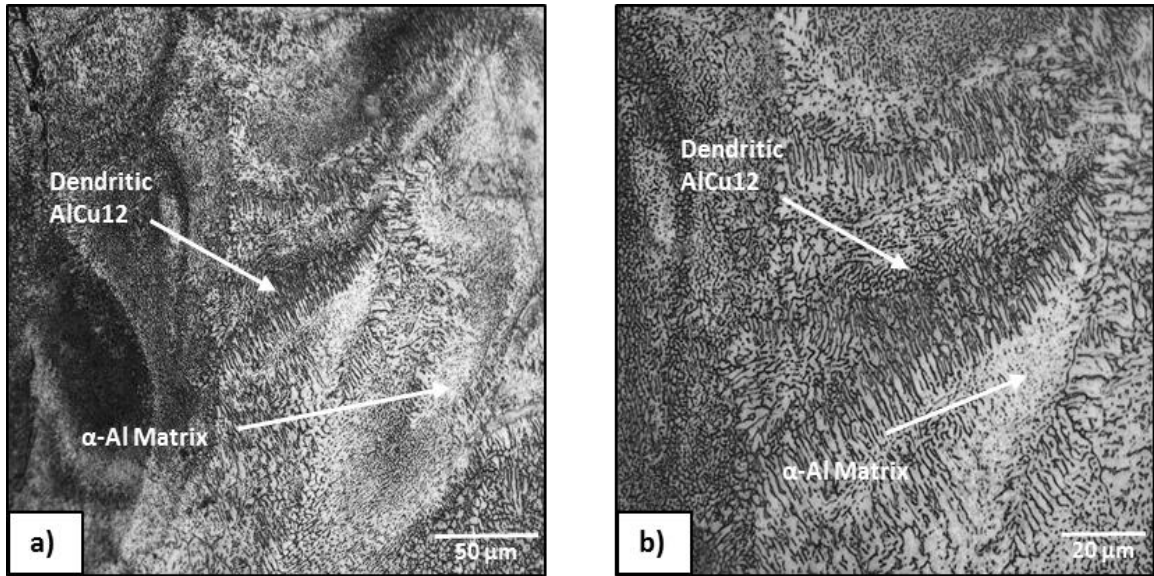
Figure 5-2 Optical microscope images of etched Al-Cu12 sample showing

dendrite orientation (a) 20 μm (b) 50 μm.
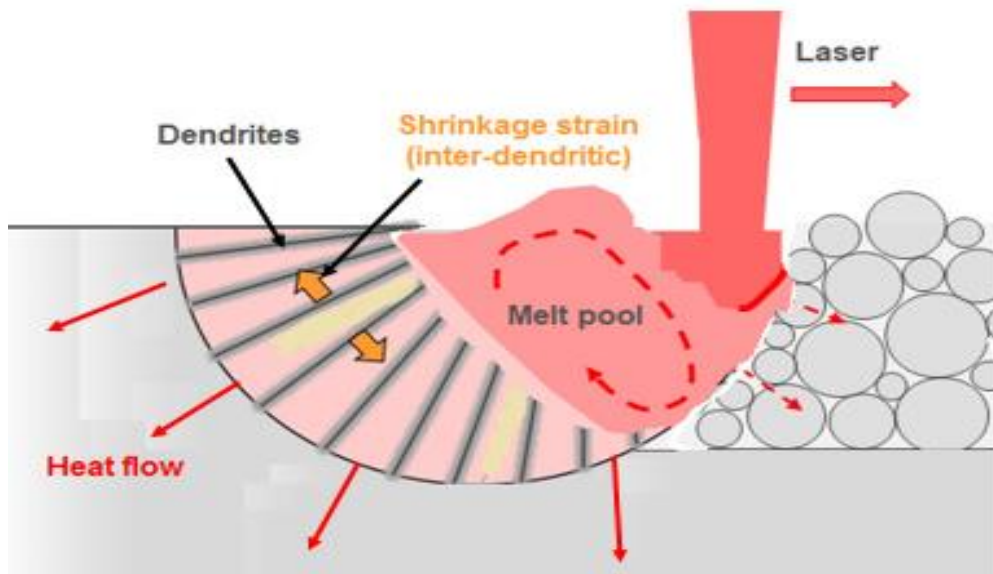
Figure 5-3 Schematics of SLM dendritic microstructure formation towards the

outer edge of melting pool (Adapted from Saunders 2018)

Figure 5-4 shows Cu rich zones in some regions of etched samples, this is likely due to the differences of the melting point for both elements with insufficient laser energy time and Cu limited solute diffusivity in Al. In Figure 5-4 (b) a non-diffused Cu rich zones are shown larger than Cu average particle size within the feedstock. Even though the re-melting overlap provides extra diffusion sites to Cu particles, larger particles cannot fully diffuse into the *α*-Al matrix due the short exposure time of molten pool.

As complementary information it is important to mention that for the in-situ mechanical mixing powder processing it is believed that would be segregation of powder within the blend which may reduce the uniformity of powder feedstock or even agglomeration during the mixing stage due the differences on weight of each particular powder (Louvis et al. 2011). This non-uniform build-up of highly reflective Cu powders with high melting temperature (1085°C) in comparison to Al particles (660°C), may create un-alloyed defect sites or weakness that will act as initiation failure points during mechanical testing. Figure 5-5 shows EDS mapping for Cu rich zones not well distributed during the deposition for selected samples processed at room temperature.
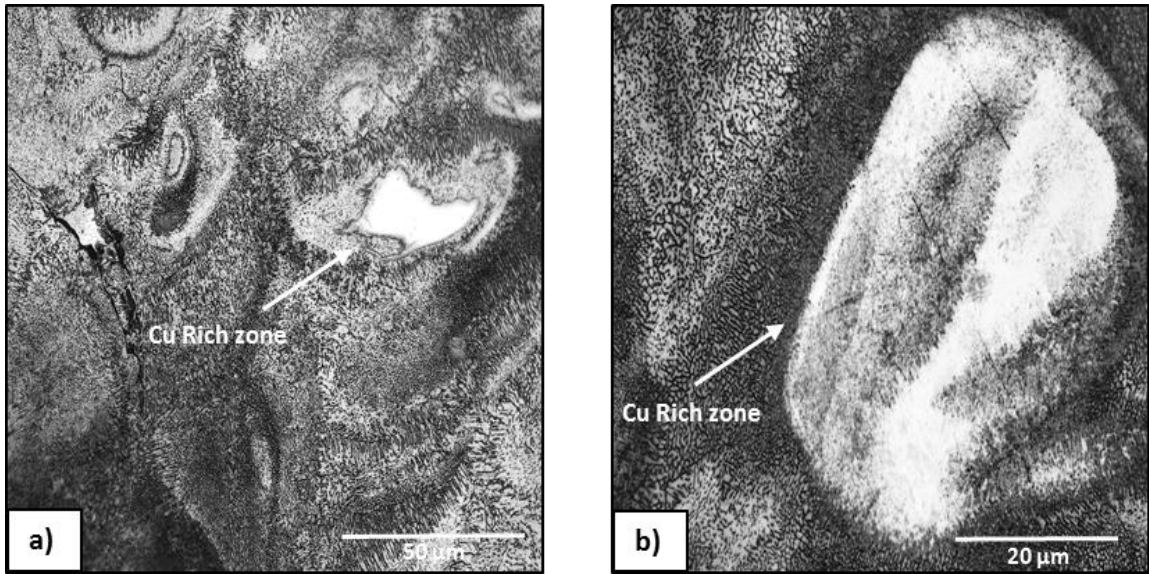
Figure 5-4 Non-fully diffuse Cu-rich zones at room temperature (a) 50 μm (b)

20 μm
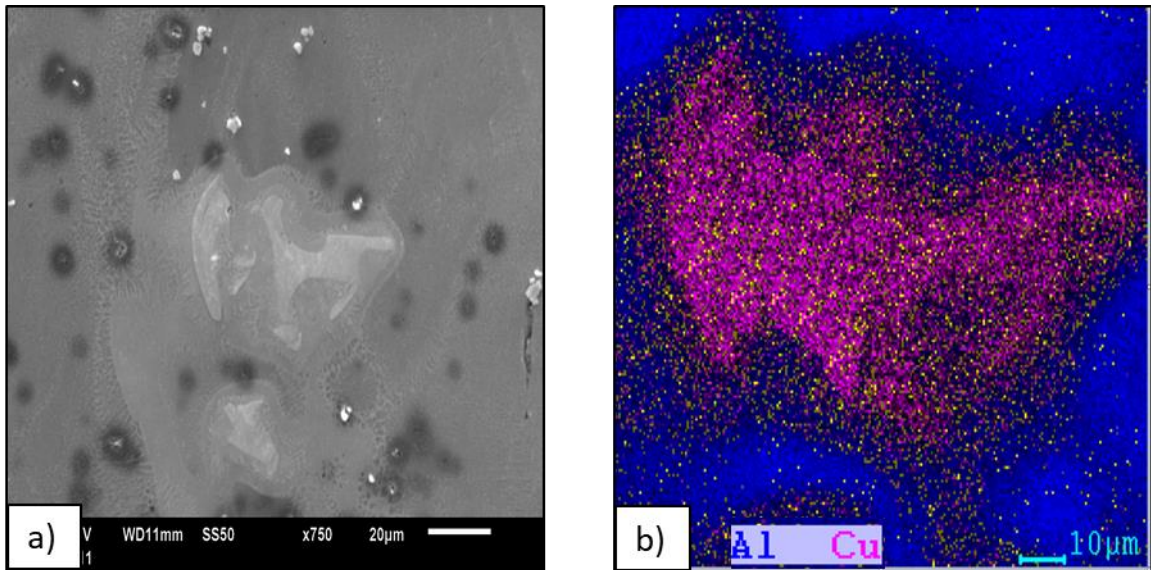
Figure 5-5 Cu rich zones not fully melted within Al-matrix at different

magnifications a) SEM analysis, b)EDS element mapping at higher

magnification

5.1.2 Heated bed processing

A set of samples processed with optimal process parameters for high temperature were selected for microstructure analysis. Figure 5-6 shows the polished cross-section of test samples built using high-temperature pre-heating substrate of 400ºC. In all etched samples, it can be observed that there is a uniform α-Al matrix with coarser dendritic cells compared to samples built at room temperature powder bed pre-heating. This is a result of the elevated pre-heating temperatures and slow cooling rates to room temperature over a period of 4-5 hours creating the effect of in-situ age heat treatment. This in-situ heat treatment may result favourable for mechanical properties due the growing AlCu2 precipitates within the matrix.

The α-Al matrix is mainly concentrated in the darker grey areas while the lighter area exhibits coarser higher α-Al (Cu) content. EDS elemental mapping analysis was performed to observe the distribution of individual elements for the samples processed at 400º C to assess homogeneity and distribution of elements for selected samples. Figure 5-7 shows the results of element mapping where is possible to appreciate a clearly differentiation by colour the distribution for both element in the final alloy processed at high temperature.

147

For all selected etched samples, it was found that both elements in the blended alloy Al and Cu were uniformly distributed over the analysed cross section, indicating a well-blended uniform microstructure. Al_2Cu intermetallic phase transformation found well distributed in the α-Al matrix with no evidence of Cu rich zones or non-diffused Cu particles as shown in some processed samples for room temperature. The absence of this Cu-rich zones may be the resulted of elevated temperature improving melting behaviour and allowing the material to remain within its diffusional temperature range while processing for a prolonged time compared to normal processing without assistance of pre-heating temperature.
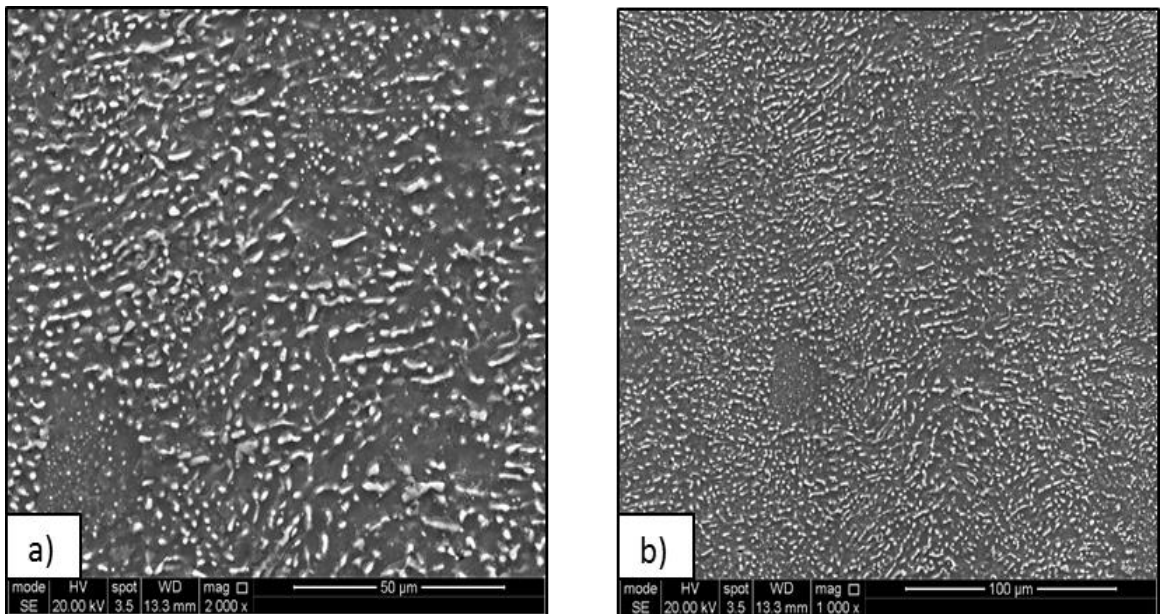
Figure 5-6 SEM micrographs of in-situ SLM Al-Cu12 samples processed at 400ºC, (a) 50µm, (b) 100µm scale bar.

148
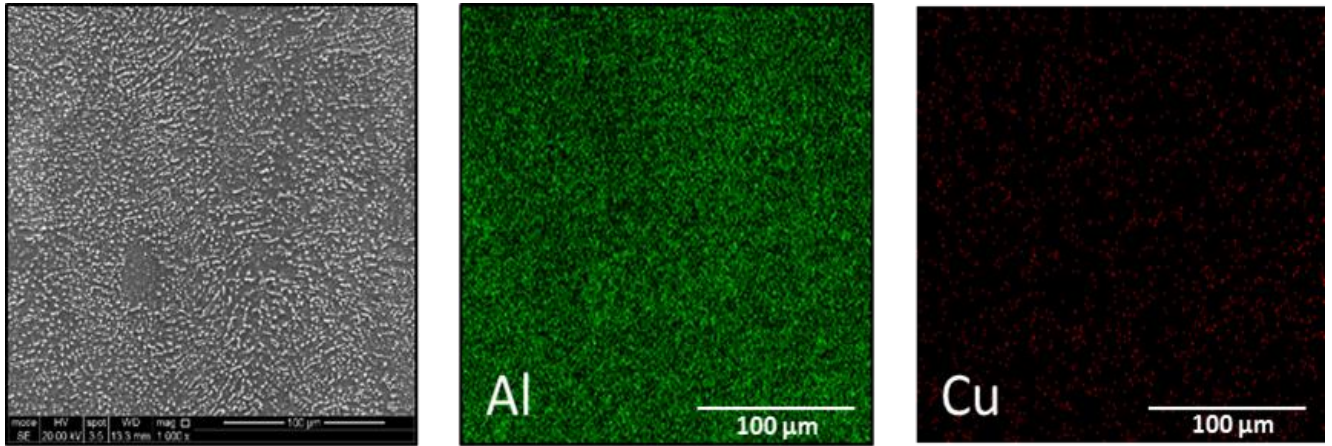
Figure 5-7 EDS mapping of elements and distribution of Al (in green) and Cu (in red) for a sample processed at 400º C

Figure 5-8 shows the comparison of room and high temperature in-situ Al-Cu12 SLM samples processed and AlCu12 alloy produced by casting process where it is possible to observe a notable difference between microstructures. In samples processed at 400º C, Figure 5-8 (c) a coarser microstructure with a very fine intermetallic compounds (θ phase) resulted from the preheating substrate assistance and the slow cooling rates after processing are distributed homogeneously within the Aluminium $α$ matrix, Figure 5-8 (b) shows a fine hypo-eutectic microstructure with dendritic arms resulted from standard SLM processing.

Figure 5-8 (a) is a master sample of AlCu12 alloy processed by casting where it can be seen a large coarser globular microstructure with fine eutectic

microstructure compared with SLM processed samples at room and high temperature. Is possible to observe how samples with dendritic arms structure belonging to the room temperature condition processing has effectively disappeared and replaced by a globular microstructure. For samples processed at a maximum temperature of 400 ºC. For the microstructure obtained in samples processed at higher temperature, is similar to the observed in semi-solid processing this findings correlates the ASLM novel processing method to produce in-situ alloys with no supports.
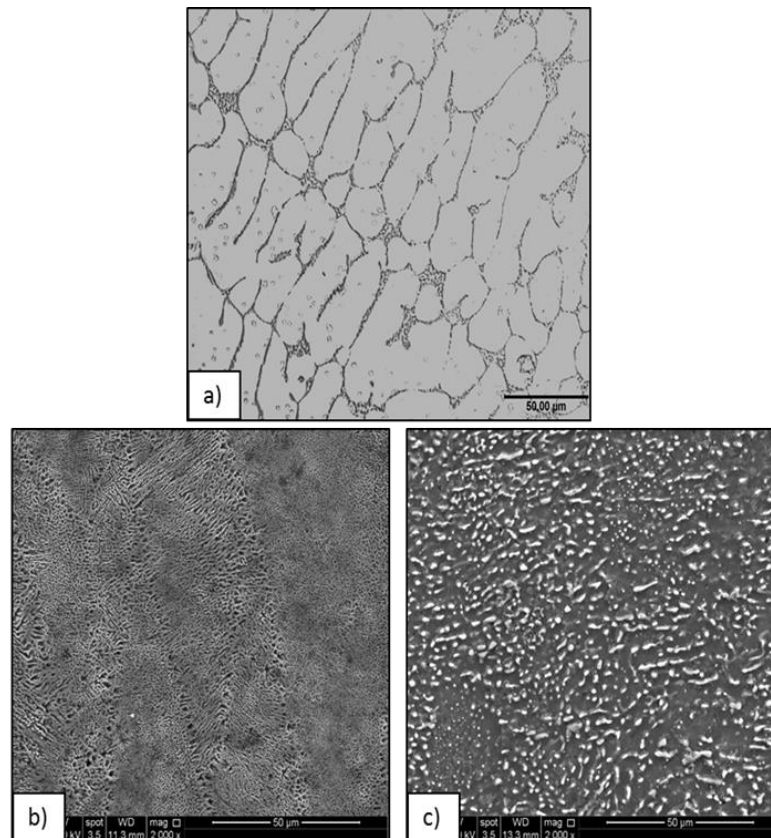
Figure 5-8 Microstructural comparison of (a) Cast AlCu12 alloy and in-situ Al-Cu12 SLM samples from elemental powder, (b) as built with fine eutectic features and (c) high-temperature (400ºC) with uniform coarser microstructure

5.2   X-Ray diffraction analysis

The X-ray diffraction analysis was performed for in-situ Al-Cu12 alloy selected solid samples using optimised parameters for room temperature and high temperature (400°C). The XRD phase pattern is presented in Figure 5-9 showing patterns at different processing temperatures. Pure aluminium and Al_2Cu intermetallic compound peaks were identified. The low intensity of Al_2Cu peak in the in-situ Al-Cu12 alloy samples at room temperature may be due its inhomogeneity zones inside the alloy.

For the in-situ Al-Cu12 samples processed at high temperature (400 °C), a higher intensity of Al_2Cu were detected, this may be attributed to the in-situ heat treatment (ageing) experienced at high temperature processing promoting the growing of Al_2Cu phase precipitates and the slow cooling rate post processing to enable enough time for diffusion of elements within the microstructure.
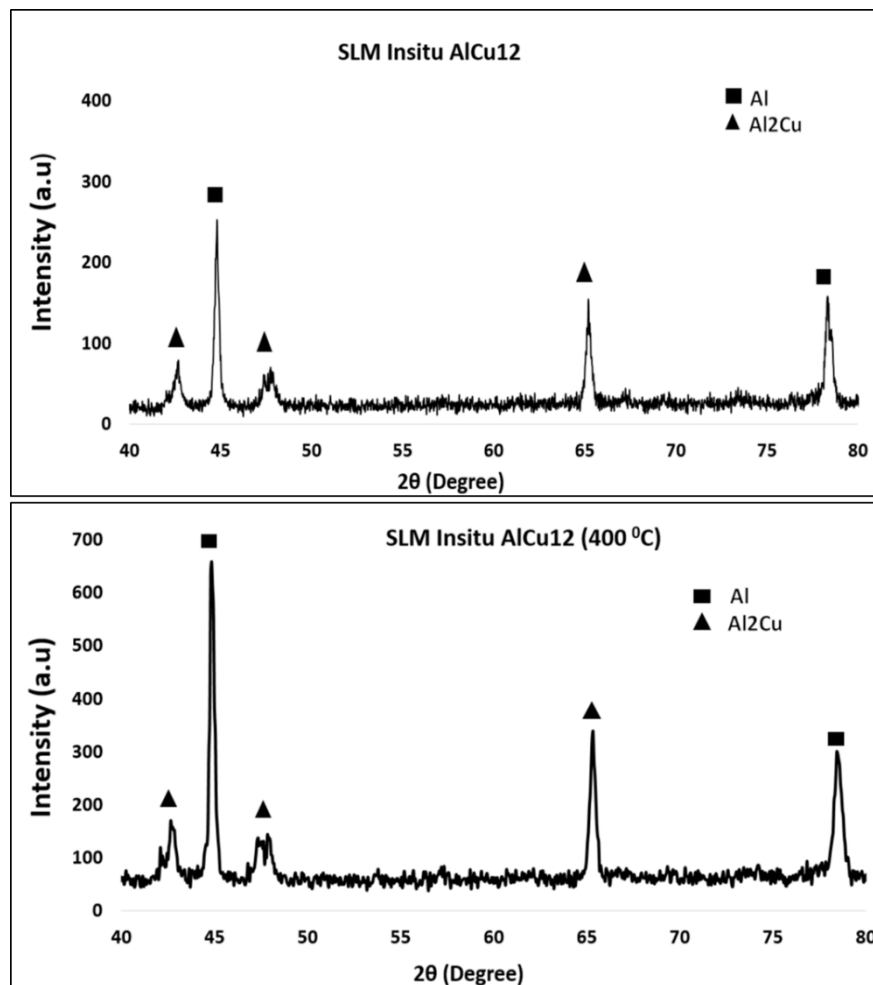
Figure 5-9. XRD patterns of SLM in-situ Al-Cu12 processed samples at (a)

room temperature and (b) preheating temperature of 400ºC

5.3   Effect of in-situ heat treatment

Based on microstructure shown for samples processed at room temperature and a maximum temperature of 400ºC, samples manufactured at high temperature exhibits a coarser homogeneous microstructure with no evidence of dendritic arms as shown for samples processed at room temperatures.

152

Figure 5-10 shows how the dendritic microstructure practically dissolved into granular microstructure with very fine particles of Al$_2$Cu (θ) intermetallic phase distributed into the Al-α matrix resulted of the prolonged in-situ annealing heat treatment provided by the pre-heated substrate used for processing. The use of preheating substrate at temperatures close to the range of annealing state creates a stress relaxation within the building part, maintaining the Cu particles in diffusion state and the large cooling rates enhance Al$_2$Cu precipitates out around the Al-α matrix. The preheating temperature represents 70% of the solid solution treatment for this binary composition.
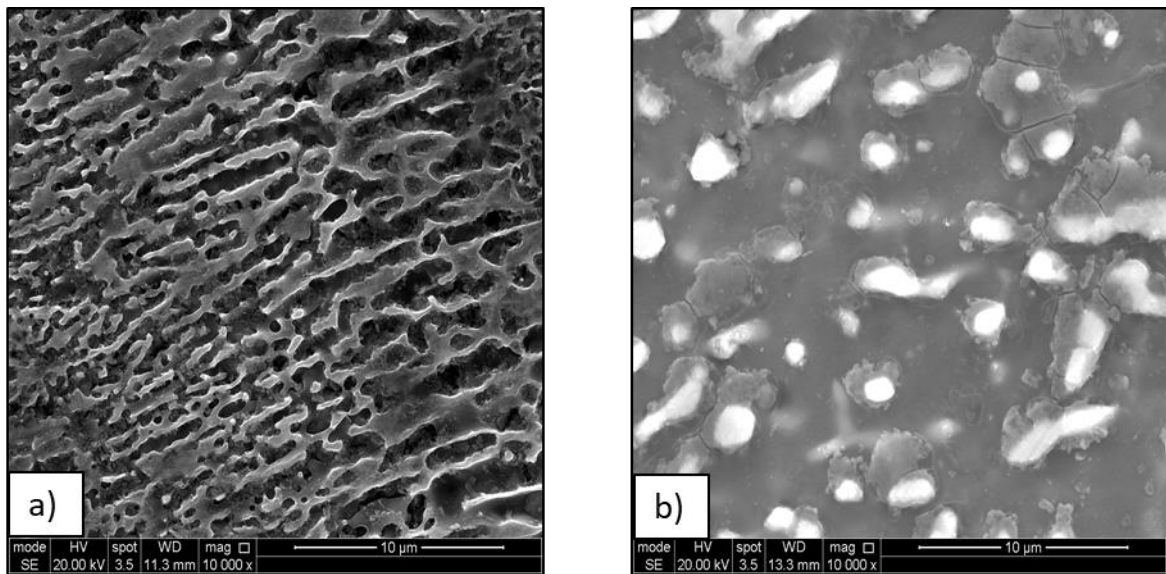
Figure 5-10 Comparison of the effect of in-situ heat treatment for samples processed at different temperatures: a) room temperature at higher magnification showing a fine dendritic microstructure, b) coarser microstructure with Al$_2$Cu precipitates resulted of in-situ heat treatment

It was noted that the presence of other intermetallic strengthening phases, that are stable in temperatures between 200-500 ºC such as, ζ (Al$_3$Cu$_4$) and γ (Al$_4$Cu$_9$) for this binary composition might be present surrounding in rich Cu zones within the microstructure in a very small quantities. However, with the SEM microscope used for this investigation was not able to confirm their presence within the microstructure of processed samples.

Additional microscopy analysis such as TEM may be needed to identified if this phase transformations precipitated during the prolonged period of high temperature exposure, for a more in deep analysis of the effects of pre-heating assistance processing.

5.4   Conclusions and summary

The main conclusions relating to the microstructure features are summarized as follows:

- The microstructure of in-situ Al-Cu12 alloy processed samples are influenced dramatically by the pre-heating substrate.

- Grain size of in-situ Al-Cu12 alloy processed at room temperature are fine due the rapid solidification of SLM process.

- Elevated temperature in-situ processing introduce a more homogeneous microstructure but also produce a coarser microstructure.

- A cellular-dendritic microstructure were observed in each individual sample.

- Al_2Cu (θ) intermetallic phase is well distributed into the Al-α matrix resulted of the prolonged in-situ annealing heat treatment.

- Two type of internal voids, the spherical voids produced by trapping gas and irregular shape voids which are induced by lack of fusion were identified

Chapter 6: Mechanical properties, influence of in-situ heat treatment

This chapter focuses on the mechanical properties of SLM samples fabricated at room temperature and high temperature conditions built by using the optimum parameters in different build directions for tensile testing. An additional build set using a pre-heating temperature of 350 ℃ was used to assess the influence of different pre-heating processing temperatures.

6.1   Tensile testing

Mechanical properties were measured using dog bone tensile specimens (previously showed in section 3.8) according to ASTM E8-16a Method B with a free-running crosshead speed of 2 mm/min manufactured using optimum process parameters for room and high temperatures.

Two sets of 6 samples using a pre-heating substrate temperature of 350 ℃ and 400 ℃ were tested for more understanding of the variability of mechanical properties at different pre-heating temperatures of SLM processing using the optimised parameters developed for high temperature. A reference values for sand and permanent mould aluminium alloys were taken from literature (Mondolfo, 1976) and (Polmear, 1995) with the purpose of compare

mechanical properties of similar to aluminium alloy AlCu12 processed by casting method. Figure 6-1 shows cylinders created for mechanical testing using optimised properties.
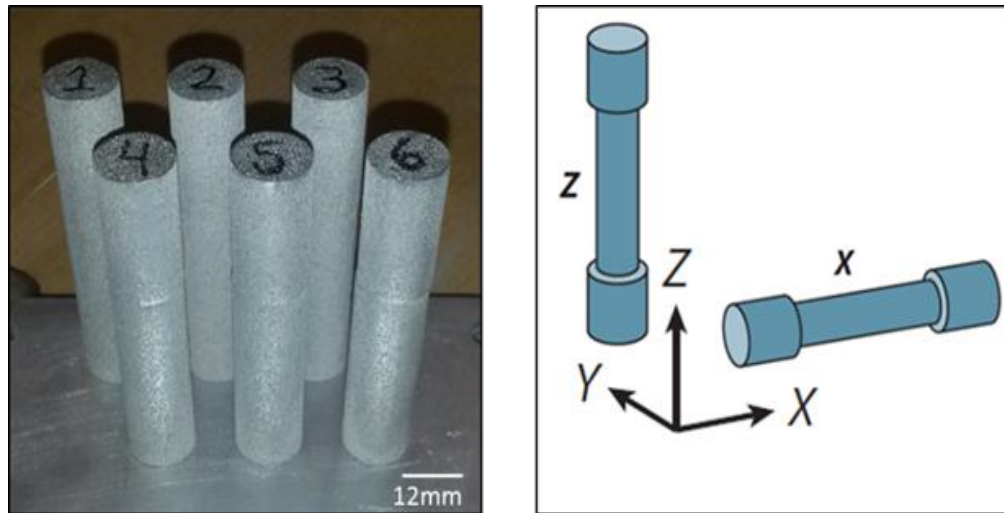
Figure 6-1 In-situ Al-Cu12 SLMed cylinder bars as built for tensile testing (65 mm height) and schematics of the different build orientations used for comparison of mechanical properties

Figures 6-2 compares the ultimate tensile strength (UTS), the yield strength (YS) and the percentage of elongation of all samples processed in "*Z*" and "*X*" axis build orientation at room temperature and the two sets of high temperature (350°C and 400°C) for in-situ Al-Cu12 alloy. Figure 6-3 shows the stress-strain plot for all processed tensile samples. The in-situ age heat treatment resulted by the use of high temperature substrate, greatly influences the mechanical properties for SLM in-situ Al-Cu12 alloy. During the processing the pre-

heating substrate keeps a temperature below solvus (below 500ºC), at this temperature the atoms of Cu can diffuse at short distances because the supersaturated α is not stable and the additional Cu atoms diffuse in nucleation sites and precipitates grow.

A maximum UTS of 172 MPa, was achieved for a tensile test specimen produced with pre-heating temperature of 400º C, this values are comparable to casting AlCu12 alloys of 120-180 MPa reported in literature by Mondolfo (Mondolfo, 1976) as shown in table 6-1 and A295 and A319 casting alloys reported by (J.R. Davies, 2001).
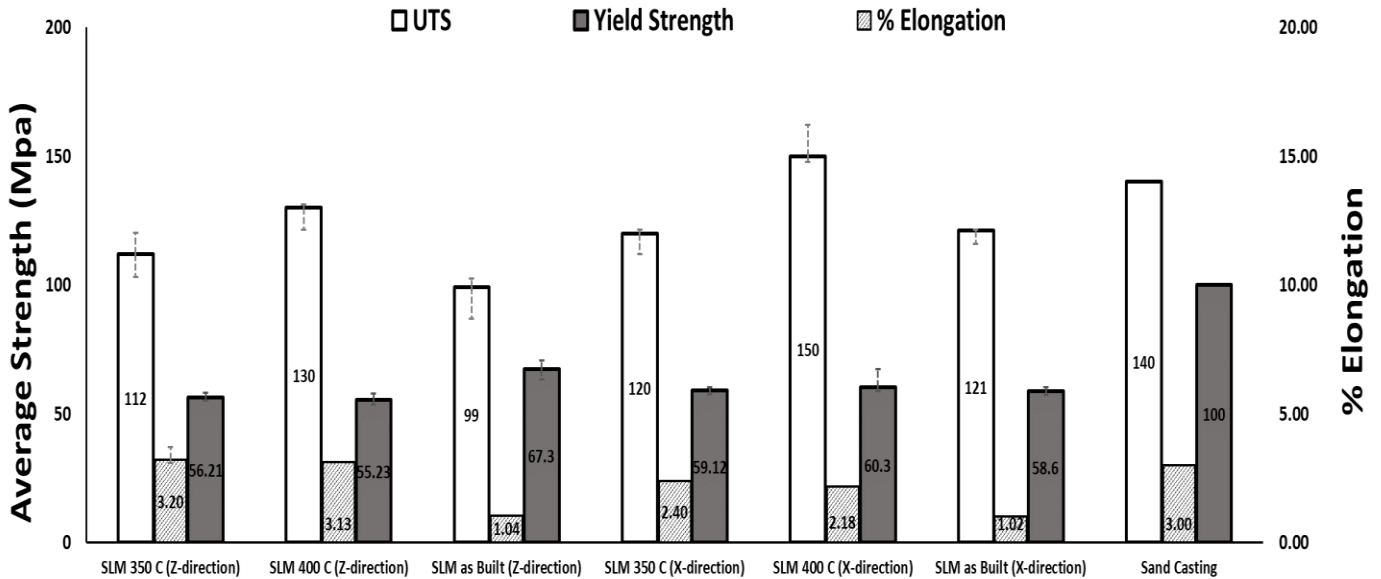
Figure 6-2 Mechanical properties comparison (UTS, yield strength and elongation) for SLM samples processed at room temperature and high temperature

The maximum values of UTS obtained were observed in the samples processed using the maximum temperature of 400º C produced in "*X*" build orientation, this represents an increase of 60% of UTS compared to the room temperature SLM samples built processed in the "*Z*" axis direction, which exhibits a UTS of 103 MPa. It is believed that samples processed at room temperature contained more defects (i.e un-melted Cu particles mentioned in section 4.3.1.1) than high temperature processed SLM parts and therefore significantly weaker mechanical properties.
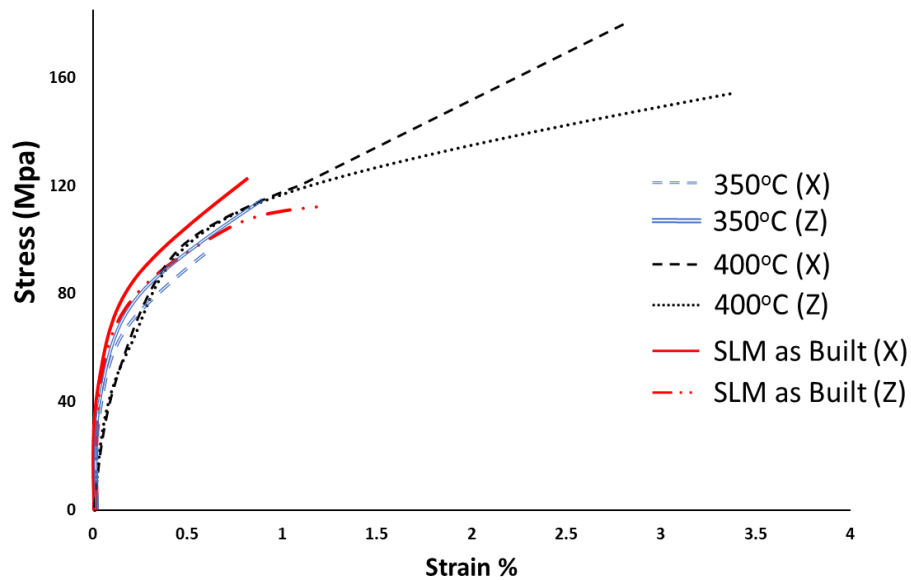
Figure 6-3 Stress-Strain curve for in-situ Al-Cu12 SLM at different build temperatures and build directions (Z and X)

Table 6-1 Mechanical properties of Aluminium-copper alloys (from

Mondolfo 1976)

MECHANICAL PROPERTIES OF ALUMINUM–COPPER ALLOYS

A. CAST

Property	Temper	5% Cu		8% Cu		12% Cu		Al–Cu–Ni	
		Sand	PM	Sand	PM	Sand	PM	Sand	PM
H_V in MN/m²	F	500–700	600–900	500–700	600–900	700–900	800–1 200	700–900	800–1 000
	T_4	600–900	700–1100			800–1 200	900–1 300	800–1 100	900–1 200
	T_6	1 000–1 200	1 100–1 400			1 000–1 400	1 000–1 500	950–1 300	1 100–1 400
UTS in MN/m²	F	100–200	150–250	120–150	150–250	120–180	150–200	150–250	200–300
	T_4	200–300	250–350			150–250	200–300	150–250	200–300
	T_6	250–350	300–450			200–300	250–350	200–300	250–350
YS in MN/m²	F	100–150	120–180	60–80	80–120	100–150	150–200	120–180	150–250
	T_4	120–200	150–250			150–200	200–250	120–200	150–250
	T_6	200–300	250–350			200–250	250–300	180–250	200–300
%E	F	3–6	2–5	2–5	2–3	0–2	0–2	0–2	0–3
	T_4	5–10	2–10			0–4	0–3	0–4	0–5
	T_6	1–5	0–5			0–2	0–1	0–2	0–2

For materials processed by SLM it is well know that interlayer voids will increase in "Z" building direction specimens due the high number of layers resulting in lower UTS by a high accumulation of porosity in the final component.

It was found that yield strength is inherently poor for samples processed at room temperature condition; these results would most likely be due to presence of internal defects as un-melted Cu particles and possible not fully optimised parameters. Ali reported similar behaviour in mechanical properties of Ti6Al4V using a pre-heating substrate via SLM (Ali et al. 2017). These findings suggested an incremental of strength (UTS) for parts processed using high temperature substrate, nevertheless it showed that processing with high

temperature substrate at the point to reach the maximum annealing temperature exhibits a sharp decline of 58% in UTS values regarding the martensitic temperatures for Ti alloy. The lower results of elongation could be attributed to low ductility of Cu rich zones presented in the microstructure and the supersaturated structure presented in Al-based SLM alloys.

It was found that samples processed at 350º C are just slightly better in mechanical properties than room temperature samples, this may have been caused by the precipitation of Al_2Cu intermetallic phase compared with the samples processed at room temperature and the internal stress reduction caused by pre heating the substrate.

6.2   Micro Hardness

Cross-sectioned cubes were used for Micro-hardness (Vickers) analysis. Results of micro hardness test of in-situ Al-Cu12 samples processed at different temperatures using optimum combination of parameters for SLM are shown in Figure 6-5. An increment of hardness of approximately 16% has been observed for samples processed under high temperature pre-heating substrate.

The hardness values achieved for in-situ Al-Cu12 samples are similar to sand casting values (70-90 Hv) and permanent mould (80-120 Hv) AlCu12% alloys. This increment may be attributed to a more uniform microstructure presented in all high temperature samples also to the increasing volume fraction of Al_2Cu intermetallic phase resulting from the in-situ artificial age treatment during the ASLM process.

Even though tensile testing had a variation of 60% between the maximum and minimum values the difference for hardness test samples are closer resulting in 16% of variation between the optimum hardness values achieved processed using a maximum temperature of $400^o\,C$ with 104 $HV_{0.1}$ and the samples for room temperature which achieved 88 $HV_{0.1}$. Schwab reported an increased hardness of 60% by using a high temperature substrate for processing Ti-5553, it was reported that the influence of high temperature in addition with slow cooling rates promoted α-phase precipitates increasing micro-hardness properties (Schwab et al. 2017).
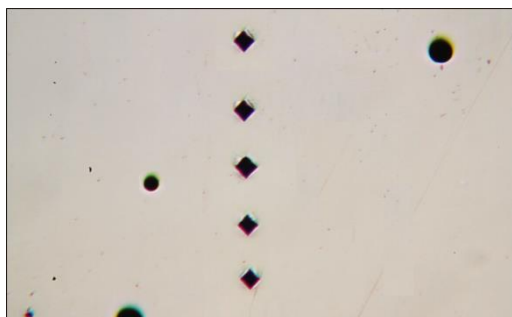
Figure 6-4 Micro-hardness results for in-situ Al-Cu12 alloy from elemental powder at room temperature (as-built)
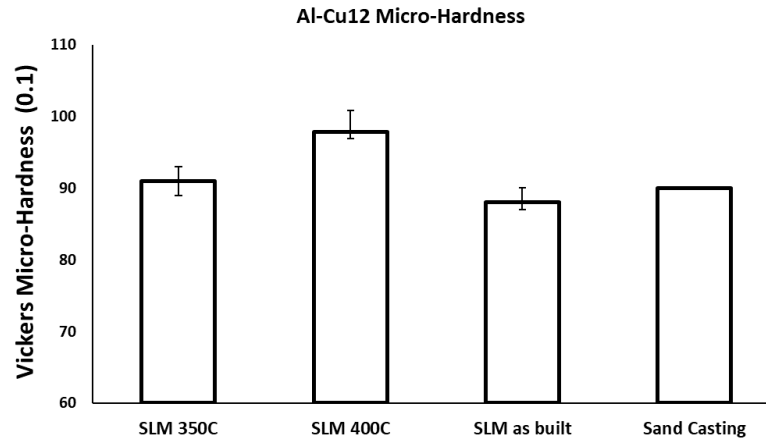
Figure 6-5 Micro-hardness results for in-situ Al-Cu12 alloy from elemental powder at 350°C, 400°C and room temperature (as-built)

6.3   Fracture analysis

Fracture analysis was performed for selected samples of in-situ Al-Cu12 processed at different temperatures using optimum combination parameters for SLM. To perform the fracture analysis is necessary to set the failed tensile specimens into SEM microscope in vertical position to analyse the top surface. The Figure 6-6 shows the fracture morphology SEM images of dense (>99%) in-situ Al-Cu12 samples built at room temperature and 400°C degrees. The analysis was performed only for samples achieved higher and lower UTS.

In Figure 6-5 (a) a fracture surface is observed for room temperature selected samples showing a typical ductile fracture developed during the tensile test. Figure 6-5 (b) shows a higher magnification image of the analysed fracture zone which reveals the presence of un-melted fine Cu particles distributed along the layer surface, this un-melted Cu particles within the solid structure acts as a weakness points promoting a premature failure during tensile test leading to poor UTS and elongation.

Even though process parameters were optimised to produce >99% density components, there were still difficulties to process the material and fully melt Cu particles, requiring a narrow optimized window processing parameters.

The fracture surface for high-temperature samples shows spherical dimples of gas trapped, due local vaporization of alloying elements during melt pool dynamics and a trace of an internal crack fracture generated during the tensile test, as shown in Figure 6-5 (c). Figure 6-5 (d) shows a higher magnification of the sample where it is possible to observe traces of un-melted particles of Al surrounding the vicinities of the internal crack fracture.

The un-melted Al particles trapped during the molten turbulence generated by Marangoni forces, resulting in poor homogeneity in the affected zone, causing the internal crack fracture due a weak metallurgy bonding. This un-melted

particles indicates that despite achieving nearly dense parts, still there are inhomogeneous areas and the processing parameters need still be further optimised to eliminate the presence of un-melted powder particles and gas occluded porosity on the final part.
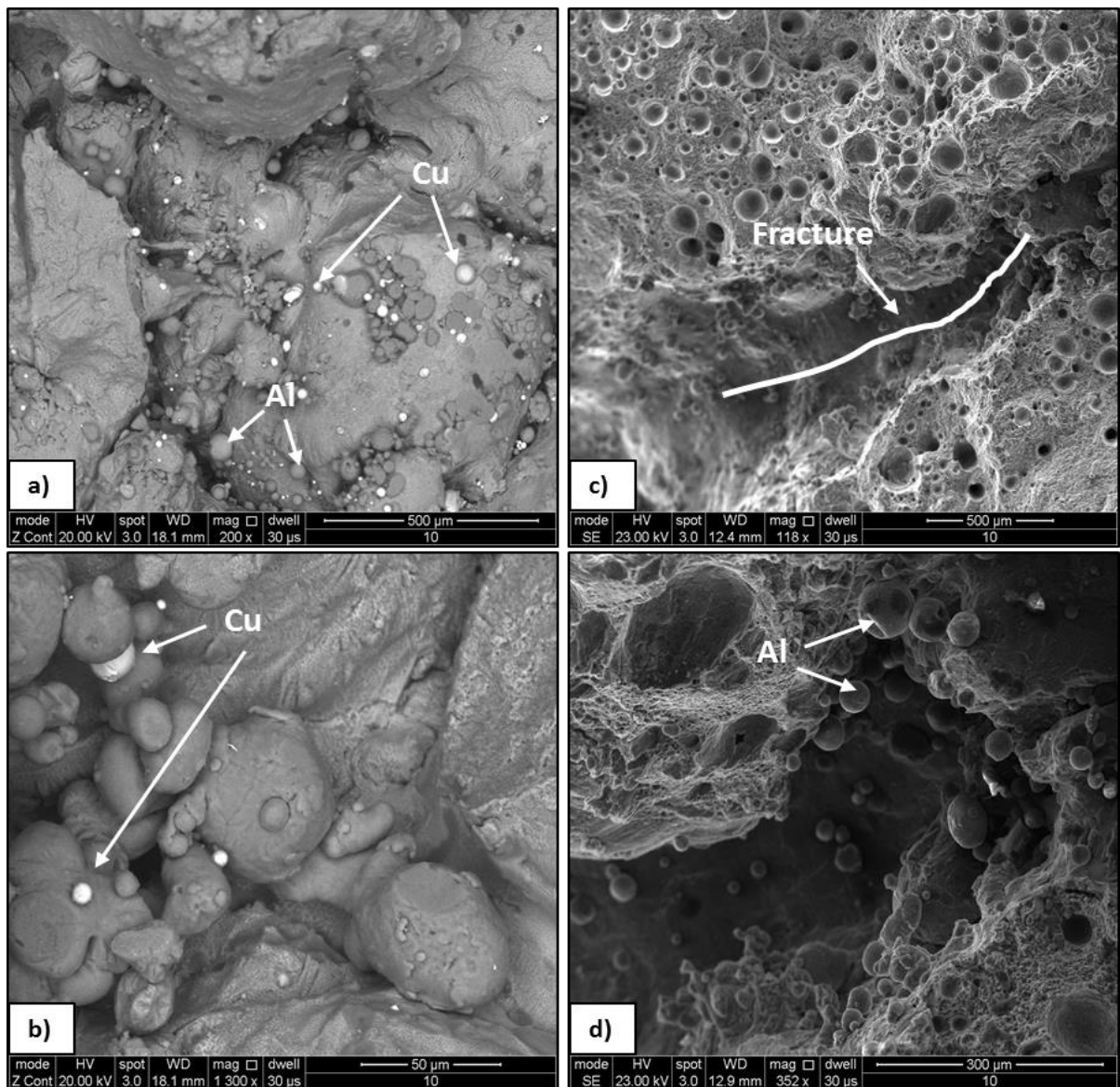
Figure 6-6 Backscattered SEM micrographs from the tensile fracture surface of in-situ Al-Cu12 as build a) and b) and heated bed processing (400°C) c) and d)

6.4 Residual stress

There are several techniques for measuring the residual stress in AM components such as X-ray diffraction and hole drilling methods. Studies by Ceglias, showing a comparison of both methods, concluding in an experimental error of 2.9% in compressive stress (Ceglias et al. 2016). Since there is a significant difference in cost due to the hole drilling method required qualified set up and is a destructive technique, the X-ray diffraction method for the residual stress measurements was selected.

A Non-destructive X-ray residual stress analysis method was performed for selected samples of in-situ Al-Cu12 processed at four different temperatures (room temperature, and preheating temperatures of 300ºC, 350C and 400 ºC) using optimum combination parameters for SLM previously developed for each condition. The residual stress was measured on the 30x30x10 mm block manufactured at different conditions using a portable x-ray residual stress analyser. Figure 6-7 shows the test block sample created to measure residual stress in five random points across the surface.
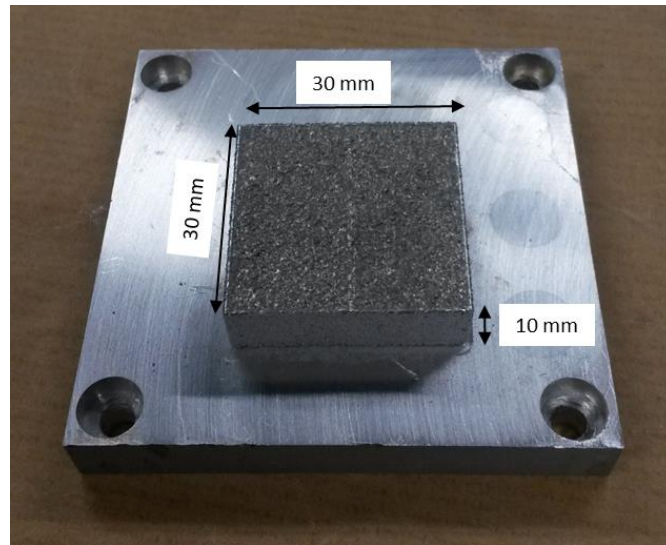
Figure 6-7 SLMed test block built to measure residual stress across different

point at the surface

Figure 6-8 shows an inverse relation between the sample created at different temperature conditions and residual stress. All sample were tested in cool down conditions after build. For the samples built at room temperature resulted in 77 MPa residual stress. Increasing the pre-heating temperature to 300ºC just at 10 degrees prior the beginning of annealing temperature the sample condition T2 resulted in 63.6% reduction in residual stress compared to room temperature condition T1. Increasing the pre-heating temperature to 350ºC representing the medium range for annealing temperature the sample condition T3 resulted in further decrease of 71.4% compared with room temperature sample and 21.14% lower in residual stress than condition T2 built at 300ºC. Increasing the pre-heating temperature just 10 degrees below the maximum temperature

for annealing range of 310 °C - 410 °C for condition T4 resulted in samples with nearly no residual stress.
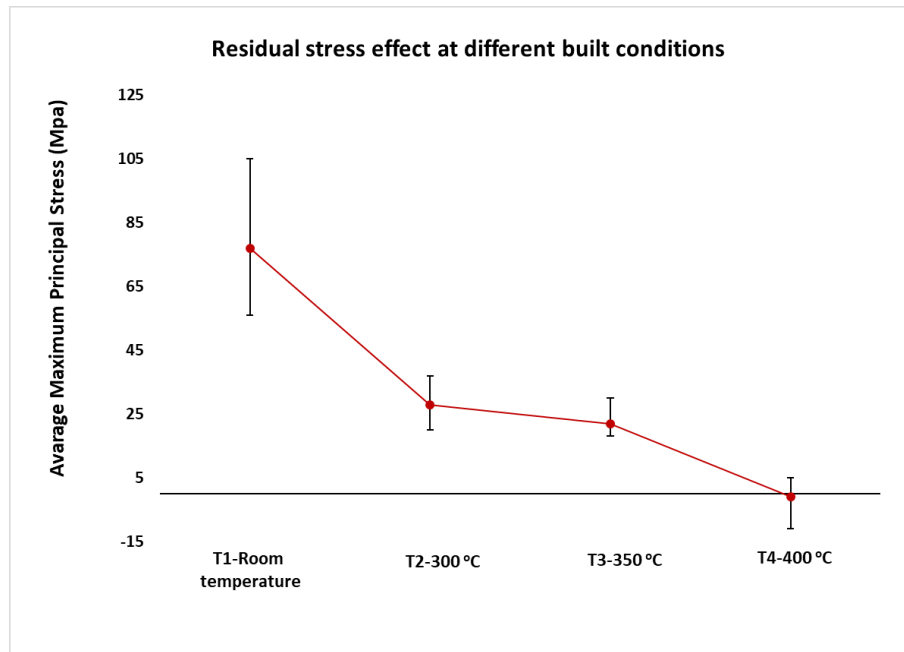
Figure 6-8 Effect of different in-situ bed pre-heating conditions on residual stress

6.5   Conclusions and summary

The main conclusions of the mechanical properties tested for in-situ AlCu-12 alloy are:

- SLM samples processed using pre-heating substrate at 400°C degrees built in *X* direction achieved the higher UTS compared with samples built as room temperature.

168

- SLM cube samples processed using pre-heating substrate at 400ºC degrees achieved the higher micro-hardness compared with samples build at room temperature.

- Findings suggested that the improvement in UTS is attributed to the homogenized microstructure resulting from the in-situ age hardening during the processing and a more complete diffusion of Cu particles within the α-matrix.

- The fracture analysis shows regions with the presence of un-melted powder particles, which give rise to cracking failures. Further optimisation parameter is required to eliminate these zones.

- The ductility for samples processed using pre-heating substrate showed a minimum improvement; however, the yield strength showed a reduction due to the high temperature during operation was set to the maximum annealing temperature of the material.

Chapter 7: Fabrication of unsupported geometries using ASLM

As mentioned in section 2.5 metal additive manufacturing does not exhibit super cooling behaviour, and still requires supports or overhang structures acting as sacrificial components to make the part buildable. Even though there are designing techniques, which exist such as Design for Additive Manufacturing (DFAM) to minimise the requirement of overhang structures, the design for additive manufacturing is ruled for geometrical limitations when the part includes an overhangs of 45° degrees or lower. Nowadays additive manufacturing designers are forced to include this supports to avoid thermal warping and build distortions during fabrication to prevent failures.

7.1   Unsupported overhang fabrication limits

Unlike polymers, metal processes has more complex problems to solve, the metal powders can be explosive, reactive, powders change characteristics in presence of oxygen increasing the level of processing them. For metal powder bed fusion AM process, the mayor limitation in the geometrical design is the requirement for support structures that can limit the geometric freedom of the SLM process and increase post-processing operations (Vora et al. 2014). Figure 7-1 shows how the distortion occurs at the absence of supports; this distortion is due internal residual stresses induced by laser processing. Internal

residual stress in powder bed fusion processes can be destructive as the process involves creating layers by layer, the internal stresses build up and result in warping edges pulling up away from their own supports.

Design for metal AM includes the following two mayor limitations (Calignano 2014):

- Melt pool requires anchors during solidification to prevent distortion or warpage.
- The critical angle to fabrication in additive manufacturing using SLM is 45° degrees (in some cases up to 35° degrees).

Printing metal components not following these rules will compromise the integrity of the build and may end in part deformation or build failure due to the coalition of the recoating system with the built part. It can be concluded, that under this limitations the design of freedom in metal additive manufacturing is still unsolved.
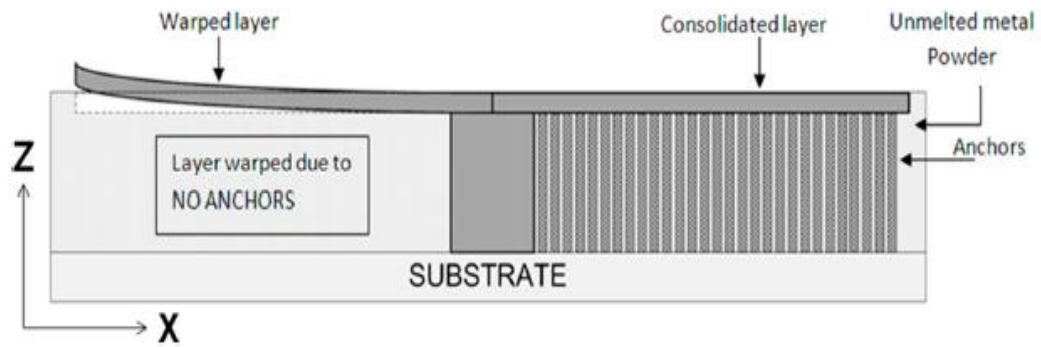
Figure 7-1 Schematics of un-supported layer susceptible to warp distortion for

SLM processing (Martinez et al. 2017)

7.2 Part design validation

Parts with multiple overhang geometries were designed for the initial experiments using the optimum processing parameters for in-situ Al-Cu12 SLM alloy previously developed.

Figure 7-2 shows the designed geometry for this study. Two build configurations to produce the parts were used. The first configuration was using room temperature and the second configuration with high temperature using the internal preheating system of Renishaw AM125 machine with a maximum capability to preheat substrate up to 140ºC degrees. The experiment

was designed to analyse the maximum possible overhang with standard SLM process without anchors/supports.

Multiple overhangs of 1mm, 2mm, 5mm, and 10mm were built for several thicknesses; however, parts with an overhang thickness of 0.5mm, 1mm, 2mm and 3mm were built with a partial success. Parts with 5mm and 10mm overhang thickness features resulted in build failures. This initial study provided a better understanding of the relationship between unsupported overhang features using different thickness for standard SLM process as shown in Figure 7-3. During the trials, sample parts developed failures and distortion.

Produced parts were analysed for warping (curling of layers) by an exhaustive method employing image analysis techniques. The overhang geometries were captured as high definition images using Olympus SZ61 microscope at 6.7x magnification and several images were taken as shown in Figure 7-4.
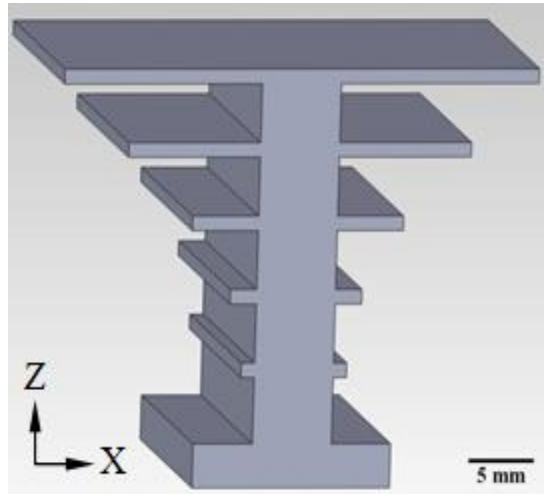
Figure 7-2 Experimental part design (CAD drawing of 1mm thick overhangs features)
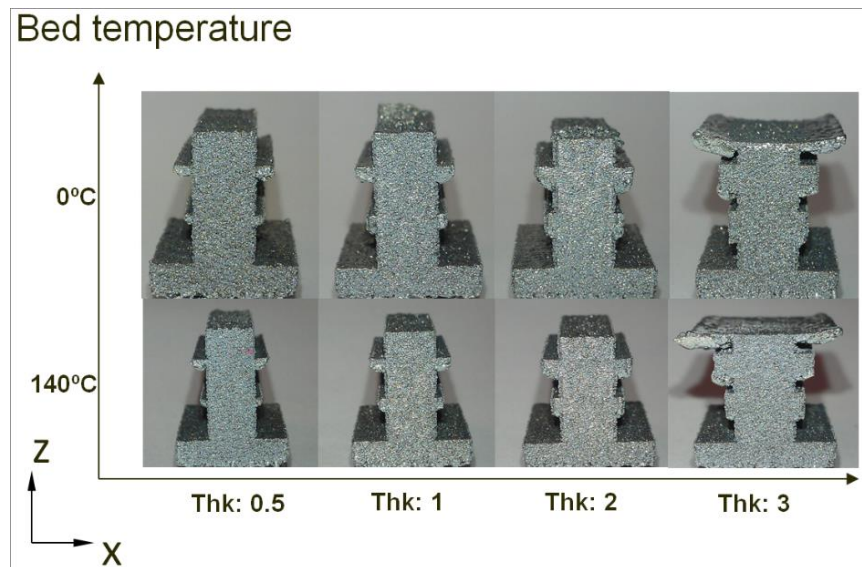
Figure 7-3 Initial support less experimental parts with different overhangs created using conventional SLM.

In Figure7-3 is possible to observe a part distortion failure resulted by the inherent residual stress created by the rapid heating and cooling behaviour of SLM laser processing for almost all geometries created using in-situ Al-Cu12 alloy at room and maximum temperature of 140 °C. The parts produced using a thickness from .5 mm to 2 mm, is clearly to observe that the third overhang was removed by the coalition of recoating system due to part warping distortion caused by residual stress.

For parts created using a thickness of 3 mm, is possible to observe that the using of preheating substrate base plate kept the surface with less distortion warping. Even though parts with 3mm thickness overhangs were built with partial success, this parts received an extra help/aid from the worn rubber coater part, which is in the recoating system, resulting beneficial to continue processing the part. Overhangs of 5mm to 10 mm were not possible to build in more than 10 attempts due part distortion.

The maximum overhang geometry achieved by the initial experiments for room temperature and a maximum pre-heating temperature substrate of 140°C was 3mm. Findings of the experimentation concluded that the use of pre-heating substrate was beneficial for the overhang features.
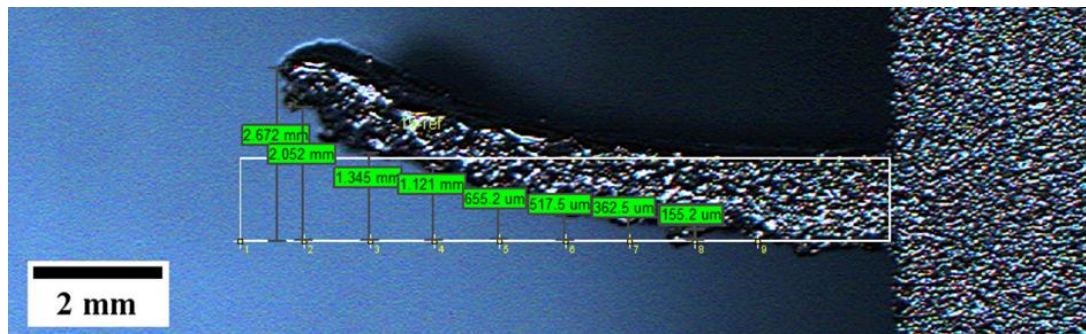
Figure 7-4 Warp distortion measurement using Olympus SZ61 microscope

7.3 ASLM overhang geometries

Two different in-situ aluminium alloys were created using ASLM with the challenge to achieve a minimum building angle of 0º degrees obtaining a flat overhang geometry with no distortion or warping after build. The experiments were produced using the Renishaw AM125 fitted with the modular heated bed system designed and developed for this project described in section 3.6 using a controllable high temperature of preheating substrate up to 400ºC.

The first material tested was the in-situ Al-339 which is a blend of 2 in-situ powder mixing A+B (*AlMg + SiCuNi)* and the second material tested was the in-situ Al-Cu12 aluminium alloy developed for this research project. Figure 7-5 shows the in-situ Al-339 aluminium alloy part designed for creating an overhang structure geometry using ASLM process. The part was created using

optimised parameters developed in previous published work by (Martinez et al., 2017).

Two different shapes were tested for the experimental overhang geometries. The first shape is described in Figure 7-5, which contains two overhangs in a "*T*" shape structure considered impossible to build according the DFAM rules. The first shape was designed to produce the in-situ Al-339 alloy for ASLM. A second shape described in Figure 7-6, was designed for in-situ Al-Cu12 by increasing the complexity with four overhangs and a total overhang of 20 mm.
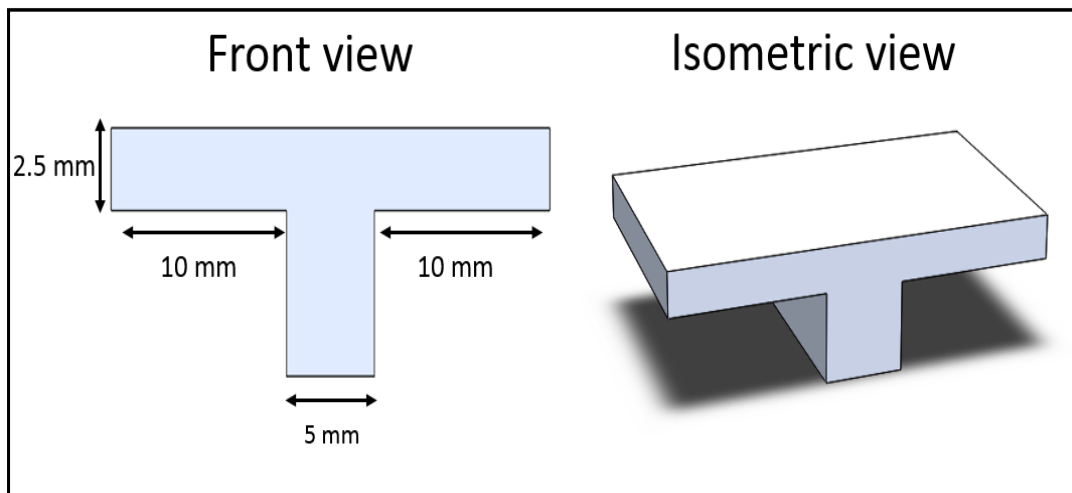
Figure 7-5 Designed component with two overhangs features (0º degrees) for in-situ Al-339 ASLM experimentation.
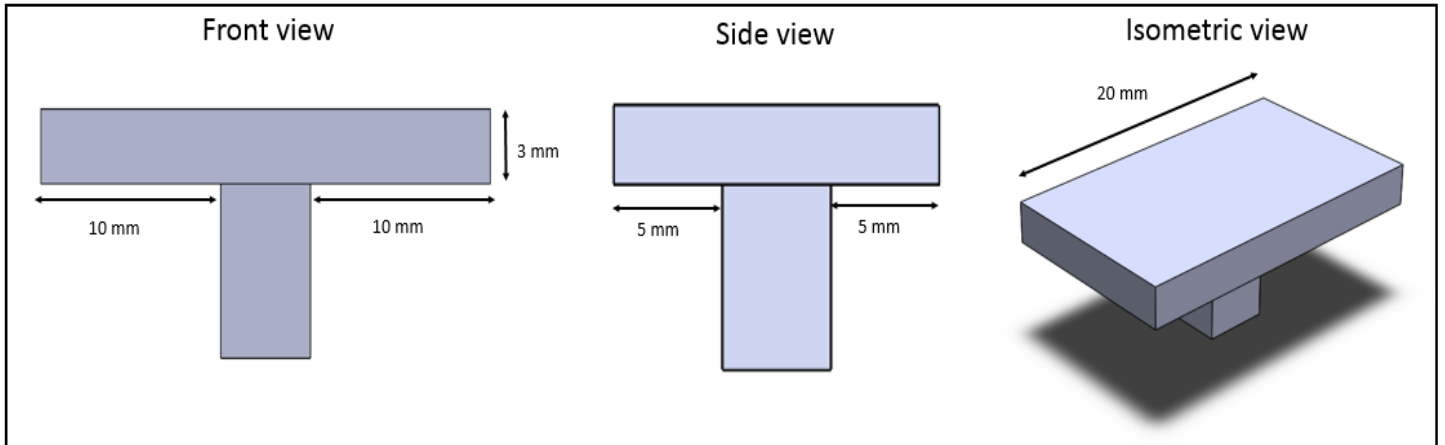
Figure 7-6 Designed component with four overhangs (0º degrees) for in-situ

Al-Cu12 ASLM experimentation.

7.4 High temperature substrate modelling

Prior processing using high temperature preheating substrate, a simulation of the process under high temperature were analysed for a better understanding of ASLM process. It is worth mentioning that, at this stage due lack of licenced Abaqus software, used to performed high engineering analysis, SolidWorks educational version was used instead. It is believed the heat from preheated substrate will transfer to the built as this growing layer by layer. SolidWorks FEA thermal analysis was used to perform this heat transfer modelling prior produce overhang geometries to validate thermal condition involved in the ASLM process.

A 66 x 66 x 15mm substrate base plate is attached to the modelled part described in section 7.3 used for the overhang experiment. Figure 7-7(a), (b) shows the heat-transfer model boundary conditions for applied temperature and convection losses. A four node linear tetrahedral mesh element was used to mesh the model for the heat transfer simulation. A total of 21283 nodes were applied to the total assembly. Figure 7-7(c) shows the meshing model for the parts.

Temperature-dependant material properties for solid in-situ Al-Cu12 used for this simulation are presented in table 7-1 below.

Table 7-1 Selected thermal properties for solid in-situ Al-Cu12

Temperature T(°C)	Density ρ(kg/m3)	Specific Heat Cp(J/kg.K)	Thermal Conductivity (W/m K)
400	3374	800	140
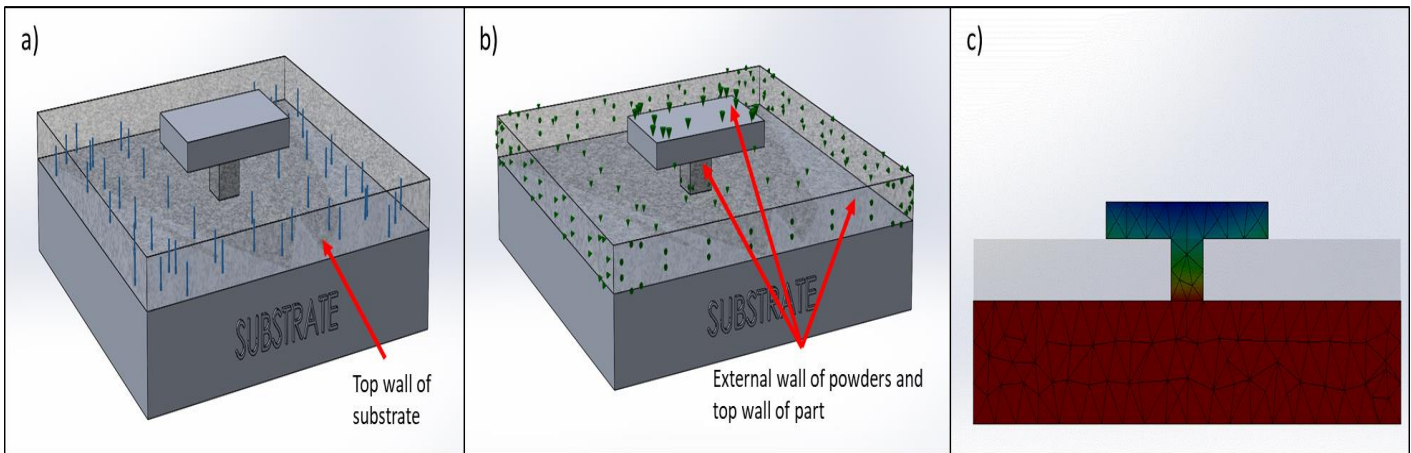
Figure 7-7 Heat Transfer simulation model using SolidWorks FEA. (a),(b)

Model boundary conditions for temperature and convection losses (b) Model

mesh in the substrate and overhang part

A constant maximum temperature condition of 400ºC was set to the top surface

of substrate. The powder bed has had been treated as a single body for this

modelling. In this simulation radiation heat losses were not considered. The

convective heat losses were set to the powder layer internal walls that are in

contact with the built material and the external wall in contact with the build

chamber. The convective heat transfer coefficient of $64 \, \frac{W}{(m^2 \, K)}$ was used.

Figure 7-8 shows the results of the thermal analysis conducted using

SolidWorks FEA. It is possible to observe that at the overhanging layer the

temperature predicted is just 4-5 degrees below the 400ºC, just 2% less than

the expected temperature at the top surface. Using this FEA prediction results, the heated bed temperature controller was set up at 408°C for processing experimental parts, to compensate heat losses during the process and the fluctuation in temperature of the heating system.
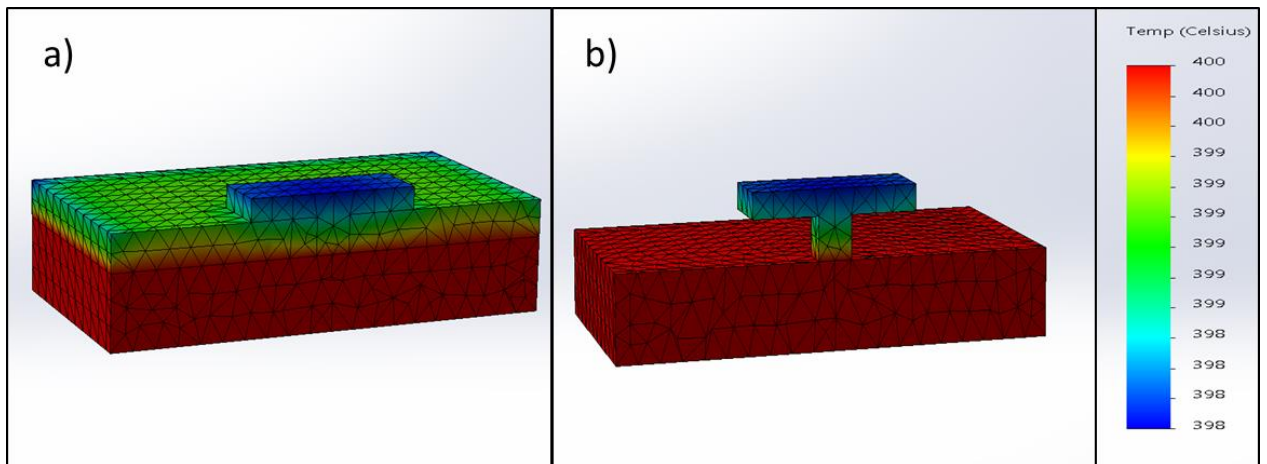
Figure 7-8 SolidWorks FEA thermal analysis results for conductive heat transfer experiments. (a) View with powder bed (b) View without powder bed

7.5 Fabrication of ASLM overhang geometries

Initial trials were performed to assess the heating system while using high temperature pre heating substrate. A Temperature of 350°C were used to start with the experiments. Initial findings suggested that it was necessary to re-design the internal rubber part within the recoating system, it was found that

the maximum temperature operation for the rubber part was 250°C, the rubber experienced a partial melting in operation.

Figure 7-9 shows a failed part with the pattern created for the melted rubber. In addition the failed part had shown warping distortion in both cantilever overhangs features. A new wiper rubber part designed for working under 450°C operation conditions was installed to proceed with the experiments. Additional software part preparation adjustments were required to process the experimental overhang parts.
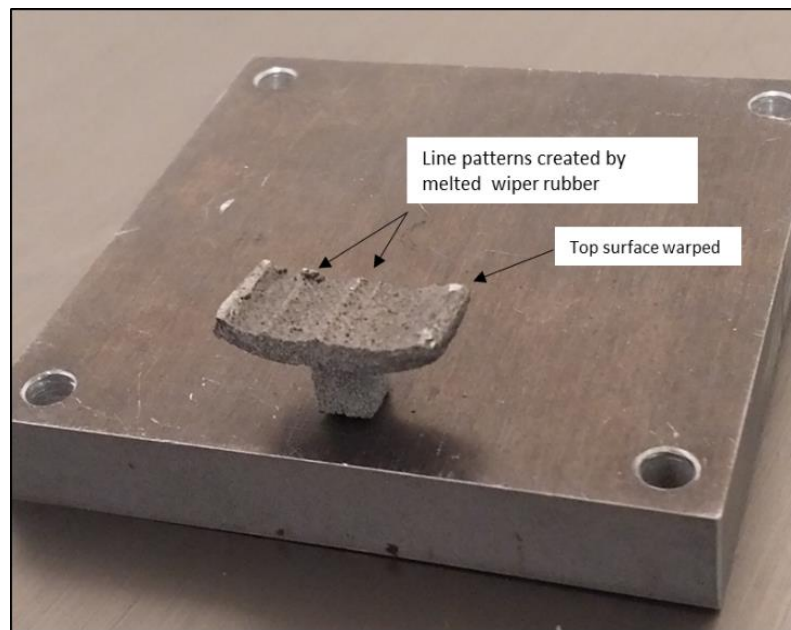
Figure 7-9 ASLMed in-situ Al-Cu12 overhang structure warped sample during processing with recoating damage at the top surface

Relaxation of internal stress normally initiates from 40 to 60 % of the solidification temperature of the material for aluminium alloys (Martinez et al. 2017). During the first trial using a maximum pre-heating substrate temperature of 350 °C, it was found that this temperature was still not enough to promote relaxation of internal stresses, such that warping distortion would not occur.

Al-339 and Al-Cu12 in-situ aluminium alloys were successfully fabricated using a 0° degree overhangs features with less than .1 mm warping distortion at the top surface resulted from the reduced residual stress state promoted by the assistance of the pre-heating substrate during the process.

Figure 7-10 shows the twin cantilever structure created using ASLM method. This part configuration exhibits 2 overhangs of 10 mm using optimised parameters previously reported (Martinez et al. 2017).
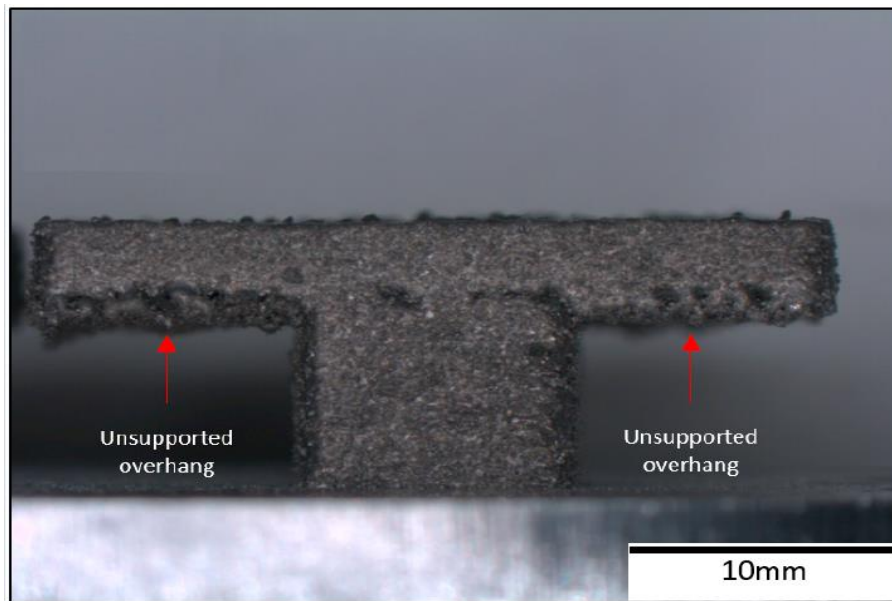
Figure 7-10 ASLM in-situ Al-339 twin cantilever part processed from powder

mixing A+B (AlMg + SiCuNi)(from Martinez et al. 2017)

Figure 7-11 shows the ASLMed in-situ Al-Cu12 aluminium alloy created with a double twin cantilever overhang, processed using a maximum pre-heating substrate temperature of 400ºC with success. The part show a maximum overhang of 20mm using optimised parameters reported in chapter 4.
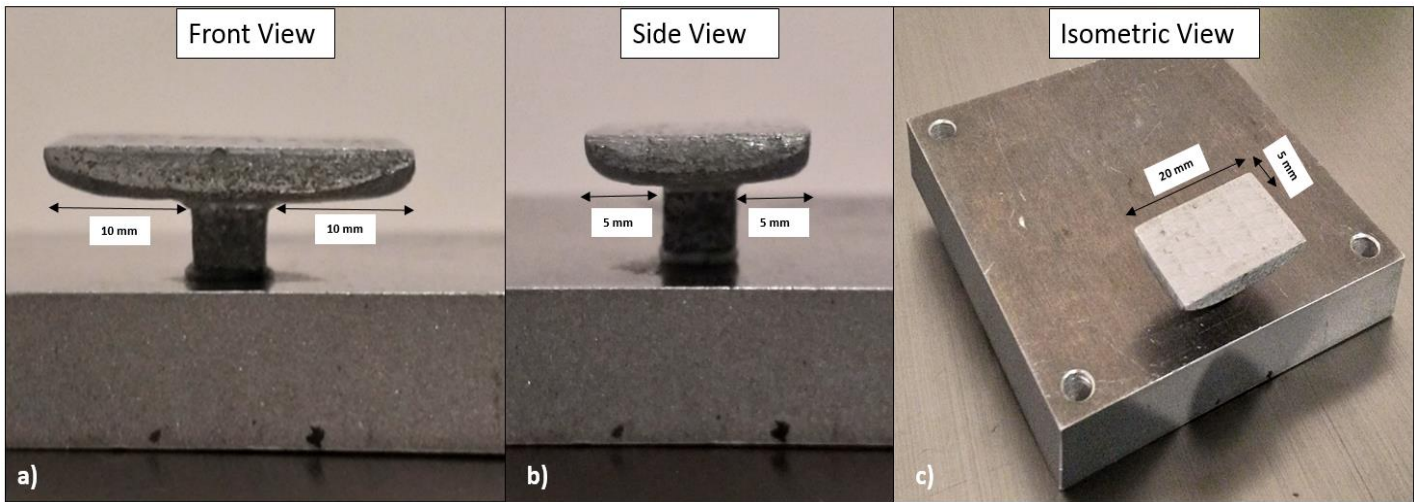
Figure 7-11 ASLM in-situ Al-Cu12 with double twin cantilever overhang processed from elemental powder mixing

For overhang processed parts, shown in Figures 7-9 and 7-10 is possible to observe that downfacing area may require further adjustments or different strategy in down skin parameters to improve the average roughness surface within the final component. In figure 7-9, dross formation is visible. This undesirable phenomenon may be promoted by a deep unstable melt pool created by the lack of a solidified material below, making heat conduction lower than supported structures, this situation created instabilities in the melt pool behaviour indicating further optimisation of scan downskin parameters to avoid dross formation.

Figure 7-10 does not shows dross formation, however, it seems like a minimum material from the down corner edges detached from the built part, this may be attributed to the same instabilities experienced in the melt pool when there are no solid support zones affecting the heat conduction rate, resulting in poor energy absorption. Cooper reported a melt pool thermal simulation comparing laser processing using solid substrate and powder support resulting in larger melt pool when processing overhang features, this finding indicates further downskin parameter optimisation improvements (Cooper et al. 2016).

Other reason for this corner edges failures, may be attributed to the geometrical starting point of the laser scanning processing raster, which is always beginning at the corner edges from the part, leaving this area waiting a long period for the next layer to be processed. Cooper reported a similar deformation when tried to build overhang features with a method called contact free support structures (Cooper et al. 2016). Unfortunately the Autofab Renishaw build preparation Software used for all overhanging experimentation does not allows to change this scanning pattern for the sequence of layer processing as well as the geometrical point to start of a new scanning across the build geometry. This may indicate changes needed in the scan strategy to perform the scanning pattern from the centre axis of the part toward the edges to minimize instabilities created by powder supported zones. Figure 7-12 shows the representation of the melt pool in overhang zones.
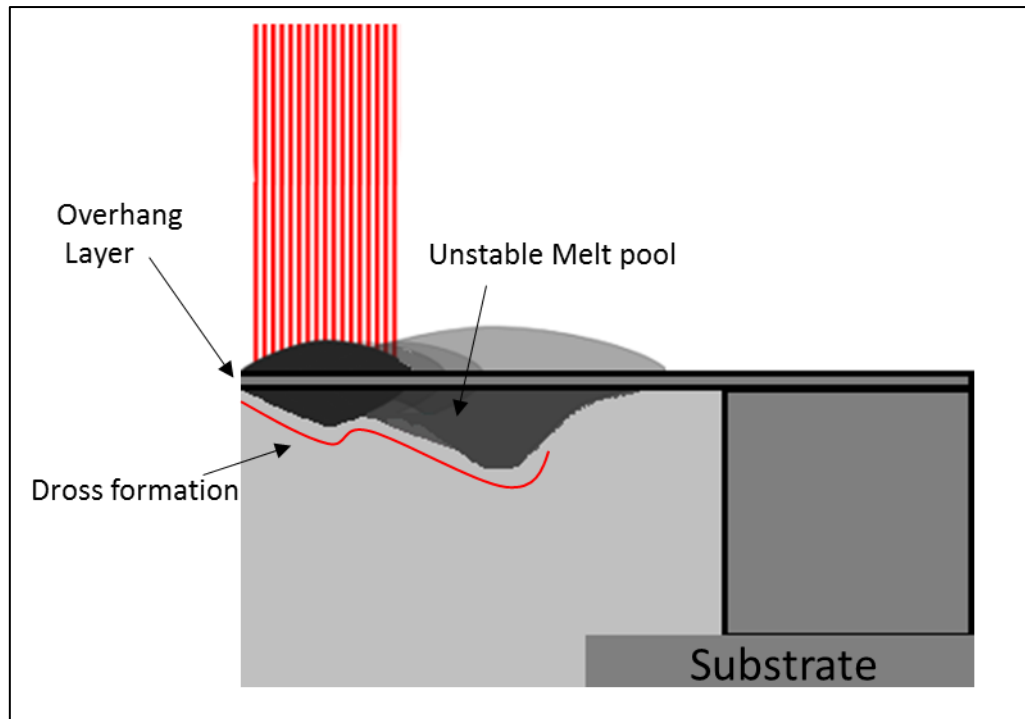
Figure 7-12 Schematics of dross formation on overhanging downskin feature during powder bed laser processing (Adapted from McMahon 2018)

7.6 Engineering applications

For current AM designs is necessary to add sacrificial supports as part of their design, avoid this structures become a real challenge as the part complexity increases (Saunders 2018). A successful part for an AM engineering application has been created for in-situ Al-Cu12 ASLM alloy using optimised parameters previously developed in this thesis and detailed in Chapter 4. The

build time process had been improved by 30% by removing all the internal supports needed to produce the part traditionally using SLM.

Figure 7-13 shows an example of a printed part with similar characteristics (with supports included) to the part created successfully using ASLM. Figure 7-14 shows a typical AM application design that requires anchors due the numerous overhangs lower than 35° degrees. For such geometry it is mandatory to include supports, besides a part with this features require more time for build preparation to add the supports in the correct areas to avoid failure during processing.
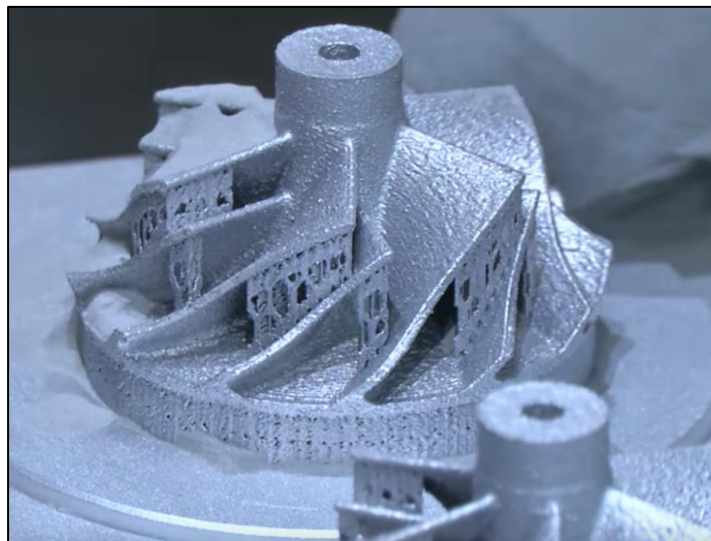
Figure 7-13 Impeller created using SLM with support structures. (DMG-Mori SLM 2018)

In Figure 7-14 (d) is possible to observe that areas between the blades shows a rough surface finish, this may indicate some adjustments in scan strategy due

the part geometry is bigger than previous experimental overhangs samples, ASLM processing impacts directly in productivity, reducing not only supports preparation but also material waste and post processing time.
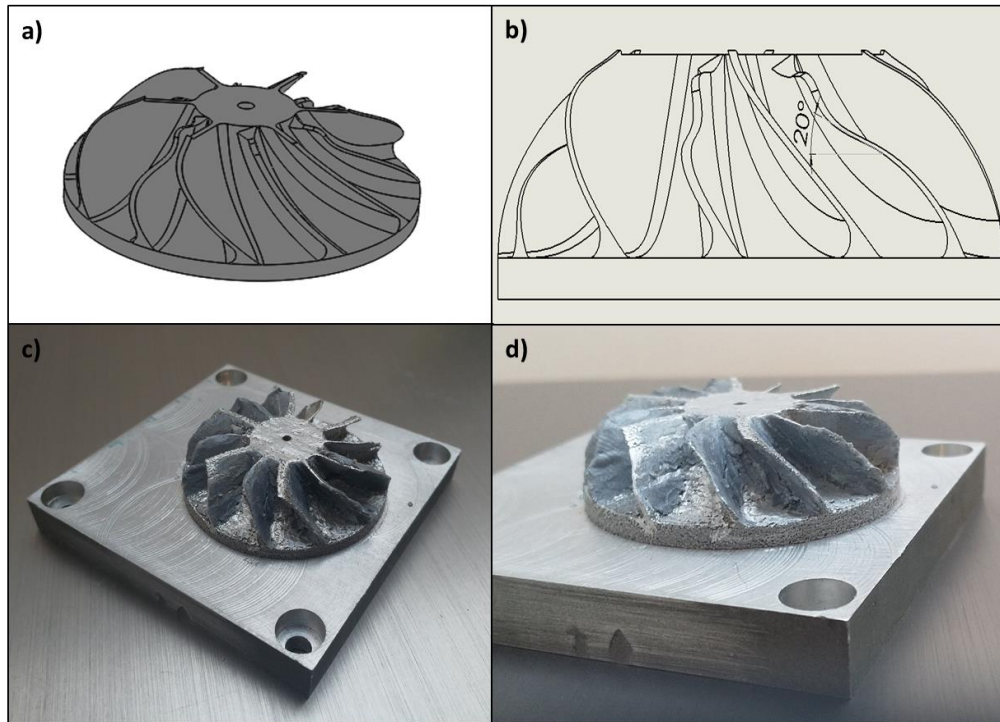
Figure 7-14 Impeller with internal overhangs less than 35º degrees creating using ASLM

The novel ASLM processing conditions allowed the experimental part to be built in a stress-reduced state, enabling the buildability of overhanging areas and unsupported features reducing the overall cost of manufacturing parts using additive manufacturing.

7.7 Conclusions and summary

The main conclusions of the efficiency of ASLM method for in-situ AlCu-12 alloy are:

- Impossible geometries according DFAM rules were created using ASLM method with optimised parameters for in-situ Al-Cu12 pure elemental blend.

- Parts were manufactured showing a minimal dross formation for overhang features. This observation suggested a change of scanning strategy to avoid the dross formation.

- A processing time reduction of 30% resulted of using ASLM for the fabrication of an impeller engineering application part using the novel method of ASLM.

Chapter 8: Conclusions and future work

This chapter briefly summarizes the main conclusions shown in chapters 4, 5, 6 and 7 as well as the suggestions for future research for in-situ Al-Cu12 Aluminium alloy and ASLM.

This work explored the in-situ fabrication of an Al-Cu12 alloy from pure elemental blend of aluminium and copper powders created by SLM and ASLM. This work also highlighted the issues with the conventional metal AM processes and described the feasibility of a novel concept to overcome the issue of warping distortion of overhanging structures using conventional SLM and thus restricting capability of buildability.

The effect of SLM parameters on porosity and mechanical properties was studied using a commercial Renishaw AM125 fitted with a heated bed device, designed and developed for this study to perform ASLM process of ins-situ aluminium alloys. A finite element model was creating for a better understanding of the melt pool formation during SLM processing to minimize parameter optimization time.

8.1 Effect of SLM parameters

A detailed study on the effect of room temperature and high temperature SLM parameters on density optimization and mechanical properties was carried out using a modified Renishaw AM125 SLM machine.

8.1.1 SLM parameter optimization

SLM parameters were developed to process elemental blends of Al and Cu powder creating a hypo-eutectic high dense in-situ Al-Cu12 alloy fabricated using room and high temperature conditions. The optimisation trials to determine optimum combination of power and scan speed for achieving nearly fully dense parts were carried out. A reduced scanning speed and high energy input were found to improve melting for this highly reflective material.

- 180W laser power and 160µs exposure time and a point of distance of 20µm resulted in 99.5% dense in-situ Al-Cu12 room temperature SLM cubes.

- 170W laser power and 160µs exposure and a point of distance of 20µm time resulted in 99.1% dense in-situ Al-Cu12 high temperature SLM cubes.

- FEA model accurately predicted melt pool size layer penetration by comparison with SLM experimental single track.

8.1.2 Effect of scan strategy and layer thickness

The effect of scanning strategy on density optimisation trials was investigated by comparing 3 different strategies: Chessboard Island 2X2mm, rotation 67º Strip and rotation 67º Meander scanning strategy.

- 67º Meander scanning strategy resulted in the lowest porosity using Renishaw AM 125 SLM machine.

Two different layer thickness (40μm and 50μm) were studied to understand the effect on density optimisation of SLM Al-Cu12 parts.

- A layer thickness of 40μm resulted in the lowest porosity values using Renishaw AM 125 SLM machine.

8.1.3 Effect in particle size

The effect of particle size on density optimisation trials was investigated by comparing 2 different particle size for pure Cu powders: 20-40 µm and 5-25 µm average size.

- Parts produced using particle size from 5-25 µm resulted in the lowest porosity values using Renishaw AM 125 SLM machine in a total of 30 samples using same processing parameters for the 2 different powders size tested.

8.2 Effect in microstructure

A finer dendritic cell microstructure resulted for standard SLM processing at room temperature, meanwhile, a uniform coarser dendritic cell microstructure consisting of supersaturated Al-rich with a uniform intermetallic Al_2Cu phase microstructure resulted for SLM processing at high temperature for all in-situ Al-Cu12 processed samples.

- All samples of in-situ Al-Cu12 elemental blend resulted in a fine supersaturated cellular dendrite microstructure similar to pre-alloys while processing by SLM.

- Cu rich zones were observed for a number of samples processed at room temperature conditions.

- For all samples a resulted microstructures consisted in cellular rich α-Al matrix with presence of intermetallic θ phase Al2Cu.

- All samples built using optimizing parameters show no evidence of crack formation

8.2.1 Effect of bed pre-heat temperature in microstructure and mechanical properties

A custom heated bed device was designed to ASLM processing capable of achieving up to 860ºC degrees temperature was fitted to Renishaw SLM125 machine to perform ASLM trials and assess the effect of be pre-heat temperature on porosity, microstructure and mechanical properties.

- SLM in-situ Al-Cu12 microstructure was completely transformed into granular coarser microstructure with higher intensity of intermetallic Al_2Cu.

- The use of heated bed preheating during ASLM processing enabled an artificial age hardening producing an equilibrium $\alpha + \theta$ microstructure.

- An increment of 50% in UTS resulted of preheating the powder bed to 400°C degrees compared with processed parts at room temperature conditions.

- An increment of Vickers micro-hardness increases 11% resulted of samples processed at 400°C compared with samples build at room temperature the increase in hardness was attributed to the increase in Al_2Cu content.

- The improvement in UTS is attributed to the homogenized microstructure resulting from the in-situ age hardening during the processing and a more complete diffusion of Cu particles within the matrix.

- The fracture surfaces presented resulted from analysed samples shows regions with the presence of un-melted powder particles, which give rise to cracking failures. Further optimisation parameter is required to eliminate these zones.

- The ductility for samples processed at high temperature showed a minimum improvement, however the yield strength showed a reduction due to the pre-heat temperatures operating close to the maximum annealing temperature of the material.

- It was found that in-situ annealing of metal 3D processing is a very promising approach that has so far not been integrated into commercial metal 3D machines in full capacity.

8.3 ASLM overhang geometries

A series of experiments were carried out to produce stress reduced parts with no distortion warpage. A Successful twin cantilever geometry was produced with a minimal distortion for two different in-situ aluminium alloys built at high temperatures using ASLM processing method. In addition a common application part was produced with success providing a better understanding of the ASLM capabilities.

- Impossible geometry "*T*" shape designed with two overhangs with a maximum length of 10 mm was created using ASLM with optimised parameters for in-situ Al-339 elemental mixture of alloy A+B (*AlMg + SiCuNi)*

- Impossible geometry "*T*" shape designed with four overhangs with a maximum length of 20 mm was created using ASLM with optimised parameters for in-situ   Al-Cu12 pure elemental blend.

- A minimal dross formation were observed for overhang structures created by ASLM, this observations suggest a change of scanning strategy.

- A processing time reduction of 30% resulted of using ASLM for the fabrication of an impeller engineering application part.

- It was demonstrated the efficiency of ASLM for processing and post processing times eliminating the support removal process.

8.4   Suggestions for future work

8.4.1   Al-Cu12 in-situ alloy

Since in-situ annealing showed potential benefits to SLM such promoting more homogenous microstructure and positive impact in mechanical properties, further research needs to be done in order to evaluate and create a deep understanding of the effect on mechanical properties after post heat treatment T6 suitable for age hardening aluminium copper alloys to assess the evolution in the growing of intermetallic phase θ Al_2Cu after quenching and ageing phases and create a data base to optimize mechanical properties for in-situ Al-Cu12.

Due the complex behaviour of layer melting processing and various controllable processing parameters involved in SLM, a pore-free structure cannot be obtained even in those samples processed by optimum parameters. An additional post-processing technique such as Hot Isostatic Pressure (HIP) is also recommended to create a comprehensive study on the microstructure, density and mechanical properties of processed SLM in-situ Al-Cu12 samples.

As the optical microscope porosity analysis approach is limited to only the upper polished layer of the processed sample, a different technique for a deep evaluation and pore formation should be included to develop a more comprehensive study in porosity optimization. X-ray tomography allows to evaluate the porosity volume and distribution across the entire processed sample through segmentations of high resolution images to finally perform the reconstruction of the sample in 3D and the distribution of pores.

Additional TEM analysis will be also favourable for in deep analysis of the effects of pre-heating substrate within the microstructure, to probe the presence of nano ζ (Al_3Cu_4) and γ (Al_4Cu_9) precipitates in the microstructure of in-situ Al-Cu12.

The exploration of new techniques for in-situ allying should be beneficial to improve powder mixing to improve wettability and flowability, powder batch distribution ratio for achieve a more homogenous distribution of elements when spreading material across the substrate.

8.4.2   Anchorless Selective Laser Melting

Limited research is going on ASLM but the method is still in developmental stages and therefore offers several opportunities for further research improvements. Exploring new alloy design using ASLM may be more cost-effective than investing in expensive gas atomisation manufacturing for the creation of pre-alloyed powders for initial testing of alloy.

The current research focused in the creating of a new in-situ Al-Cu12 alloy for ASLM. A further materials development and the understanding of the properties for in-situ alloying from elemental blends should be tested in order to expand the range of alloys/materials available for the ASLM process today.

The current approach of adapting the development of ASLM to a commercial technology as the Renishaw AM125 machine limits the capabilities of this method due insufficient access to software and hardware to have full control of the operation system. For this project, the build preparation file took several

hours to prepare due the lack of control in software adjustments. The software Autofab owned by Renishaw does not allow full control in adjusting scan strategies and parameter control for each layer in particular. This software problems suggested that ASLM method could have a better performance if it is adapted to an open source machine with access to the hardware and software to eliminate this problems, this may open new research for developing an open source AM machine fitted with a custom heated bed able to preheat until 880ºC.

It was found that one of the mayor barriers to produce effective overhangs was the recoating system due the fact that is the only part which is in contact with the deposited powder layer by layer during the entire build, a further adjustments in the design of this recoating system is required to improve the performance of this methodology. A flexible brush recoating system is suggested to avoid coalition and distortion during build processing. A second option is design a contactless system to avoid mechanical contact with the deposited layer powder to minimize distortion.

Enable a high temperature pre-heating substrate has shown promising results in reducing the warping distortion, changes in microstructure and enhancement of mechanical properties. This represent a new window for further investigation in optimising parameters for different bed temperatures using

different combinations of metal alloys from elemental powders and studying the effect in microstructure and mechanical properties for customised applications.

Bibliography

A. Popovich, et al (2016) "Microstructure and mechanical properties of additive manufactured copper alloy," *Acta Materialia*. Letter, vol. 179, pp. 38–41.

Aboulkhair, Nesma T., et al (2014). "Reducing porosity in alsi10mg parts processed by selective laser melting." *Additive Manufacturing* 1: 77–86.

Agarwala M., et al. (1995). "Direct selective laser sintering of metals." *Rapid Prototyping Journal*, 1(1), 26-36.

Ahmadein, Mahmoud, et al (2014). "Analysis of macrosegregation formation and columnar-to-equiaxed transition during solidification of aluminium alloy" no. March 2015.

Ahuja, Bhrigu, et al (2014). "Fabrication and characterization of high strength Al-Cu plloys processed using laser beam melting in metal powder bed." *Physics Procedia* 56 (C): 135–46.

Ali, Haider, et al (2017). "In-situ residual stress reduction, martensitic decomposition and mechanical properties enhancement through high temperature powder ped pre-heating of selective laser melted Ti6Al4 V" *Materials Science and Engineering* A 695: 211–220.

Allmen M. V. and Blatter A. (2002). Laser-beam interactions with materials: *Springer*.

ASTM, E8 / E8M-13a, (2013) Standard Test Methods for Tension Testing of Metallic Materials, *ASTM International*: West Conshohocken, PA.

ASTM, ISO/ASTM 52921:2013 (2013)-Standard Terminology for Additive Manufacturing—Coordinate Systems and Test Methodologies, *ASTM International*: West Conshohocken, PA.

Aversa, A., et al. (2017) "Effect of process and post-process conditions on the mechanical properties of an A-357 alloy produced via laser powder bed fusion". *Metals and alloys*, 68.

Aversa Alberta, and Marchese, Giulio. (2019). "New aluminium alloys specifically designed for laser powder bed fusion: a review" *MDPI materials journal*", 12-19.

Aziz M. and Kaplan T. (1988). "Continuous growth model for interface motion during alloy solidification" *Acta Metallurgica* 36, 2335-2437

Bansal R. K. (2005). A Textbook of Fluid Mechanics and Hydraulic Machines: *Laxmi Publications*.

Beaman J. J., et al. (1996). Solid Freeform Fabrication: A New Direction in Manufacturing: *Springer*.

Beer S. Z. (1972). Liquid metals: chemistry and physics: *M. Dekker, New York.*

Boivie K. (2012) "Limits of loose metal powder density in the sinterstation." *Presented at proceedings of the solid freeform fabrication symposium*.

Buchbinder, D., et al (2011). "High Power Selective Laser Melting (HP SLM) of Aluminum Parts." *Physics Procedia* 12 (part 1): 271–78.

Buchbinder, Damien, et al (2015). "Components using selective laser melting investigation on reducing distortion by preheating during manufacture of aluminum components using selective laser melting" *Journal of materials & design* 01-24.

Calignano, F. (2014). "Design optimization of supports for overhanging structures in Aluminum and Titanium alloys by selective laser melting." *Journal of materials & design* 64: 203–13

Chaudhuri B., et al. (2006). "Cohesive effects in powder mixing in a tumbling blender." *Powder Technology*, 165(2), 105-114.

Chia-Wei Lin, et al (2016). "Microstructure evolution and high-temperature compressibility of modified two-step strain-induced melt activation-processed Al-Mg-Si Aluminum alloy" Advanced Engineering Materials, 23(5) 112-120

Cibula A., et al (1949). "Solidification of pure metals" *Journal of the Institute of Metals* 17, 321-322

Cooper K., et al (2016). "Contact-free support structures for part overhangs in powder-bed metal additive manufacturing", *Elsevier editorial system* 1, 11.

Czerwinski, Frank. (2006). "The Basics of Modern Semi-Solid Metal Processing," *Powder Technology*, 17–20.

Das S. (1998). Direct selective laser sintering of high performance metals: Machine design, process development, and process control. *The University of Texas at Austin*.

Das S. (2003). "Physical aspects of process control in selective laser sintering of metals." *Advanced Engineering Materials*, 5(10), 701-711.

Daumann B., et al. (2011). "Discontinuous powder mixing of nanoscale particles." *Chemical Engineering Journal*, 167(1), 377-387.

Debroy T. and David S. A. (1995). "Physical Processes in Fusion-Welding." *Reviews of Modern Physics*, 67(1), 85-112.

Dickens Jr E. D., et al. (1994). "Sinterable semi-crystalline powder and near-fully dense article formed therewith", A. T. Dtm Corporation, *City: Google Patents*: United States.

Doru Michael Stefanescu, (2009), Second Edition. Science and Engineering of Casting Solidification.

E. D. Palik, (1981), Handbook of Optical Constants of Solids (*Academic Press, Orlando*).

E. Louvis, and C. J. Sutcliffe, (2011) "Selective laser melting of aluminium components," *Journal Materlias Processing Technologies,* vol. 211, no. 2, pp. 275–284.

E. O. Olakanmi, (2013) "Selective laser sintering/melting (SLS/SLM) of pure Al, Al-Mg, and Al-Si powders: Effect of processing conditions and powder properties," *Journal Materlias Processing Technologies*, vol. 213, no. 8, pp. 1387–1405.

El-Eskandarany M. Sherif, et al. (1991). "Effect of ball-to-powder weight ratio on the amorphization reaction of Al50Ta50 by ball milling." *Journal of the Less Common Metals,* 169(2), 235-244.

Eustathopoulos N., et al (1999). Wettability at High Temperatures Pregamon Materials Series, Vol. 3: *Elsevier, UK*.

Fast J. D. (1965). Interaction of metals and gases: *Philips Technical Library*.

Fischer P., et al. (2003). "Sintering of commercially pure titanium powder with a Nd : YAG laser source." *Acta Materialia*, 51(6), 1651-1662.

Flemings Merton C. (2004) : in Solidification Process Microstructures, (*TMS, Warrendale PA*).

Flemings, Merton C. (2005). "Coarsening in Solidification Processing" 46 (5): 895–900.

Fuh J. Y. H., et al. (1995). "Improvement of the Uv Curing Process for the Laser Lithography Technique." *Materials & Design*, 16(1), 23-32.

Fujii H. and Nogi K. (2004). "Formation and disappearance of pores in aluminum alloy molten pool under microgravity." *Science and Technology of Advanced Materials*, 5(1-2), 219-223.

Furlong Michael Thomas, et al. (2011). "A Method, Apparatus, Computer Readable Storage Medium and Computer Program for forming an object". *City: United kingdom*.

Goodridge R. D., and Hague R. J. M. (2012). "Laser sintering of polyamides and other polymers." *Progress in Materials Science*, 57(2), 229-267.

Gremaud, M., et al. (1990). "The microstructure of rapidly solidified AlFe alloys subjected to laser surface treatment." *Acta Metallurgica et Materialia* 38(12): 2587-2599.

Gu, D D., et al. (2012). "Laser additive manufacturing of metallic components: materials, processes, and mechanisms." *International Materials Reviews* 57 (3): 133–64.

Hadadzadeh, A., et al. (2015) "Strengthening mechanisms in direct metal laser sintered AlSi10Mg: Comparison between virgin and recycled powders" *MDP journal* 45-52.

Harrison Neil J., et al. (2015). "Reduction of micro-cracking in nickel superalloys processed by Selective Laser Melting: A fundamental alloy design approach." *Acta Materialia*, 94, 59-68.

Hauser C. (2003). "Selective laser sintering of a stainless steel powder". *Thesis University of Leeds*.

Hogg R., and Austin L. G. (1974). "Axial transport of dry powders in horizontal rotating cylinders." *Powder Technology*, 9(2-3), 99-106.

Jia, Q., et al. (2018) "Characterisation of AlScZr and AlErZr alloys processed by rapid laser melting." *Scripta. Materialia*. 2018, 151, 42–46

K. Kempen, L., et al. (2011). "Process optimization and microstructural analysis for selective laser." *Rapid Journal Prototyping* 484–95.

Kajima, Yuka., et al. (2018). "Journal of the mechanical behavior of biomedical materials e ff ect of adding support structures for overhanging part on fatigue strength in selective laser melting." *Journal of the Mechanical Behavior of Biomedical Materials* 78(5) 210-222

Karapatis P. (2002). "A Sub-process approach of Selective Laser Sintering", *Ecole polytechnique fédérale de Lausanne*.

Kaufmann, F., et al. (2016). "Influence of process parameters on the quality of aluminium alloy EN AW7075 using selective laser melting (SLM) ". *Physics. Procedia*, 83, 918–926.

Khan Mushtaq. (2010). Selective laser melting (SLM) of gold (Au). Wolfson School of Mechanical and Manufacturing Engineering, *Loughborough University.*

Kiuchi, M I, and R Kopp. (2002). "Mushy / Semi-Solid Metal Forming Technology - Present and Future" 2 (1).

Kruth J. P., et al. (2004). "Selective laser melting of iron-based powder." *Journal of Materials Processing Technology*, 149(1-3), 616-622.

Krycer I., and Hersey J. A. (1980). "Fine Powder Mixing in a Vibratory Ball Mill." *International journal of pharmaceutics*, 6(2), 119-129.

Kurochkin, A. R,, et al. (2013). "Density of copper–aluminum alloys at temperatures up to 1400 ° c determined by the gamma ray technique" *Journal of alloys and compounds* 51 (2): 224–32.

Kurz, W, and D J Fisher. (1992). "Fundamentals of Solidification" third edition.

Lacey P. C. (2007). "Developments in the theory of particle mixing." *Journal of Applied Chemistry*, 4(5), 257 - 268.

Legendre F., et al.. (2007). "Synthesis of nanostructured SnO2 materials by reactive ball-milling." *Journal of Alloys and Compounds*, 434-435, 400-404.

Li, Ruidi, et al. (2012). "Balling Behavior of Stainless Steel and Nickel Powder during Selective Laser Melting Process," *Journal of Alloys and Compounds* 1025–35.

Li, Yali, and Dongdong Gu. (2014). "Parametric analysis of thermal behavior during selective laser melting additive manufacturing of aluminum alloy powder." *Materials and Design* 63: 856–67.

Li, Zhonghua, et al. (2017). "A lightweight and support-free design method for selective laser melting," *Journal of Alloys and Compounds* 2943–53.

M.N.Mohammed, et al. (2014). "An Overview of Semi-Solid Metal Processing" *Materials and Design* 8 (19): 369–73.

Marc Saunders (2018) Modulation matters - how to build all features great and small, *Linkedin Publications*

Marchese Giulio, et al.. (2017). "Microstructural investigation of as-fabricated and heattreated inconel 625 and inconel 718 fabricated by direct metal laser sintering: contribution of politecnico di torino and istituto italiano di tecnologia (iit) di torino", *Elsevier Metal Powder Report*, Volume 71, 273-278.

Martin Eden Glicksman, (2011), Principales of Solidification, "An introduction to Modern Casting and Crystal Growth Concepts" .

Martin McMahon (2018) "Viso profundum et latius", *Linkedin Publications*, https://www.linkedin.com/pulse/viso-profundum-et-latius-martin-mcmahon/.

Martinez R., et al. (2017). "Customised Alloy Blends for in-Situ Al339 Alloy Formation Using Anchorless Selective Laser Melting." *MDP Technologies* 5 (2): 24.

Mauduit, A. (2017) "Study of the suitability of aluminum alloys for additive manufacturing by laser powder bed fusion". *Science Bulletin*, 79, 219–238.

Mills, K. C., et al. (1998). "Marangoni effects in welding. Philosophical Transactions of the Royal Society of London", *Mathematical, Physical and Engineering Sciences*, 356, 911-925.

Mondolfo, L. F. (1976). "Aluminium alloys : structure and properties". Edited by APA. 16th ed. London: *Butterworth*.

Montero Sistiaga, et al. (2016). "Changing the alloy composition of al7075 for better processability by selective laser melting." *Journal of Materials Processing Technology* 238: 437–45.

Morgan R., Sutcliffe C. J., and O'Neill W. (2004). "Density analysis of direct metal laser re-melted 316L stainless steel cubic primitives." *Journal of Materials Science*, 39(4), 1195-1205.

Mumtaz K. (2008). Selective laser melting of Iconel 625 using pulse shaping, *Loughborough University*.

Mumtaz K., and Hopkinson N. (2011). "A method to eliminate anchors/supports from directly laser melted metal powder bed processes"Solid Freeform Fabrication. *City: University of Texas: Texas.*

O'Neill W., et al. (2012) "Investigation of short pulse Nd: YAG laser interaction with stainless steel powder beds." Presented at *Proceedings of the Solid Freeform Fabrication Symposium, University of Texas, Austin, Texas.*

Okamoto H. (1997). "Bi-zn (bismuth-zinc)." *Journal of Phase Equilibria*, 18(2), 218-218.

Olakanmi, E. O., et al. (2015). "A review on selective laser sintering/melting (sls/slm) of aluminium alloy powders: Processing, Microstructure, and Properties." *Progress in Materials Science* 74: 401–77.

Over C. (2003). "Generative Fertigung von Bauteilen aus Werkzeugstahl X38CrMoV5-1 und Titan TiAl6V4" mit, *Selective Laser Melting journal* p68-74.

Polivnikova T. (2015) "Study and modelling of the melt pool dynamics during selective laser sintering and melting" *École Polytechnique Fédérale de Lausanne* 80 1-105

P. Mercelis and J. Kruth, (2006) "Residual stresses in selective laser sintering and selective laser melting," *Rapid Prototyping Journal*, pp. 254–265,.

Polmear, I. J. (1995). Light Alloys : Metallurgy of the Light Metals. 3rd ed. London: *Butterworth*.

Rehme Reinhart. (2011). Tailored Light 2: Laser Application Technology (RWTHedition): *Springer*.

Pratik Vora, et al. (2014). "AlSi12 in-situ alloy formation and residual stress reduction using anchorless selective laser melting." *Elsevier Editorial System* 1: p30.

Read, Noriko, et al. (2015). "Selective laser melting of AlSi10Mg alloy: process optimisation and mechanical properties development." *Materials and Design* 65: 417–24.

Rehme O. and Emmelmann C. (2006)."Reproducibility for properties of Selective Laser Melting products." Presented at Proceedings of the *Third International WLT-Conference on Lasers in Manufacturing,* Munich.

Rietzel Dominik, et al. (2008). "New thermoplastic powder for selective laser sintering." *Springer*, 42-45.

Robert M. Suter, and He Liu,. (2017) Rollett, presented at *SSSAP Chicago*.

Rombouts M., et al. (2006). "Fundamentals of selective laser melting of alloyed steel powders." *Cirp Annals-Manufacturing Technology*, 55(1), 187-192.

Sahu, Ashutosh, and Ajit Behera. (2015). "Semi-Solid processing and tribological characteristics of Al-Cu Alloy." *Materials Today: Proceedings* 2 (4–5): 1175–82.

Salmoria G. V.,et al. (2009). "The microstructural characterization of PA6/PA12 blend specimens fabricated by selective laser sintering." *Polymer Testing*, 28(7), 746-751.

Schmidtke, K., et al. (2011). "Process and mechanical properties: applicability of a scandium modified al-alloy for laser additive*" Manufacturing Phys. Procedia*, p12, 369–374.

Schwab, Holger, et al. (2017). "Materials & design processing of Ti-5553 with improved mechanical properties via an in-situ heat treatment combining selective laser melting and substrate plate heating." *Materials & Design* p130: 83–89.

Sercombe, T.B. and Li, X. (2016). Selective laser melting of aluminium and aluminium metal matrix composites: *Review Materials Technology*. p31, 77–85.

Simchi A., and Pohl H. (2003). "Effects of laser sintering processing parameters on the microstructure and densification of iron powder." *Materials Science and Engineering a-Structural Materials Properties Microstructure and Processing*, 359(1-2), 119-128.

Singheiser L., et al. (2001). "Failure aspects of thermal barrier coatings." *Materials at High Temperatures*, 18(4), 249-259.

Steen William M., and Mazumder Jyotirmoy. (2010). Laser Material Processing: *Springer*.

Stwora, A, and G Skrabalak. (2013). "Influence of selected parameters of selective laser sintering process on properties of sintered materials." *Journal of Achievements in Materials and Manufacturing Eingineering* 61 (2): 375–80.

Suryanarayana C. (2001). "Mechanical alloying and milling." *Progress in Materials Science*, 46(1-2), 1-184.

Sze. (2009). Outlines and Highlights for Semiconductor Devices: *Academic Internet Publishers*.

Thýn Jiři, and Duffek Karel. (1976). "Powder mixing in a horizontal batch mixer." *Powder Technology*, 15(2), 193-197.

Tolochko N. K., et al. (2004). "Balling processes during selective laser treatment of powders." *Rapid Prototyping Journal*, 10(2), 78-87.

Tontowi A. E., and Childs T. H. C. (2001). "Density prediction of crystalline polymer sintered parts at various powder bed temperatures." *Rapid Prototyping Journal*, 7(3), 180-184.

Van Elsen M. (2007). Complexity of selective laser melting: a new optimisation approach, *Katholieke Universiteit Leuven*.

Wang, Di, et al. (2013). "Study on SLM Fabrication of Precision Metal Parts with Overhanging Structures" *Rapid Prototyping Journal*, 222 20–25.

Wang, L. and Deng, K.G. (2018). "Microstructure and mechanical properties of Al-Cu alloys fabricated by selective laser melting of powder mixtures" *Journal of alloys and compounds*, 735 ,2263-2266. Letter

Watanabe H. (1999). "Critical rotation speed for ball-milling." *Powder Technology*, 104(1), 95-99.

Wendel B. and Schmachtenberg E. (2007) "New Developments in Selective Laser Sintering of Polymers." *Presented at Proc. 5th Laser Assisted Net-shape Engineering Conf Erlangen*.

X. W. and K. Chou, (2013) "Residual Stress in Metal Parts Produced by Powder-Bed Additive Manufacturing Processes," *Journal Chemical. Information Model*, vol. 53, no. 9, 1689–1699.

Yadroitsev I., et al. (2010). "Single track formation in selective laser melting of metal powders." *Journal of Materials Processing Technology*, 210(12), 1624-1631.

Yap, C Y, at al. (2015). "Review of selective laser melting for metals" *Materials and Applications*," p.154-161

Yilbas B. et al. (2012) "Laser straight cutting of Ti-6Al-4V alloy: Temperature and stress fields." *Materials and Surface Engineering* 243-265

Zhang, Hu, et al. (2016). "Selective laser melting of high strength al-cu-mg alloys: processing, microstructure and mechanical properties." *Materials Science and Engineering* A 656: 47–54.
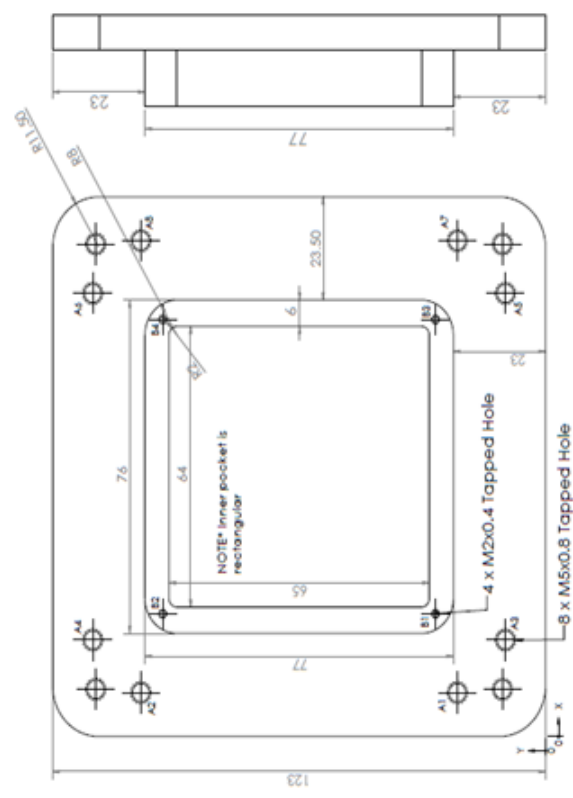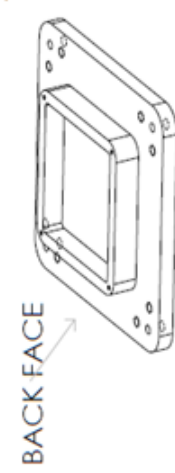
Appendix-A   Powder Certification

AMG

AMG Alpoco UK

Certificate of Analysis	Certificate No. 50801	Advice Note 48312	Date 25-NOV-2016
	Contract GB41276	Customer University of Sheffield	
	Cust. Order No. XJO / 4500780418		

Shipping Marks	Material
PO : XJO / 4500780418	**Aluminium Powder 99.7% (D50: 20-40microns)**
	No and Kind of Packages
DELIVERY LOCATION: UNIVERSITY OF SHEFFIELD CIVIL/MECH ENGINEERING GOODS INWARDS ROOM D121 - MAPPIN BUILDING MAPPIN STREET SHEFFIELD S1 3JD	**1 Drum**

```
Chemical      Test Values %
Al *          99.81
Fe            0.100
Si            0.062
Cu            <0.001
Mn            0.001
Pb            0.001
Mg            0.001
Zn            0.002
Ni            0.004
Ti            0.006
Zr            0.002
Cr            0.001
Ga            0.009
Others
Physical
MALVERN
D10 8.39
D50 24.55
D90 55.32



* Al by difference

We certify that the Aluminium Powder supplied against the above numbered invoice conforms
to the specification given.  The Quality Control arrangements adopted in respect of these
supplies are consistent with the conditions of our Accreditation BS EN ISO 9001:2008.
This certificate is in accordance with BS EN 10204 Part 3.1.B.
Lab Rep No: 20721
Analysis No: 18702
University of Sheffield
```

AMG ADVANCED METALLURGICAL GROUP N.V.
Registered Office: Fullerton Road, Rotherham, S60 1DL, United Kingdom
Registered in England & Wales No. 961050 V.A.T. No. GB 789 6326 65
amg-s.com | amg-nv.com

Page   1   of   1

Telephone: +44 (0)121 351 6119
Facsimile: +44 (0)121 351 7604

212

Appendix-B   Heated Bed Design

UNLESS OTHERWISE SPECIFIED:

DIMENSIONS ARE IN INCHES
TOLERANCES:
FRACTIONAL±
ANGULAR: MACH±   BEND ±
TWO PLACE DECIMAL   ±
THREE PLACE DECIMAL ±

INTERPRET GEOMETRIC
TOLERANCING PER:

MATERIAL

FINISH

DO NOT SCALE DRAWING

	NAME	DATE
DRAWN		
CHECKED		
ENG APPR.		
MFG APPR.		
Q.A.		
COMMENTS:		

TITLE:

SIZE DWG. NO.   REV
A NEWDESIGN

SCALE: 1:5 WEIGHT: SHEET 1 OF 1

APPLICATION

SOLIDWORKS Educational Product. For Instructional Use Only

TOP FACE

BACK FACE

BACK FACE HOLES

TAG	X LOC	Y LOC	SIZE
A1	10	22	Ø 4.20 THRU ALL / M5X0.8 - 6H THRU ALL
A2	10	100	Ø 4.20 THRU ALL / M5X0.8 - 6H THRU ALL
A3	22	113	Ø 4.20 THRU ALL / M5X0.8 - 6H THRU ALL
A4	22	10	Ø 4.20 THRU ALL / M5X0.8 - 6H THRU ALL
A5	101	101	Ø 4.20 THRU ALL / M5X0.8 - 6H THRU ALL
A6	101	113	Ø 4.20 THRU ALL / M5X0.8 - 6H THRU ALL
A7	113	22	Ø 4.20 THRU ALL / M5X0.8 - 6H THRU ALL
A8	113	100	Ø 4.20 THRU ALL / M5X0.8 - 6H THRU ALL
B1	27.96	27.96	Ø 1.60 ▼ 4.20 / M2X0.4 - 6H ▼ 5
B2	27.96	95.04	Ø 1.60 ▼ 4.20 / M2X0.4 - 6H ▼ 5
B3	95.04	27.96	Ø 1.60 ▼ 4.20 / M2X0.4 - 6H ▼ 5
B4	95.04	95.04	Ø 1.60 ▼ 4.20 / M2X0.4 - 6H ▼ 5

TOP FACE HOLES

TAG	X LOC	Y LOC	SIZE
C1	10.75	10.75	Ø 4.20 ▼ 12.40 / M5X0.8 - 6H ▼ 10
C2	10.75	112.25	Ø 4.20 ▼ 12.40 / M5X0.8 - 6H ▼ 10
C3	112.25	10.75	Ø 4.20 ▼ 12.40 / M5X0.8 - 6H ▼ 10
C4	112.25	112.25	Ø 4.20 ▼ 12.40 / M5X0.8 - 6H ▼ 10
D1	33.32	33.49	Ø 3.30 ▼ 6.50 / M4X0.7 - 6H ▼ 6
D2	33.32	89.49	Ø 3.30 ▼ 6.50 / M4X0.7 - 6H ▼ 6
D3	89.32	33.49	Ø 3.30 ▼ 6.50 / M4X0.7 - 6H ▼ 6
D4	89.32	89.49	Ø 3.30 ▼ 6.50 / M4X0.7 - 6H ▼ 6

TOP FACE

4 x M4x0.7 Tapped Hole
4 x M5x0.8 Tapped Hole

R11.50
R8

23
77
23

BACK FACE

4 x M2x0.4 Tapped Hole
8 x M5x0.8 Tapped Hole

NOTE* Inner pocket is rectangular

123
76
23.50
23.50
13
21
8

77
76
64
65
6
23.50

11

214

SOLIDWORKS Educational Product. For Instructional Use Only

	123
116	
R20	
R11.50	
14.80	
26.80	

TAG	X	Y	SIZE
A1	10	22	⌀ 5.50 THRU ALL ⌴ ⌀ 12.24 ⤓ 3.58
A2	10	101	⌀ 5.50 THRU ALL ⌴ ⌀ 12.24 ⤓ 3.58
A3	22	10	⌀ 5.50 THRU ALL ⌴ ⌀ 12.24 ⤓ 3.58
A4	22	113	⌀ 5.50 THRU ALL ⌴ ⌀ 12.24 ⤓ 3.58
A5	101	10	⌀ 5.50 THRU ALL ⌴ ⌀ 12.24 ⤓ 3.58
A6	101	113	⌀ 5.50 THRU ALL ⌴ ⌀ 12.24 ⤓ 3.58
A7	113	22	⌀ 5.50 THRU ALL ⌴ ⌀ 12.24 ⤓ 3.58
A8	113	101	⌀ 5.50 THRU ALL ⌴ ⌀ 12.24 ⤓ 3.58

* All units in mm

UNLESS OTHERWISE SPECIFIED:

DIMENSIONS ARE IN INCHES
TOLERANCES:
FRACTIONAL±
ANGULAR: MACH± BEND ±
TWO PLACE DECIMAL ±
THREE PLACE DECIMAL ±

INTERPRET GEOMETRIC TOLERANCING PER:

MATERIAL

FINISH

DO NOT SCALE DRAWING

	NAME	DATE
DRAWN		
CHECKED		
ENG APPR.		
MFG APPR.		
Q.A.		
COMMENTS:		

APPLICATION

TITLE:

SIZE A | DWG. NO. lower plate | REV

SCALE: 1:2 | WEIGHT: | SHEET 1 OF 1

TAG	X LOC	Y LOC	SIZE
A1	10	22	Ø 5 THRU ALL
A2	10	101	Ø 5 THRU ALL
A3	22	10	Ø 5 THRU ALL
A4	22	113	Ø 5 THRU ALL
A5	101	10	Ø 5 THRU ALL
A6	101	113	Ø 5 THRU ALL
A7	113	22	Ø 5 THRU ALL
A8	113	101	Ø 5 THRU ALL

NOTE : All units are in mm

MATERIAL: AISI 310

Inner radio 1mm

D Middle plate

216

NOTE: All units are in mm
MATERIAL: Alumina Insulation Type SALI-2

TAG	X LOC	Y LOC	SIZE
A1	10	22	Ø 5 THRU ALL
A2	10	101	Ø 5 THRU ALL
A3	22	10	Ø 5 THRU ALL
A4	22	113	Ø 5 THRU ALL
A5	101	10	Ø 5 THRU ALL
A6	101	113	Ø 5 THRU ALL
A7	113	22	Ø 5 THRU ALL
A8	113	101	Ø 5 THRU ALL

Ceramic gasket

SIZE DWG. NO. REV

SCALE: 1:2 WEIGHT: SHEET 1 OF 1

TITLE:

UNLESS OTHERWISE SPECIFIED:

DIMENSIONS ARE IN INCHES
TOLERANCES:
FRACTIONAL±
ANGULAR: MACH±   BEND ±
TWO PLACE DECIMAL ±
THREE PLACE DECIMAL ±

INTERPRET GEOMETRIC
TOLERANCING PER:

MATERIAL

FINISH

	NAME	DATE
DRAWN		
CHECKED		
ENG APPR.		
MFG APPR.		
Q.A.		
COMMENTS:		

DO NOT SCALE DRAWING

APPLICATION

PROPRIETARY AND CONFIDENTIAL

THE INFORMATION CONTAINED IN THIS
DRAWING IS THE SOLE PROPERTY OF
<INSERT COMPANY NAME HERE>. ANY
REPRODUCTION IN PART OR AS A WHOLE
WITHOUT THE WRITTEN PERMISSION OF
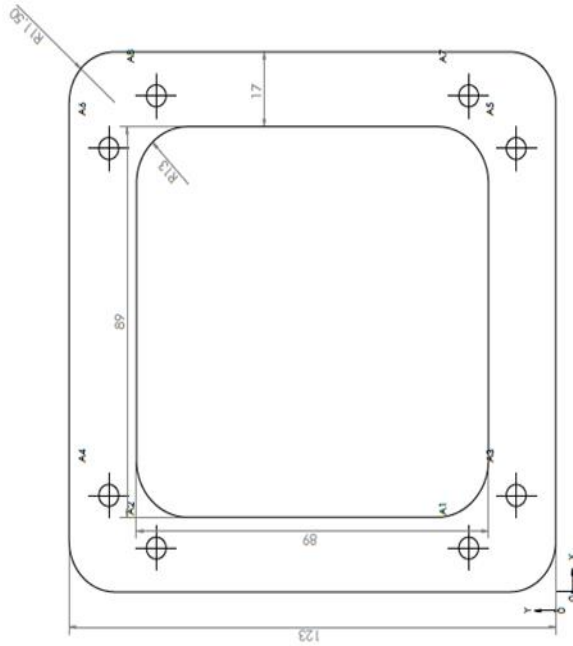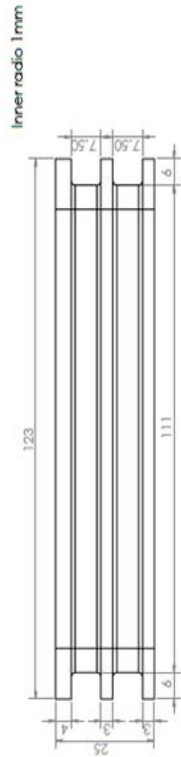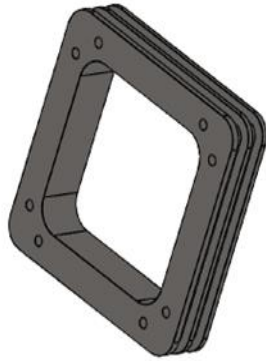<INSERT COMPANY NAME HERE> IS
PROHIBITED.

SOLIDWORKS Educational Product. For Instructional Use Only

R11.50

R13

5

123

89

68

89

123

A1 A2 A3 A4 A5 A6 A7 A8

X

Y

O

217

Appendix-C   ABAQUS Program Subroutine

```
c   Program Test Rafael Martinez Aluminium Alloy
    subroutine                          dflux(flux,sol,kstep,kinc,time,noel,npt2
,coords,jltyp,temp,press)
    include 'ABA_PARAM.INC'
    dimension flux(2),time(2),coords(3)
    parameter (PI=3.1415926535)
    integer NI, MI, SpotNumber, LineNumber, SpotsPerLine
    real*8 x0,y0,z0,yx,y,z,L0,L1,SpotDistance,exposure
    real*8 xinc, W, H, yinc, TimeToSwitchLines
    real*8 vw,r,rp,rs,d,lt
    real*8 q,tho,Hs,Iz,S
    real*8 omega
    real*8 temp
    real*8 M,N
c    Defining heating speed in m/sec
    PARAMETER(vw=122)
c    Defining the laser's spot size in meters
    PARAMETER(rlas=0.05)
    PARAMETER(d=0.07)
c    Laser's Efficiency
    PARAMETER(eff=.18)
c    Sheet thickness in meters
    PARAMETER(th=1.05)
  Power of Laser in Watts
    PARAMETER(pow=180000)
c    Define the hatch distance (Distance between two scan lines).
    xinc=0.065
    yinc=0.065
c    Width of the plate
    W=5.95
c    Height of the plate
    H=1.04
c    Layer Thickness
    lt=0.04
c ------------------------------------------------------------------
    ts=time(1)
c    Define Spot Distance
    SpotDistance=0.02
c    Define Exposure
    Exposure=0.00016
c    Define Line Number
    LineNumber=(ts*vw)/H
```

218

```fortran
      LineNumber=INT(LineNumber)
c     Define Number of Spots per Line
      SpotsPerLine=H/SpotDistance
      SpotsPerLine=INT(SpotsPerLine)
c     Define Spot Number
c      SpotNumber=ts/Exposure
      SpotNumber=INT(SpotNumber)
      SpotNumber=((ts-(LineNumber*Exposure))/Exposure)
c     Iniatilize tool centre.
      x0=0
      y0=0
c      x0=0.000208333
c     y0=-0.0000632911
c      z0=0.55
      L0=((y0)+(vw*ts))
      L1=((x0)+(vw*ts))
      N=L0/H
c      N1=L1/W
      NI=INT(N)
      N=REAL(NI)
      If (MOD((KSTEP-3),8).eq.0) THEN
c     Increment X by (0.00008 the hatch distance).
      x0=x0+(LineNumber*xinc)
c     Condition for scanning Odd vectors from bottom-end at 0 to top-end 0.025.
        IF ((MOD (NI,2).eq.0)) THEN
c      Keep the Laser moving in Positive-Y direction till the top-end of Odd
vectors (1,3,5...) at 0.025 is reached.
c        y0=y0+(SpotDistance)*((SpotNumber-LineNumber)
c     2  -(LineNumber*SpotsPerLine))
       y0=y0+(SpotDistance)*(SpotNumber-(LineNumber*SpotsPerLine))
      Else
c     Keep the Laser moving in Negative-Y direction till the bottom-end of Even
Vectors (0,2,4,6...) at 0 is reached.
c        y0=H-(SpotDistance)*((SpotNumber-LineNumber)
c     2    -(LineNumber*SpotsPerLine))
      y0=H-(SpotDistance)*((SpotNumber)-(LineNumber*SpotsPerLine))
        END IF
      ELSE IF (MOD((KSTEP-5),8).eq.0) THEN
c     Increment Y by (0.00008 the hatch distance).
      y0=y0+(LineNumber*yinc)
        IF ((MOD (NI,2).eq.0)) THEN
c     Keep the Laser moving in Negative-X direction till the Left-end of Even
Vectors (0,2,4,6...) at 0 is reached.
        x0=W-(SpotDistance)*((SpotNumber-LineNumber)
    2   -(LineNumber*SpotsPerLine))
        Else
```

c   Keep the Laser moving in Positive-X direction till the Right-end of Odd
vectors (1,3,5...) at 0.025 is reached.
      x0=x0+(SpotDistance)*((SpotNumber-LineNumber)
     2   -(LineNumber*SpotsPerLine))
        END IF
      ELSE IF (MOD((KSTEP-7),8).eq.0) THEN
c   Decrement X by (0.00008 the hatch distance).
      x0=W-(LineNumber*xinc)
c   x0=(W-0.00005)-(LineNumber*xinc)
c   Condition for scanning Odd vectors from bottom-end at 0 to top-end 0.025.
        IF ((MOD (NI,2).eq.0)) THEN
c   Keep the Laser moving in Negative-Y direction till the bottom-end of Even
Vectors (2,4,6...) at 0 is reached.
      y0=H-(SpotDistance)*((SpotNumber-LineNumber)
     2   -(LineNumber*SpotsPerLine))
        Else
c   Keep the Laser moving in Positive-Y direction till the top-end of Odd
vectors (1,3,5...) at 0.025 is reached.
      y0=y0+(SpotDistance)*((SpotNumber-LineNumber)
     2   -(LineNumber*SpotsPerLine))
        END IF
      ELSE IF (MOD((KSTEP-9),8).eq.0) THEN
c   Decrement Y by (0.00008 the Hatch distance).
      y0=H-(LineNumber*yinc)
c   y0=(H-0.00005)-(LineNumber*yinc)
        IF ((MOD (NI,2).eq.0)) THEN
c   Keep the Laser moving in Positive-X direction till the Right-end of Odd
vectors (1,3,5...) at 0.025 is reached.
      x0=x0+(SpotDistance)*((SpotNumber-LineNumber)
     2   -(LineNumber*SpotsPerLine))
        Else
c   Keep the Laser moving in Negative-X direction till the Left-end of Even
Vectors (0,2,4,6...) at 0 is reached.
      x0=W-(SpotDistance)*((SpotNumber-LineNumber)
     2   -(LineNumber*SpotsPerLine))
        END IF
      END IF
c Calculation of polar coordinates
      x=coords(1)
      y=coords(2)
      z=coords(3)
      r=sqrt((x-x0)**2+(y-y0)**2)
c
c Test of node position and flux assignment
c   q=pow/(PI*rlas*rlas)
ccccc This works   Hs=(pow/(pi*(rlas**2)*lt))*exp((-(r**2))/rlas**2)

```fortran
c      Hs=(pow/(pi*(rlas**2)*lt))*exp((-2*(r**2))/rlas**2)
c THis model is for Aluminium-Copper  Hs=(2.6*pow/(pi*(rlas**2)))
      Hs=(2.6*pow/(pi*(rlas**2)))
c this workssss      Hs=(pow/(pi*(rlas**2)*lt))
c      z=(x**2/rlas)+(y**2/rlas)+0.05
c      z=sqrt((x**2/rlas**2)+(y**2/rlas**2))+0.05
ccccccccccccccccccccccccc      Iz=(-6*(z)**2+2*(z)+1)
ccccccccccccccccccccccccc      Iz=(-5*(z)**2+2*(z)+1)
c      Iz=(0.9*(z)+ 0.8)
cc      Iz=(-15*(z)**2+0.8*(z)+1.4)
ccc      Iz=(-15*(z)**2+0.1*(z)+1.1)
      Iz=(-15*(z)**2+4*(z)+2)
c      Hs=q*eff*0.1*0.846
c      Iz=(1/0.75)*((-2.25*(z)**2)+(1.5*(z))+0.75)*exp(-z)
c      Iz=(1/0.75)*((-2.25*(z/S)**2)+(1.5*(z/S))+0.75)
c      z=(((x)**2+(y)**2)-0.02)
      temp=sol
c      If (temp.le.1660) then
      if (r.le.rlas) then
c      if ((r.le.rlas).AND.(z.ge.-0.05)) then
c        flux(1)=q*eff*0.18*exp(-2*r*r/(rlas*rlas))
c        flux(1)=(0.18*(Hs*Iz)/S)
ccccccccc This is the want that works for a single scan line
flux(1)=(0.6*0.846*(Hs*Iz))
       flux(1)=(0.6*0.846*(Hs*Iz))
      Else
       flux(1)=0
      end if
      Else
       if (r.le.rlas) then
       flux {1} =q*eff (efficiencia)*1*exp(-2*r*r/(rlas*rlas))
       flux{1} = q* eff efficiencia)*1*0.846
       Else
       flux(1)=0
      end if
      End If
      return
      end
      QSUBROUTINE
~QUSDFLDQ(FIELDQ,STATEVQ,PNEWDT,DIRECT,T,CELENT,
   1
TIME,DTIME,CMNAME,ORNAME,NFIELD,NSTATV,NOEL,NPT,LAYE
R,
   2
KSPT,KSTEP,KINC,NDI,NSHR,COORD,JMAC,JMATYP,MATLAYO,
   3 LACCFLA)
```

**221**

```fortran
      INCLUDE 'ABA_PARAM.INC'
      CHARACTER*80 CMNAME,ORNAME
      CHARACTER*3  FLGRAY(15)
      DIMENSION FIELD(NFIELD),STATEV(NSTATV),DIRECT(3,3),
     1 T(3,3),TIME(2)
      DIMENSION ARRAY(15),JARRAY(15),JMAC(*),JMATYP(*),
     1 COORD(*)
C
C Get temperatures from previous increment
      call getvrm('TEMP',array,jarray,flgray,jrcd,
     1    jmac, jmatyp, matlayo, laccfla)
      TEMP = array(1)
C**************************************************
C define the melting temperature and create logic to change field
C variable
      TMELT=1412
      If (TEMP.GT.TMELT) then
c     TOL=1E-6
c     IF ((TEMP.GT.TMELT).AND.
c    1      (ABS(STATEV(1)-1).lt.TOL))then
C     FIELD(1)=2.0
      STATEV(1) = 2.0
      ENDIF
      FIELD(1)=STATEV(1)
C Escribir Aqui para ver si hay cambios
C-- FOR This will QQ print the value  QQ in the command window
c     write(*,*) time(1), field(1),STATEV(1)
      RETURN
      END
```

Appendix-D   Beam profiling measurements
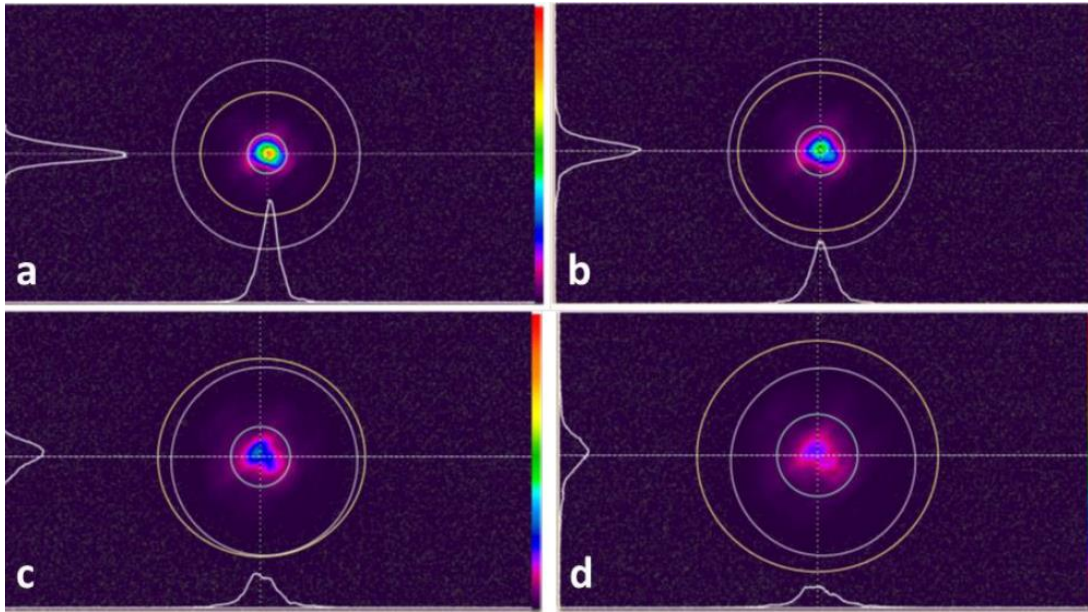
Beam profile using 200W with different focus offsets a) 0.0 mm b) 2.0 mm c)

4.0 mm and d) 6.0 mm
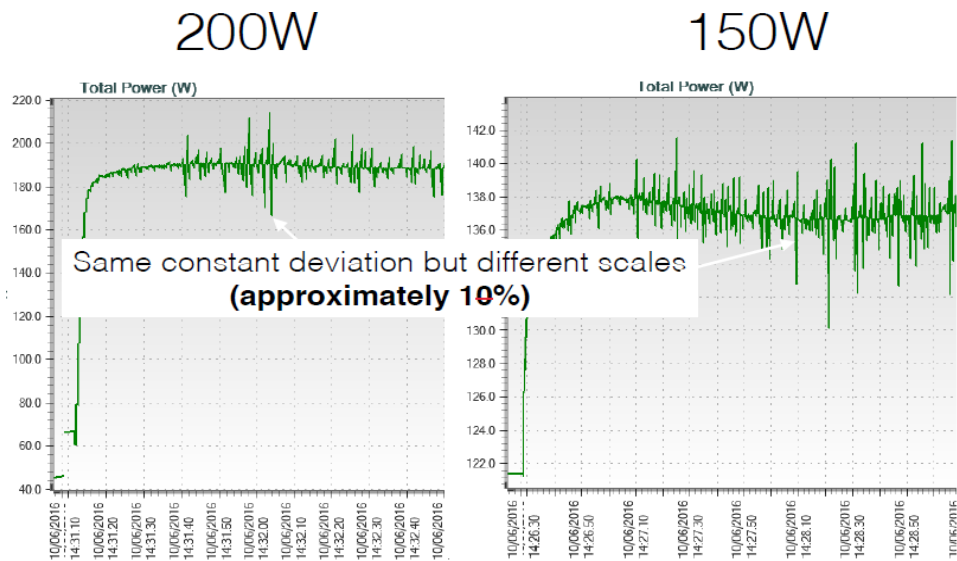
Laser Power (W)	Actual Laser Power (W)	Difference (W)
50	40	10
100	93	7
150	142	8
200	192	8